ISTANBUL TECHNICAL UNIVERSITY ★ GRADUATE SCHOOL OF SCIENCE ENGINEERING AND TECHNOLOGY

GEOCHEMICAL CHARACTERIZATION AND PREDICTION OF ACID MINE DRAINAGE GENERATION POTENTIAL OF KURE VOLCANOGENIC MASSIVE SULFIDE DEPOSITS

M.Sc. THESIS

Cansu DEMİREL

Department of Geological Engineering

Geological Engineering Programme

MAY 2015

ISTANBUL TECHNICAL UNIVERSITY ★ GRADUATE SCHOOL OF SCIENCE ENGINEERING AND TECHNOLOGY

GEOCHEMICAL CHARACTERIZATION AND PREDICTION OF ACID MINE DRAINAGE GENERATION POTENTIAL OF KURE VOLCANOGENIC MASSIVE SULFIDE DEPOSITS

M.Sc. THESIS

Cansu DEMİREL
(505121303)

Department of Geological Engineering

Geological Engineering Programme

Thesis Advisor: Assoc. Prof. Dr. Nurgül ÇELİK BALCI

MAY 2015

İSTANBUL TEKNİK ÜNİVERSİTESİ ★ FEN BİLİMLERİ ENSTİTÜSÜ

KÜRE VOLKANOJENİK MASİF SÜLFİD YATAKLARININ JEOKİMYASAL KARAKTERİZASYONU VE ASİT MADEN DRENAJI ÜRETME POTANSİYELİNİN KESTİRİMİ

YÜKSEK LİSANS TEZİ

Cansu DEMİREL
(505121303)

Jeoloji Mühendisliği Anabilim Dalı

Uygulamalı Jeoloji Programı

Tez Danışmanı: Doç. Dr. Nurgül ÇELİK BALCI

MAYIS 2015

Cansu DEMİREL, a **M.Sc.** student of ITU **Graduate School of Science, Engineering & Technology** student ID **505121303**, successfully defended the **thesis** entitled "**GEOCHEMICAL CHARACTERIZATION AND PREDICTION OF ACID MINE DRAINAGE GENERATION POTENTIAL OF KURE VOLCANOGENIC MASSIVE SULFIDE DEPOSITS**", which she prepared after fulfilling the requirements specified in the associated legislations, before the jury whose signatures are below.

Thesis Advisor :	**Assoc. Prof. Nurgül ÇELİK BALCI** Istanbul Technical University	.....
Jury Members :	**Prof. Dr. Namık ÇAĞATAY** Istanbul Technical University	.....
	Assoc. Prof. Erol SARI Istanbul University	.....

Date of Submission : 04 May 2015
Date of Defense : 29 May 2015

To my family,

FOREWORD

Mining industries, particularly base metal mines, are irrevocable parts of the world's economy. With increasing population, exploration and operating of new ore deposits is inevitable. Operating ore deposits particularly with low tenor cause a vast amount of wastes. Oxidation of these wastes around active and inactive mining sites upon exposure to the atmosphere create one of the most common environmental problem known as acid mine drainage (AMD). Located in the Kastamonu province, Northern Turkey, Küre volcanogenic massive sulfide (VMS) copper deposits is a great candidate for AMD generation. Despite its long mining history, there is no systematic study related to environmental impacts of Kure VSM deposits. Despite the high risk for AMD, the lack of environmental studies about Küre copper deposits was the main motivation for this particular subject and study area. I owe special thanks to Prof. Dr. Yüksel Örgün for inspiring me to be aware of the environmental problems related to mining activities. In addition, I would like to thank Prof. Dr. Namık Çağatay, and my bachelor degree supervisor Assoc. Prof. Yılmaz Mahmutoğlu for their motivation during my studies. Most importantly, I have my supervisor to thank for supporting every single phase of my thesis financially and intellectually; encouraging me to try everything in her laboratory to achieve my goals and letting me fail and learn, which helped me to design projects and fix related problems on my own.

I also thank Prof. Dr. Aral Okay, Prof. Dr. Paul Schroeder, Asst. Prof. Şeref Sönmez, Assoc. Prof. Dr. Emin Çiftçi, Res. Asst. Hatice Ünal Ercan, and my friends Res. Asst. Alp Ünal, Geological Engineer Serra Gül and Ahmet Metin Öteleş, and Genetics Engineer Meryem Menekşe Kılıç for their support during mineralogical and geochemical studies. Moreover, I thank Dr. Cengiz Zabcı, Res. Asst. İrem Elitez and my friend Res. Asst. Murat Şahin for their technical support in digital mapping techniques. Eventually, I thank every academic member of ITU Department of Geological Engineering for supporting me during my studentship, starting with my bachelor degree at ITU.

I thank ITU Scientific Research Projects (BAP) Division for funding this study.

I owe special thanks to my parents Malike and Eren Demirel, who have raised me to become who I am today; to my brother Alper Demirel, who have always supported me; and finally, to Fatih Güler, who has been always there for me no matter what with his big heart.

May 2015

Cansu DEMİREL
(Geological Engineer)

TABLE OF CONTENTS

Page

FOREWORD ..... **ix**
TABLE OF CONTENTS ..... **xi**
ABBREVIATIONS ..... **xiii**
LIST OF TABLES ..... **xv**
LIST OF FIGURES ..... **xvii**
SUMMARY ..... **xxi**
ÖZET ..... **xxv**
1. INTRODUCTION **1**
1.1 Literature Review 1
1.1.1 Copper bioleaching studies 4
1.2 Purpose of Thesis 5
1.3 Acid Mine Drainage 6
1.3.1 Acid generating mechanisms 7
1.3.1.1 Thiosulfate mechanism 9
1.3.1.2 Polysulfide mechanism 10
1.3.2 Role of microbial activity 12
1.3.3 Characterization and prediction of acid mine drainage 13
2. STUDY AREA **15**
2.1 Geographical Features 15
2.2 Geological and Tectonic Setting 18
2.3 Mining Operations on the Study Area 21
3. MATERIALS AND METHODS **25**
3.1 Field Studies 25
3.1.1 Field exploration and geological investigations 25
3.1.2 Sampling and in-situ applications 26
3.2 Laboratory Studies 30
3.2.1 Water analyses 30
3.2.2 Solid phase analyses 30
3.2.3 Mixing zone chemistry simulation titrations 35
3.2.4 Geochemical static AMD prediction tests 36
3.2.4.1 Paste pH 33
3.2.4.2 Initial neutralization potential 34
3.2.4.3 Standard acid-base accounting 35
3.2.4.4 Net acid generation 35
3.2.5 Biological and chemical leaching of the massive ore 38
3.2.5.1 Bacterial culture growth 36
3.2.5.2 Experimental setup 37
3.2.5.3 Sampling and analytical techniques 37
4. RESULTS AND DISCUSSION **41**

4.1 Simplified Geology of the Area Around Mining Operations 41
4.2 Geochemical and Mineralogical Features of the Ore and Wastes 47
4.2.1 Bulk chemistry 47
4.2.2 Mineralogical investigations 48
4.2.3 Evaluation of static AMD prediction test results 51
4.2.3.1 Paste pH 53
4.2.3.2 Initial neutralization potential 54
4.2.3.3 Standard acid-base accounting 55
4.2.3.4 Net acid generation 56
4.2.4 Neutralizing and Acid Generating Potential of Küre VMS Deposits 56
4.2.4.1 Limitations of the static test methods 58
4.3 Bacterial and Chemical Leaching of the Massive Ore 59
4.3.1 Chemical and mineralogical features of the ore after leaching 64
4.3.2 Comparative leaching characteristics 67
4.3.3 Implications on microbial oxidation mechanisms 72
4.4 Geochemical and Mineralogical Features of the Küre Mining Environment 73
4.4.1 Water chemistry 73
4.4.2 Geochemical and Mineralogical Characterization of Streambeds 74
4.4.2.1 Bulk chemistry of the sediments and secondary precipitates 75
4.4.2.2 Mineralogy of the sediments and secondary precipitates 75
4.4.3 Simulated Geochemical Shifts in Mixing Zones 80
4.5 Mechanisms Operating on Küre AMD System 82
4.5.1 Possible contamination pathways derived from bioleaching experiments 82
4.5.2 Effect of lithological features on water acidity 86
4.5.3 Sources and fate of metals around Küre VMS deposits 88
5. CONCLUSIONS 91
REFERENCES 95
CURRICULUM VITAE 111

ABBREVIATIONS

ABA : Acid-Base Accounting
AC : Acid Consumption
AMD : Acid Mine Drainage
ARD : Acid Rock Drainage
AP : Acid Potential
ASTER : Advanced Spaceborne Thermal Emission and Reflection Radiometer
B : Basalt
EC : Electrical Conductivity
EDS : Energy-Dispersive X-Ray Spectroscopy
Eh : Redox potential
EPA : Environmental Protection Agency
GDEM : Global Digital Elevation Model
GIS : Geographic Information Systems
ICP-MS : Inductively Coupled Plasma Mass Spectrometry
INP : Initial Neutralization potential
m : Meter
M : Molarity
mg/L : A milligram of a substance per a liter of solution
ml : Milliliter
METI : Ministry of Economy, Trade, and Industry (Japan)
MPA : Maximum Potential Acidity
MTA : Mineral Research & Exploration (Maden Tetkik ve Arama)
mV : Millivolt
MWW : Municipal Waste Water
N : Normality
NAG : Net Acid Generation
NASA : National Aeronautics and Space Administration (USA)
NP : Neutralization Potential
NPR : Neutralization Potential Ratio
O : Ore
OBR : Ore Bearing Rock
pH : Negative Logarithm of the Hydrogen Ion Activity
ppb : Parts per Billion
ppm : Parts per Million
ppt : Parts per Tons
PRW : Polluted River Water
rpm : Revolutions per Minute
SABA : Standard Acid-Base Accounting
SEM : Scanning Electron Microscope
TS : Turkish Standards
UTM : Universal Transverse Mercator
USW : Unpolluted Stream Water

UV **:** Ultraviolet
WEP **:** Waste Effluent Precipitate
WEW **:** Waste Effluent Water
WHO **:** World Health Organization
XRD **:** X-Ray Diffraction
XRF **:** X-Ray fluorescence
% **:** Percentile
µm **:** Micrometer
µS/cm **:** Microsiemens per Centimeter

LIST OF TABLES

Page

Table 4.1 : Bulk chemical composition of the rock samples……..……...…48
Table 4.2 : Amounts and concentrations of acid or base used in the experiments.... 52
Table 4.3 : Formulations and parameters used in static test calculations.. ..... ….52
Table 4.4 : Results of the geochemical static AMD prediction tests…….……57
Table 4.5 : EDS analysis (% concentration) of selected surfaces that were subjected to SEM imaging. Lower case letters represent analyzed surfaces displayed in Figure 4.18…….……...67
Table 4.6 : Selected elemental composition (%) of experimental residues collected after 6 months for B1 experiments and 2 months for B2 experiments, determined by XRF analysis……..67
Table 4.7 : Selected physicochemical parameters and chemical compositions of the surface water, groundwater and drinking water samples representing the Küre mine drainage environment……..76
Table 4.8 : Selected elemental compositions (%) of the riverine sediments and ochre precipitates and the ochre crustation on gravels…….....76
Table 4.9 : EDS results (% mass concentration) of selected sections of SEM images. Lower case letters represent analyzed surfaces displayed in Figure 4.24 and Figure 4.25…...……... 81
Table 4.10 : Chemical composition (%) of the supernatants after residue collection after 6 months for B1 experiments and 2 months for B2 experiments.....83
Table 4.11 : Drinking and tap water quality standards showing maximum acceptable levels for human health (TS 266, 2005; WHO, 2008; EPA, 2012)……..……..……85

LIST OF FIGURES

Page

Figure 2.1 : Location map of the study area, marked (with a red square) on Western Black Sea Region (yellow plotted cities) map of Turkey. Units of the geological coordinates are in degrees. Map at the lower right (unscaled) displays the position of the base map (by a red rectangle), which is focused on Western Black Sea Region and Küre (by a red star) in Turkey……15

Figure 2.2 : Topography and drainage network map of Kastamonu E31-a3sheet. Coordinates are in UTM (European Datum 1950 36N) and black rectangle defines the study area……...17

Figure 2.3 : General geology map and geological cross-section of the area around Küre (in Okay et al., 2014)..……...20

Figure 2.4 : Entrance to ancient underground adits of Küre copper mines……..….22

Figure 2.5 : General views from the Küre mining sites: (a) Bakibaba open-cut mine (inactive). (b) Gossan outcrop near Bakibaba open-cut mine. (c) Waste effluent dam. (d) New tunnel boring operation at 512 m elevation in Bakibaba underground mining tunnels. (e) Ancient slag heaps. (f) Processed product storage area…...……..23

Figure 2.6 : Waste dumping areas in the field (black arrows represent flow directions). (a) Ancient slags and relatively recent mining and gossan waste heaps dumped on the slopes of AMD impacted Karanlık Stream (location AMD-5 in Figure 3.1). (b) Mining waste, core and core case dumping into green colored Zemberekler River (location PRW in Figure 3.1)……..…….24

Figure 3.1 : Sampling location map plotted on the topography model (Coordinate system (UTM): European Datum 1950 36N)……..……..……26

Figure 3.2 : Sampling and in-situ measurement locationts of 2013 field study: (a) pH measurements on Karanlık Stream (SWE-1 or AMD-2). (b) Water sampling from Karanlık Stream and filtering (SWE-2 or AMD-7). (c) Sediment sampling from Zemberekler River (SWE-3 or PRW). (d) Water sampling from boreholes (GW) in Bakibaba underground mining tunnels. (e) Water sampling from sidewall leakages (GW) in Bakibaba underground mining tunnels. (f) Illustration of effluent input to the waste dam by piping system and WEW sampling location……27

Figure 3.3 : In-situ pH measurements of the unnamed mine drainage (black arrows point to flow directions): (a) AMD-6. (b) AMD-7, just above the mixing zone with MWW……...……..28

Figure 3.4 : 2014 field geochemistry locations (black arrows point to flow directions): (a) Uncontaminated Küçükali Stream (USW). (b) Section of Karanlık Stream (AMD-1) before mixing with Küçükali Stream. (c) General view from Karanlık Stream (AMD-4). (d) Ochre sample (Ochre2)collection (AMD-4) from Karanlık Stream. ……29
Figure 3.5 : In-situ geochemical applications of 2014 field trip: (a) Fountain (drinking) water (DW) sampling and pH measurement. (b) In-situ water filtering with Nagel bottle……..…….30
Figure 3.6 : Examples from water chemistry analyses: (a) Spectrophotometry. (b) Laboratory pH measurements. ……..31
Figure 3.7 : Examples of instrumentations used for geochemical and mineralogical characterization of the solid phases: (a) Bruker D8 XRD instrument. (b) Philips XL30 ESEM-FEG SEM instrument coupled with EDS……..…32
Figure 3.8 : Mixing zone chemistry simulations: (a) Titration experiments (AMD-7+MWW, AMD-1+USW). (b) Freshly forming precipitates from NaOH titration experiment (AMD-1+NaOH)…….…..……...33
Figure 3.9 : Illustration of paste pH experiments……..……..……. 34
Figure 3.10 : Illustration of INP experiments: (a) Sample stirring using magnetic stirrer. (b) Back titration of the experiment……...……..35
Figure 3.11 : Illustration of SABA experiments: (a) Samples subjected to fizz rating. (b) Acid addition to flasks before heat treatment in water bath……..……....35
Figure 3.12 : Illustration of NAG experiments: (a) Heat treatment in water bath. (b) Titrations after heat treatment……..……..36
Figure 3.13: Illustration of the steps of bioleaching experiments: (a) Laminar flow (Biosafety Cabinet) used as sterile environment. (b) Bacterial culture growth on shaker. (c) Elemental sulfur sterilization under UV light in laminar flow. (d) Chemical control and bioleaching flasks after four months of experiments…….…….....38
Figure 3.14 : Filtering system with Nagel bottle and automated pump…….39
Figure 4.1 : Akgöl Formation: (a) Subgreywacke. (b) Alterated black shale……...41
Figure 4.2 : Tectonic contact of basalt and black shale on a roadcut on Kastamonu-İnebolu main road. Red line depicts the contact between two lithological units; whereas the yellow line indicates a fault plane, which obviously generated a deformation zone.…….……..42
Figure 4.3 : Different features of pillow lavas from Küre Complex: (a) 2 meter long elliptical shape. (b) Spherical, relatively small pillow lava. (c) Chalcopyrite content visible on pillow lava displayed in Figure 4.3a. (d) Internal structure of pillow lava……...43
Figure 4.4 : İnaltı Formation: (a) Fault scarps at North of the city center. (b) Fault scarps at Northwest. (c) Biomicritic blocks at South……..….44
Figure 4.5 : Field views of Çağlayan Formation (note that photos of Çağlayan Formation were taken from different localities in Central Pontides, in scope of a structural geology project coordinated by Prof. Dr. Aral Okay): (a) A typical outcrop view. (b) Illustration of rake angle measurement in the study area. (c) Typical, well-preserved flute cast of Çağlayan Formation…….……..…….45
Figure 4.6 : UTM coordinated new geological map of the study area (after Bailey et al., 1966)…….…...……46

Figure 4.7 : X-ray diffractograms of samples subjected to static tests experiments (Alb: Albite, C: Chalcopyrite, Cal: Calcite, Cct: Chalcocite, Chl: Chlorite, Cov: Covellite, Dol: Dolomite, Gp: Gypsum, H: Hematite, I: Illite, J: Jarosite, M: Magnetite, Mnt: Montmorillonite, P: Pyrite, Q: Quartz, Sp: Sphalerite): (A) Massive sulfide ore. (B) OBR-1. (C) OBR-2. (D) OBR-3. (E) B. (F) WEP……49
Figure 4.8 : Microscopic imaging of OBR's (Ccp: Chalcopyrite, Hem: Hematite, Mgt: Magnetite, Py: Pyrite; AF: Annealing fracture, CF: Cataclastic fracture, FF: Fracture filling): (A) Pyrite grains having chalcopyrite fracture fillings, cataclastic and annealing fractures in OBR-1. (B) Disseminated pyrite grains in the matrix in OBR-1. (C) Pyrite grain being substituted by chalcopyrite and surrounded by specularite in OBR-2. (D) Pyrite, chalcopyrite, specularite and prismatic magnetite in OBR-2. (E) Specularite clusters in OBR-2. (F) Paragenetetic relationship between pyrite, chalcopyrite and specularite in OBR-3....51
Figure 4.9 : Shifts in the pH and EC values of the solution during paste pH tests…53
Figure 4.10 : Evaluation of initial neutralization potential test results…..……..…54
Figure 4.11 : Evaluation of standard acid-base accounting test results…….55
Figure 4.12 : Evaluation of net acid generation test results……..……..56
Figure 4.13 : Shifts in pH with Eh (mV) and Fe(II) with Fe(III) of the solution during B1/26 (A), B2/26 (B) and B2/40 (C) experiments; where diamonds, triangles and hollow circles refer to *Acidithibacillus ferrooxidans*, mixed enrichment cultures and abiotic control experiments, respectively. Blue colors are representing pH or Fe(II), while red colors are representing Eh or Fe(III) shifts, respectively....60
Figure 4.14 : Shifts in total Fe, SO_4^{2-}, Cu, Co and Zn concentrations and EC, during B1/26 experiments……...……61
Figure 4.15 : Shifts in total Fe, SO_4^{2-}, Cu, Co and Zn concentrations and EC, during B2/26 experiments……...……...……62
Figure 4.16 : Shifts in total Fe, SO_4^{2-}, Cu, Co and Zn concentrations and EC, during B2/40 experiments……...……63
Figure 4.17 : X-ray diffractograms of (A) Untreated massive sulfide ore and leached residue after six months of (B) B1-C, (C) B1-Af, (D) B1-E; and two months of (E) B2/40-Af and (F) B2/40-E experiments (C: Chalcopyrite, J: Jarosite, P: Pyrite, Q: Quartz, S: Sulfur, Sch: Schwertmannite, Sp: Sphalerite)……64
Figure 4.18 : SEM imaging of the surface of leached residue after six months of B1 and two months of B2/40 experiments: (A) Morphologies formed after chemical leaching. (B) Secondary precipitation in the presence of *A. ferrooxidans* in B1-Af experiment. (C) Rod shaped *A. ferrooxidans* in red circled area. (D) Deep holes (red circled) and irregular etched surface formed by mixed acidophiles in B1-E experiments. (E) Rose shaped secondary precipitate. (F) Relatively intact pyrite in B2/40-Af experiments. (G) Secondary precipitates (left), newly being oxidized surface (middle) and hexagonal quartz (top right) in B2/40-E experiments……65
Figure 4.19 : Comparative metal release efficiencies of all experiments, in terms of heavy metal release ratio (%) calculated from metal concentrations in the solution relative to initial metal concentrations in the massive sulfide ore…….……...……68

Figure 4.20 : About a micron long rod-shaped erosion pits (red circled) that were observed on the ore surface, in the presence of mixed acidophilic enrichment culture……...……....73
Figure 4.21 : X-ray diffractograms of AMD streambed sediments (Alb: Albite, C: Chalcopyrite, Chl: Chlorite, Fle: Fluoro-edenite, Gib: Gibbsite, Go: Goethite, Gp: Gypsum, I: Illite, J: Jarosite, P: Pyrite, Q: Quartz, Sch: Schwertmannite, Sp: Sphalerite, Sr-Si: Strontium Aluminum Ammine Silicate): (a) S1. (b) S2. (c) S3. (d) S4. (e) S5. (f) S6…....77
Figure 4.22 : X-ray diffractograms of neutral-alkaline streambed sediments and ochre samples (Alb: Albite, C: Chalcopyrite, Chl: Chlorite, Fle: Fluoro-edenite, Frh: Ferrihydrite, Gib: Gibbsite, Go: Goethite, Gp: Gypsum, I: Illite, J: Jarosite, K: Kaolinite, Mg-Ca: Mg-bearing calcite,P: Pyrite, Q: Quartz, Sch: Schwertmannite, Sp: Sphalerite, Sr-Si: Strontium Aluminum Ammine Silicate, Zn-Si: Zinc Hydronium Aluminum Silicate Hydroxide): (a) S7. (b) S8. (c) Ochre1. (d) Ochre2. (e) GFe……..…..78
Figure 4.23 : SEM images of the Ochre1 sample: (A) Different morphologies of secondary ochre precipitates in AMD environment. (B) A closer look to Figure 4.24A (by 5 fold): Jarosite (at left-center) and tubular akageneite-like mineral (at bottom-right). (C) Spherical or globular secondary precipitation (possibly gibbsite) around a mineral grain (possibly pyrite). (D) Gibbsite, some metal (Cu, Fe and Zn) sulfides or hydroxides/hydroxysulfates and an unidentified spherical (spore-like) morphology. (E) Al, Cu and Zn bearing secondary Fe hydroxide/hydroxysulfate precipitates (due to combined EDS results; see Table 4.9). (F) Fe and Al hydroxides/hydroxysulfates (jarosite, goethite, gibbsite, etc.) precipitates (Table 4.9)……..……..……79
Figure 4.24 : SEM images of the GFe sample: (A) Spherical Fe hydroxide/hydroxysulfate precipitates. (B) Chlorite (probably clinochlore due to EDS results) with secondary precipitates. (C) Fe, Al-silicate (clay) mineral with tension cracks and secondary precipitation on its surface. (D) Deformed Fe, Al-silicate (clay) and minerals surrounding secondary precipitates……..……..80
Figure 4.25 : Graphs illustrating the metal concentration before and after titrations……..…….82

GEOCHEMICAL CHARACTERIZATION AND PREDICTION OF ACID MINE DRAINAGE GENERATION POTENTIAL OF KURE VOLCANOGENIC MASSIVE SULFIDE DEPOSITS

SUMMARY

Base metals have an irrevocable place in any branch of industry. With emerging technologies and progressively depleting reserves, metal demand is increasing along with piles of waste material produced after mining activities of the low-grade ores. Considering the base metal need is mostly supplied from volcanogenic massive sulfide deposits; areas surrounding those mining sites are vulnerable to inevitable environmental hazards like acid mine drainage (AMD). AMD is one of the biggest and widespread environmental problems related to mining. AMD occurs due to the oxidation of the sulfur moiety of sulfidic ore deposits and result in acidic water with low pH <3 and heavy metals. Diverse chemical and biological processes co-occur during generation of AMD and the fate of heavy metals in resulting aquatic or solid phases is largely controlled by Fe oxidation. Therefore, elucidating those complex biogeochemical reactions controlled by unique geochemical, mineralogical and lithological features of an ore deposit is a crucial step for prevention and rehabilitation of AMD.

Located in the Kastamonu province of western Black Sea region of Turkey, the Küre VMS deposits hosts one of the most important and productive copper mines of Turkey. The area is a good example of ancient mining activities carried out by Genoese and Byzantines and/or the Ottoman Empire (400 to 1000 years ago) in Turkey. Because of its historical mining past, Küre VSM deposits set a great example to investigate mechanism of AMD generation and fate of heavy metals in mining impacted areas. Therefore, potential sources and acid generating potential of Küre VMS deposits were investigated for the first time with an integrated approach-involving laboratory and field based studies.

For this purpose, ore, ore bearing wall rocks, basalts and waste materials were collected during the field studies and subjected to geochemical analyses and to static AMD prediction tests. AMD prediction tests applied in this study involve paste pH, initial neutralization potential, standard acid-base accounting and net acid generation to determine acid producing or neutralizing potentials of the materials.

In addition to AMD prediction tests, the long-term comparative bioleaching characteristics of Küre's massive pyritic copper ore were investigated under various environmental conditions. The generation of AMD was simulated at 26^{o}C and leaching characteristics of pure *Acidithiobacillus ferrooxidans* and a mixed culture of *Acidithiobacillus sp.* were comparatively investigated at 26^{o}C and 40^{o}C.

Finally, the results of AMD prediction tests and laboratory leaching experiments were combined with the field data containing the water chemistry of groundwater, surface and drinking water in addition to mineralogical data involving bulk chemistry

of relevant streambed sediment and secondary precipitates. All these results were used to discuss how acidic waters were generated and to what extend affected the aquatic environment around the mining area.

AMD prediction test results were used to classify and evaluate acid production potential of the ore, ore bearing wall rocks, wall rock and precipitate from waste ponds. The net neutralization potential (NNP), neutralization potential ratio (NPR), acid production potential (AP), neutralization potential (NP) and net acid generating (NAG) values of the ore represent the upper limit values for the region. The lowest NNP (-1617.8), NP (-217.5) values with the highest AP (1400.3), maximum potential acidity (MPA) (1371.2) and NAG (206.5) values calculated for the ore sample indicate good consistency in different methods. Following the ore sample, highest acid production was determined in the waste effluent (or flotation tailings) dam precipitate (WEP) (974.03), ore bearing wall rocks (OBR-1) rich in disseminated pyrite (75.94) and basalt (B) samples referenced to wall rocks (129.6). The ore bearing wall rocks (OBR-2 and OBR-3) containing minor amounts of covellite, chalcocite and pyrite are classified as non-acid producer indicating significance of sulfide mineralogy on acid production. In general, there is good consistency between the results of ABA and NAG tests for the samples. From the ABA and NAG tests applied in the current study, it is concluded that in addition to the ore, ore bearing wall rocks that can be considered as waste and containing particularly disseminated pyrite, contribute more towards acid generation in the region. WEP also have a high acid production potential with an elevated level of toxic metals and precaution should be taken to prevent possible leakage to the environment. Consistency in results from both ABA and NAG tests justify that static tests can be used as tools for preliminary evaluation of prospective AMD generation and its impact on surface and groundwater quality in VMS mining environments.

Results of bioleaching experiments indicate that mixed acidophilic cultures containing iron and sulfur oxidizers leached the massive ore faster rate than pure culture and produced significant amount of acidity (down to pH 1.26). These results suggest that microbial reactions are the major source for acid generation in the mining area. In the early stages of AMD generation, release of Co (max. 9.37 ppm) and Cu (max. 871.4 ppm) into the water were controlled by pure culture of *Acidithiobacillus ferrooxidans*, whereas Zn (max. 201 ppm) and Fe (max. 1810 pm) release were faster in the experiments carried out by mixed *Acidithiobacillus sp*. During the bioleaching experiments, due to calculated percentile leaching ratios, *A. ferrooxidans* was found to be more effective in the leaching of Cu (31.46%), Fe (5.97%) and Co (5.42%) at higher temperatures in contrast to mixed acidophiles that are more active at optimal moderate conditions. Formation of secondary Fe-oxyhydrooxides (e.g. jarosite) were determined in the biological experiments. Significant decrease in Co, Cu and Zn concentration in the later stage of AMD generation were attributed to the co-precipitation of the respected metals with Fe oxides phases. Leaching of massif ore revealed that release of Fe, Cu, Co and Zn during the short term experiments (34 days) were generally due to the rapid bacterial oxidation unlike the long-term experiments (180 days). In the long-term experiments, more complex biogeochemical reactions such as Fe-oxidation and precipitation took place together and regulated the release and precipitation of those metals.

Results obtained from geochemical and mineralogical studies on water, sediment, ochre precipitate in addition to AMD prediction tests carried on the ore, ore bearing wall rocks showed that massive ore and ore bearing wall rocks are the major sources

of acidity and heavy metals. Consistent with this, acid production potential of massive pyritic chalcopyrite ore representing the maximum acid production rate in the region is about 1400 tons of acidity per ton of ore with a net acidity about 206 kg H_2SO_4 per a ton of ore. High concentrations of Cu (up to 40.41 ppm), Zn (up to 9.94 ppm), Fe (up to 19.6 ppm), Mn (up to 30.5 ppm) and Co (up to 7.6 ppm) determined in the surface and groundwater with low pH values (pH 2.9-4.5) indicate AMD generation in the field. Ochre chemistry and mineralogy showed that, major proportions of metals released from the ore and ore bearing rocks were precipitated and transported with secondary iron hydroxide, iron hydroxysulfate and aluminum hydroxide minerals. Moreover, combined XRD and SEM-EDS measurements also revealed the abundance of clay minerals (mainly clinochlore and illite) and secondary metal-bearing (Zn and Sr) silicate phases, which points out the importance of the stability of clay minerals in the transport, release or mobility of metals (mainly Fe, Al, Zn and Sr) in AMD systems.

KÜRE VOLKANOJENİK MASİF SÜLFİD YATAKLARININ JEOKİMYASAL KARAKTERİZASYONU VE ASİT MADEN DRENAJI ÜRETME POTANSİYELİNİN KESTİRİMİ

ÖZET

Temel metallerin, endüstrinin her alanında vazgeçilmez bir yeri vardır. Yeni gelişen teknoloji ve sürekli azalan rezervler ile metal ihtiyacı da artmaktadır. Bunlarla birlikte, düşük tenörlü cevherlerin işletilmesi ile yığınlarca atık açığa çıkmaktadır. Baz metal ihtiyacının çoğunun volkanojenik massif sülfid yataklarından elde edildiği düşünülürse; bu maden yatakları çevresindeki alanlar, asit maden drenajı (AMD) gibi kaçınılmaz çevresel risklere karşı savunmasızdır. AMD, madenciliğe bağlı en büyük ve yaygın çevre sorunlarından biridir. AMD, sülfürlü maden yataklarının sülfür bileşenlerinin oksitlenmesi sebebiyle açığa çıkar ve düşük pH (pH<3) değerlerine sahip ve ağır metallerce kirlenmiş suların oluşmasına sebep olur. AMD'nın oluşmasında çeşitli kimyasal ve biyolojik süreçler işler ve açığa çıkan katı/sıvı fazlardaki metallerin davranışlarını çoğunlukla Fe oksitlenmesi belirler. Bu nedenle; başlıca her maden yatağının kendine has jeokimyasal, mineralojik ve litolojik özellikleri tarafından kontrol edilen bu karışık biyojeokimyasal mekanizmaların açığa kavuşturulması, AMD'nı önlemek veya bertaraf etmek için en önemli adımdır.

Batı Karadeniz bölgesinin Kastamonu ilinde yer alan Küre volkanojenik masif sülfid (VMS) maden yatakları, Türkiye'nin en önemli ve verimli bakır madenlerinden birine ev sahipliği yapmaktadır. Bölge, Cenovalılar, Bizanslılar ve/veya Osmanlıların yürütmüş olduğu, Türkiye'deki eski madencilik aktivitelerine (400-1000 yıl önce) dair iyi bir örnek niteliğindeir. Küre VMS yatakları, tarihi madencilik geçmişinden ötürü, AMD oluşumu ve madencilikten etkilenen alanlarda ağır metallerin davranışını araştırmak için çok iyi bir örnek teşkil eder. Bu nedenle, Küre VMS yataklarının asit üretme potansiyeli ve üretilen asidin potansiyel kaynakları ile miktarı, multidisipliner (kimyasal, mineralojik, jeolojik ve mikrobiyolojik) yaklaşımlar kullanılarak, arazide ve laboratuvarda yapılan detaylı çalışmalar ile araştırılmıştır.

Bu amaçla arazi çalışmalarında cevher, cevher içeren yan kayaçlar, bazalt ve atık madde örnekleri toplanmış; jeokimyasal analizlere ve AMD kestirim testlerine tabi tutulmuştur. Bu çalışmada uygulanan ve örneklerin asit üretme ile nötralizasyon potansiyellerinin belirlenmesinde kullanılan AMD kestirimi testleri, çamur pH'sı, ilksel nötralizasyon potansiyeli, standart asit-baz hesaplama ve net asit üretme testlerini kapsar.

AMD kestirimi teslerine ek olarak, Küre masif piritli bakır cevherinin uzun süreli biyoliç edilme özellikleri, değişen çevresel koşullarda karşılaştırmalı olarak incelemiştir. AMD oluşumu 26^{o}C sıcaklıkta simüle edilmiş; saf *Acidithiobacillus ferrooxidans* ve karışık *Acidithiobacillus sp*. türlerinden oluşan kültürün biyoliç etme özellikleri ise 26^{o}C ve 40^{o}C'de karşılaştırmalı olarak incelenmiştir.

Son olarak, AMD kestirimi ve biyoliç deneylerinin sonuçları, yeraltı maden tünelleri ve yüzeydeki içme suyu çeşme/hayratlarından elde edilen yeraltı suyu kimyası; yüzey sularının maden drenajı kimyası ve ilgili dere sedimenti ile ikincil dere tabanı çökellerin kimyasal ve mineralojik özellikleri ile birleştirilmiştir. Tüm bu sonuçlar, asitli suların nasıl oluştuğunu ve su ortamını ne dereceye kadar etkilediğini tartışmak için kullanılmıştır.

AMD kestirimi deneylerinin sonuçları, cevher, cevherli yan kayaçlar, yan kayaç ve atık barajı çökelinin asit üretme potansiyellerinin sınıflandırılması ve değerlendirilmesinde kullanılmıştır. Cevhere ait net nötralizasyon potansiyeli (NNP), nötralizasyon potansiyeli oranı (NPR), asit üretme potansiyeli (AP), nötralizasyon potansiyeli (NP) ve net asit üretme (NAG) değerleri, bölge, için üst limitleri temsil etmiştir. Cevher için hesaplanan en büyük AP(1400.3), maksimum potansiyel asidite (MPA) (1371.2) ve NAG (206.5) değerleri ile uyum içinde olan en küçük NNP (-1617.8) ve NP (-217.5) değerleri, farklı metodların birbirleri ile iyi derecede tutarlı olduğunu göstermiştir. Cevher örneğinden sonra en büyük asit üretme potansiyeli, atık barajı çökeli (WEP) (974.03), dissemine pirit açısından zengin cevher içeren yan kayaçlar (OBR-1) (75.94) ve yan kayaçları temsil eden bazalt numunelerinde (129.6) belirlenmiştir. Az miktarda kovellit, kalkosit ve pirit içeren yan kayaçlar (OBR-2 ve OBR-3) asit üretmez olarak sınıflandırılmıştır. Bu durum, asit üretiminde sülfid mineralojisinin önemini ortaya koymuştur. Genel olarak, örneklerin asit-baz hesaplama (ABA) ve NAG testi sonuçları arasında tutarlılık vardır. Bu çalışmada uygulanan ABA ve NAG testlerine göre, cevhere ek olarak, atık olarak Kabul edilebilecek ve özellikle dissemine pirit içeren cevherli yan kayaçların daha çok asit üretimine katkıda bulunduğu sonucuna varılmıştır. WEP örneği de yüksek seviyelerde toksik metal içeriği ile birlikte yüksek bir asit üretme potansiyeline sahiptir ve çevreye olası sızıntılar için önlem alınmalıdır. Tutarlı ABA ve NAG test sonuçları, statik testlerin olası AMD oluşumu ve bunun VMS maden ortamında yeraltı suyu kalitesine etkilerinin değerlendirilmesi için ilksel bir araç olarak kullanılabileceğini doğrulamıştır.

Biyoliç deneylerinin sonuçları, Fe ve S oksitleyen bakterilerin birlikte bulunduğu karışık asidofilik kültürlerin, saf kültürlere göre cevheri daha hızlı oksitlediğini ve önemli miktarda (pH 1.26'ya kadar düşen seviyede) asit ürettiğine işaret etmektedir. Bu sonuçlar, mikrobiyal reaksiyonların, maden sahasında asit üretiminin en büyük kaynağı olduğunu göstermiştir. AMD oluşumunun erken safhalarında; AMD sularındaki Co (maksimum 9.37 ppm) ve Cu (maksimum 871.4 ppm) salınımı saf *Acidithiobacillus ferrooxidans* kültürü tarafından kontrol edilirken, Zn (maksimum 201 ppm) ve Fe (maksimum 1810 ppm) salınımı karışık kültürleri içeren biyoliç deneylerinde daha hızlı gerçekleşmiştir. Biyoliç deneyleri süresince, hesaplanan yüzde liç oranlarına göre, *Acidithiobacillus ferrooxidans* kültürünün, optimum orta sıcaklıklarda daha aktif olan karışık asidofilik türlere göre yüksek sıcaklıklarda daha iyi Cu (31.46%), Fe (5.97%) ve Co (5.42%) liç ettiği tespit edilmiştir. Biyolojik deneylerde, ikincil Fe-oksihidroksit (örneğin, jarosit) oluşumu tespit edilmiştir. Deneylerin son safhalarına doğru Co, Cu ve Zn konsantrasyonlarında görülen azalma, bu metallerin demir oksit fazlarıyla birlikte çökelmesi olarak yorumlanmıştır. Bu çalışma, kısa süreli biyoliçte (34 gün), uzun süreli deneylere (180 gün) karşıt olarak, metal (Fe, Cu, Co ve Zn) salınımının daha çok hızlı bakteriyel oksidasyondan kaynaklandığını göstermiştir. Uzun süreli deneylerde, demir oksitlenmesi ve çökelmesi gibi daha karışık biyojeokimyasal mekanizmalar birlikte devreye girmiş ve metal salınımı ya da çökelmesini kontrol etmiştir.

AMD kestirim testlerine ek olarak; su, sediment, okr çökeltisi ve cevher içeren malzeme örnekleri üzerinde gerçekleştirilen jeokimyasal ve mineralojik incelemelerin sonuçları, cevher ve cevher içeren yan kayaçların en büyük asidite ve ağır metal kaynağı olduğunu göstermiştir. Bununla tutarlı olarak, bölgenin en maksimum asit üretme kapasitesinin temsil eden massif piritli kalkopirit cevherinin yaklaşık asit üretme potansiyeli 1400 ton asidite/ton cevher olmakla birlikte, net asit üretimi bir ton cevhere karşılık 206 kg H_2SO_4 olarak hesaplanmıştır. Bölge yüzey ve yeraltı sularında tespit edilen düşük pH değerleri (pH 2.9-4.5) ile birlikte yüksek Cu (40.1 ppm), Zn (9.94 ppm), Fe (19.6 ppm), Mn (30.5 ppm) ve Co (7.6 ppm) konsantrasyonları, bölgede AMD oluşumunu göstermektedir. Okr kimyası ve mineralojisi, cevher ve cevherli yan kayaçlardan salınan metallerin büyük bir bölümünün demir hidroksit, demir hidroksisülfat ve aluminyum hidroksit mineralleri ile çökeldiğini ve taşındığını göstermiştir. Ayrıca, birleştirilmiş XRD ve SEM-EDS ölçümleri kil minerallerinin (başlıca klinoklor ve illit) ve metal (Zn ve Sr) içeren ikincil silikat fazlarının varlığını açığa çıkarmış ve AMD sistemlerindeki kil minerallerin duraylılığının metal (başlıca Fe, Al, Zn ve Sr) taşınımı, salınımı ve mobilitesindeki önemini ortaya koymuştur.

1. INTRODUCTION

Oxidation of the sulfur content of ore deposits results in the generation of acidic water bodies and an excess release of heavy metals, which is widely known as acidic mine drainage (AMD) (Schippers, 2004; Lottermoser, 2010). AMD has serious environmental impacts, affecting aquatic life and water quality. Due to the increased acidity, high heavy metal concentrations and ferric iron precipitation in hydroxide and hydrated forms, AMD disturbs the habitat of living organisms (Kelly, 1988; Gray, 1997). Likewise, acidophilic bacteria which are commonly associated with AMD like sulfur and/or iron oxidizing *Acidithiobacillus* and *Leptospirillum spp.* (Bosecker, 1997; Nordstrom and Southam, 1997; Sand et al., 2001; Rohwerder et al., 2003; Schippers, 2004) facilitate reactions that strongly affect the geochemical conditions of the environment, acting as a catalyzer (Bethke, 2008). Moreover, contaminated irrigation waters and heavy metal uptake from soil near AMD waters may result in toxic levels of heavy metals for vegetation, also affecting the human health. This is why, revealing every possible factor generating AMD and characterization of contaminated sites is crucial.

To our knowledge, this is the first study providing experimental data and focused on environmental assessment on the AMD problem of Küre VMS ore deposits. In the scope of characterizing the AMD formation in Küre; this study investigates the source and the possible chemical or biological mechanisms contributing to acid generation and heavy metal release via geochemical characterization of the ore, ore bearing rocks, waste effluent dam deposits and AMD contaminated or uncontaminated stream waters and sediments in the vicinity of the mining site.

1.1 Literature Review

To our knowledge, previous studies in the field, conducted by Asloğlu (1919), Nikitin (1925) and Kovenko (1944), consist of geology and mineralogy of Küre ore deposits and geochemical investigations on gossan and slags of ancient mining operations, as reported by Çağatay et al. (1980). Kovenko (1944) conducted further

geological and mineralogical studies on Küre ore deposits, on behalf of MTA. New improvements by Kovenko (1944) include 1:5000 scaled geological map, first reserve calculation of Aşıköy ore deposits, pointing to Aşıköy and Kızılsu gossan outcroppings after Bakibaba and implication of a hydrothermal metasomatic origin.

The first relatively detailed study was conducted by CENTO group in 1966, in the scope of a summer course on field mapping techniques (Bailey et al., 1966). Their studies included 1:10000 scaled geological map of the area, 1:1000 scaled geological and topographical map of the vicinity of Aşıköy open-cut mining site, and detailed geological, mineralogical and structural investigations on the ore deposits and lithological units. A side work of their summer course included some soil and sediment sampling and in-situ cold-extractable copper tests around the mining sites, which resulted in the first implications of potential Cu contamination (0,4-90 ppm) in Küre drainage system (James, 1966). Their results suggested that concentrations around gossan outcrops may be higher, as evident in the stream sediments (20 ppm Cu) around Aşıköy gossan. Moreover, James (1966) indicated that unidentified anomalies could be pointing to new mineralizations that were yet to be discovered.

Çağatay et al. (1980) investigated paragenesis of primary ore minerals and secondary minerals in the ore samples they collected from Bakibaba and Aşıköy mines, using their ore microscopy and chemical analysis. Their main goal was to estimate the economic value of Co and Au minerals, as those were evident in analyzed samples. Çağatay et al. (1980) reported about 0,3% Co and 2,48 g/ton Au content in the ore deposits and their economic value were determined to be exceeding the total value of copper reserves. However, bravoite forming a zoned structure with pyrite; linneite being disseminated as small particles in pyrite and chalcopyrite; and gold being present in along fracture planes and cleavages of pyrite, chalcopyrite and bornite, were reported to set back mineral processing studies and prevent production of those metals. After this report, MTA conducted several studies to enable extraction of Co, Au, Ag and Cu together (unpublished reports).

Güner (1980) studied geology, geochemistry and petrography of the Pontid chain mountains and the area around Küre copper deposits. 1:10000 scaled geological map of the area was prepared. According to Güner (1980), ore bodies are located in contact zones of black shales and basalts cut by main faults; and ore forming hydrothermal fluids found their way through faults or weak zones in basalts.

Ustaömer and Robertson (1994) proposed a model on the origin of Küre ophiolites, stating that they plot into marginal back-arc basin according to their geochemical data on basalt, clinopyroxene and chromite samples.

Çakır (1995) investigated the geology of Aşıköy-Toykondu massive sulfide deposits and listed the chain of events that may have formed the ores as following: i) formation in a back-arc marginal basin after an extensional process in Lias and following hydrothermal processes; ii) surfacing after a closing process in Dogger; and iii) remobilization due to granitic intrusions in Dogger. Çakır (1995) also indicated that, mineralization mechanism could have formed due to penetration of seawater to mid ocean ridge basalt (MORB), uprising of hydrothermal fluids due to convection currents and following sedimentation.

Koç et al. (1995) investigated the geology, geochemistry and geotectonic location of Küre ore deposits. Result indicated that Küre volcanites are tholeiitic basalts and back-arc formations deriving from hybrids of mantle originated magma with the continental crust. Koç et al. (1955) dated age of mineralization as Lias. Moreover, unlike the other studies stating that the deposit are Cyprus type, Koç et al. (1995) claimed the ore deposits to be Kieslager type.

Kuşçu and Erler (2002) studied the pyrite deformation structures on Küre VMS deposits, using microscopic investigations on the samples of Bakibaba, Aşıköy and Kızılsu mineralizations. They interpreted their findings of cataclastic, annealing and fracture filling deformation textures as progressive metamorphic deformation on the ore deposits.

Recent studies investigate different techniques for environmental-friendly and low-cost metal recovery from the pyritic chalcopyrite ore concentrate and massive ore of Küre (Arslan et al., 1995, 2003, 2004; Bulut et al., 2001a, 2001b; Kangal et al., 2001; Akçıl, 2002; Akçıl and Çiftçi, 2003; Akçıl et al., 2007; Perek and Arslan, 2010). Experimental results of those studies indicate feasible extraction of base metals via proposed methods that can be listed as ferric sulfate leaching, ferric chloride leaching, cupric chloride leaching, pressure leaching and bacterial leaching of the ore. However, regardless of the long mining history (Bailey et al., 1966); there is still no available data verifying the acid generation capacity of Küre copper deposits.

1.1.1 Copper bioleaching studies

Significance and mining activities of base metals, including copper, have dramatically increased science 1950's (Förstner, 1999). Among all copper-bearing ores, chalcopyrite ($CuFeS_2$) is the main source of copper production (Bevilaqua et al., 2004) with its widespread spatial distribution adding up to three fourth of the total copper reserves (Habashi, 1978; Third et al., 2002; Rohwerder et al., 2003; Córdoba et al., 2008). Conventional pyrometallurgical methods were used to recover copper from low-grade ores and ore concentrates, which were replaced by hydrometallurgical processes in time due to environmental concerns (Bosecker, 1997; Krebs et al., 1997). However, recalcitrant nature of chalcopyrite in hydrometallurgical processes (Dutrizac, 1978; Watling, 2006) led mining operations to apply low-cost and more environmental friendly methodologies (Olson et al., 2003). Therefore, reaction kinetics were enhanced by bacterial catalysis method that is called bioleaching (Norris and Barr, 1988), which has been used for this scope for over decades and is a current technology now (Rossi, 1990; Brierley and Brierley, 2001; Ehrlich, 2004).

Bioleaching is studied by several authors most currently for efficient and quick metal recovery from sulfidic ores and concentrates or solid wastes of industrial products (Li et al., 2013; Schippers et al., 2014; Lee and Pandey, 2012) using different leaching solutions, catalysts and oxidants with various initial redox and temperature conditions to enhance reaction rates (i.e. Feng et al., 2013; Dong et al., 2013a, 2013b, 2013c; Zhao et al., 2013a, 2013b; Bevilaqua et al., 2014). Adsorption characteristics of bacteria on mineral surfaces and its effect on bioleaching is also a common subject (i.e. Wang et al., 2012; Dong et al., 2013a, 2013b). Moreover, pre-adaptation of bacteria to the ore (i.e. Xia et al., 2008) and comparative leaching characteristics or synergistic relations between several acidophilic cultures were investigated (i.e. Stott et al., 2003; Akçıl et al., 2007). Nevertheless, there are only a few studies using bacterial oxidation of metal sulfides addressing to the role of bacteria in AMD related biogeochemical processes (i.e. Baker and Wilshire, 1970; Mielke et al., 2003; Balcı, 2010; Balcı et al., 2006, 2007, 2012; Thurston et al., 2010). Adding that, there are limited studies performed on actual ore samples (i.e. Dong et al., 2013a, 2013b; Mehta and Pandey, 2013), which is preventing the assessment of additional factors like the effect of gangue minerals on bioleaching (Li et al., 2013).

1.2 Purpose of Thesis

Like elsewhere, Turkey also have mining related AMD problem, which creates toxic conditions for the environment. There are well known and characterized AMD sites in Turkey, caused by coal or lignite mines like in Çanakkale (Sanliyuksel-Yucel and Baba, 2013) or lead-zinc mines in Balya (Aykol et al., 2003; Çelik-Balcı et al., 2014) and copper mines in Murgul (Akçay and Moon, 2004). Even though being one of the major and ancient copper mining area in Turkey, there is limited data on Küre, which might only be evaluated as a potential environmental contamination related to mining operations. CENTO group reported Cu contamination in river sediments around Küre (Bailey et al., 1966). Moreover, volcanogenic massive sulfide (VMS) deposits take the second place in the ranking made by Kwong (1993) on the potential of AMD generation (Lottermoser, 2010) and Küre ore deposits have already been identified as a possible AMD source on a potential risk map of MTA (Mineral Research & Exploration) in Turkey (www.mta.gov.tr). Despite there are bioleaching studies conducted with the ore concentrates of Küre on bacterial metal recovery (Akçıl and Çiftçi, 2003; Akçıl et al., 2007), the aim of the studies are limited to look for more economical and environmental friendly metal recovery from ore concentrates.

As emphasized in the literature review, Küre had only been a focal point of previous studies in terms of mining industry and economical geology. First objective of this study is to build up an initial database of multidisciplinary studies on the environmental impacts of mining activities around Küre VMS deposits. To fill the lack of information on today's field conditions, this study aims to geochemically characterize the AMD impacted or unaffected streams and determine the sources and possible mechanisms of heavy metal contamination, using geological, chemical and biological approaches. Moreover, to contribute to the future rehabilitation models, this study aims to reveal the fate of heavy metal in Küre groundwater and surface water drainages. Furthermore, this study aims to investigate the effects of dissolution of the lithological units of VMS deposit by AMD waters on drainage systems. Further objectives of this study can be listed as defining the limitations of well-known AMD prediction methods and integrating flask bioleaching studies to environmental assessments by combining long-term leaching results with chemical prediction tests.

1.3 Acid Mine Drainage

AMD is defined as a process, which results from the oxidation of sulfide minerals, causing the pH of the water drop to acidic levels (Lottermoser, 2010), which is the biggest environmental issue that the mining industry faces today. With considerable amounts of heavy metals released and great amounts of acid generated, aquatic environment is highly disturbed around mining sites (Kelly, 1988; Karadeniz, 2008; McLemore, 2008; Lottermoser, 2010).

Sulfur moiety of metal sulfides is chemically inert in their natural environment (Schippers and Sand, 1999; Schippers, 2004) but, during or after mining activities, metal sulfides are exposed to oxidation causing acid mine drainage (Schippers, 2004; Lottermoser, 2010). Bacteria also help the generation of AMD by biological oxidation of metal sulfides (Kelly, 1988; Schippers, 2004; Lottermoser, 2010), resulting in acidic and reddish colored drainage waters due to rich ferric iron content deriving from ferrous iron oxidation.

The main sources of AMD are metal sulfides (most commonly pyrite, pyrrhotite) of sulfidic ore deposits, along with other sulfur minerals and coals. AMD occurs where abandoned mines (Aykol et al., 2003), waste piles, tailing heaps and dams, open pit mines, underground workings, and ore stockyards get in contact with surface water, groundwater, lakes (Karadeniz, 2008; Lottermoser, 2010; Atabey, 2010; Paktunç, 1998) or other types of freshwater reservoirs (Kelly, 1988). Moreover, construction works may also cause AMD, as the weathered sulfidic material contacts with surface and groundwaters in deep excavations or road cuts (Paktunç, 1998; Lottermoser, 2010).

Due to resulting from various sources (metal sulfides, coal, etc.) mine waters can contain different types of dissolved ions, thus have different chemical characteristics. For instance, coal mine waters can be highly saline as a result of possible dissolution of chloride and sulfate salts. Wastes of metallurgical processes and extraction are other factors affecting the chemical composition of mine waters (Lottermoser, 2010).

There are other factors affecting the chemistry of AMD waters directly or indirectly. These can be defined as some processes affecting also each other. Microbial activity, precipitation and dissolution of secondary minerals, coprecipitation, adsorption and desorption, Eh-pH conditions, heavy metals, element cycling governing the source

material, pH buffering and turbidity (Lottermoser, 2010) are some of the main processes that may alter the AMD water chemistry.

AMD seriously affects the water quality by its characteristic low pH and heavy metal rich waters (Nordstrom and Alpers, 1999). Moreover aquatic environment is disturbed by the detrimental shifts in solution chemistry (McLemore, 2008) and new thriving organisms invading and controlling the habitat of the former indigenous microbial populations (Kelly, 1988; Gray, 1997; Kim et al., 2009). Among the new habitants of AMD contaminated environment, acidophilic iron and/or sulfur oxidizing *Acidithiobacillus* and *Leptosprillum* species hold the majority (Nordstrom and Southam, 1997; Baker and Banfield, 2003; Schippers, 2004). It should also be noted that acidophilic Archaea was also detected as dominant species of extremely acidic environments in some rare cases (i.e. Edwards et al., 2000).

1.3.1 Acid generating mechanisms

Acid generation is known to be a result of metal sulfide oxidation, which is a complex and widespread process that can be seen in a large variety of environments from fresh and marine water sediments, salt marshes and paddy soils (Luther et al., 2001), pyritic mine waste heaps and tailings (Schippers, 1998) to coal deposits. This large distribution of metal sulfide oxidation processes points out that they have such importance in global geochemical –especially sulfur- cycles. Metal sulfide oxidation processes control sulfur cycles, forming intermediate sulfur compounds (elemental sulfur, sulfite, sulfate, thiosulfate, polysulfide, polythionates), provided by thiosulfate and polysulfide mechanisms, while being controlled by the mineralogy of the metal sulfide and geochemistry (pH, Eh, presence of microorganisms, availability of molecular oxygen and other oxidizing agents) of the environment (Schippers, 2004). There are other factors affecting the metal oxidation like surface controlled processes (Becker et al., 2001), impurities and crystal structure related dislocations and stacking faults (Thomas et al., 2003).

The acid produced in AMD is a result of the exposure of sulfidic material to oxidizing conditions (Schippers, 2004; McLemore, 2008; Lottermoser, 2010). Being the most abundant metal sulfide on Earth's crust, pyrite oxidation is widely studied among other minerals (Luther, 1987; Moses et al., 1987; Nordstrom and Southam,

1997; Schippers et al., 2000; Schippers and Jørgensen, 2001; 2002; Schippers, 2004; Lottermoser, 2010).

Lottermoser (2010) summarized pyrite oxidation in terms of biotic and abiotic oxidation. Combined possible reactions pathways are presented below:

$$FeS_{2(s)} + 7/2\ O_{2(g)} + H_2O_{(l)} \longrightarrow Fe^{2+}_{(aq)} + 2\ SO_4^{2-} + 2\ H^+ + \text{energy} \quad \textbf{(1.1)}$$

$$4\ FeS_{2(s)} + 14\ O_{2(g)} + 4\ H_2O_{(l)} \longrightarrow 4\ FeSO_{4(aq)} + 4\ H_2SO_{4(aq)} + \text{energy} \quad \textbf{(1.2)}$$

$$4\ FeSO_{4(aq)} + O_{2(g)} + 2\ H_2SO_{4(aq)} \longrightarrow 2\ Fe_2(SO_4)_{3(aq)} + 2\ H_2O_{(l)} + \text{energy} \quad \textbf{(1.3)}$$

or,

$$Fe^{2+}_{(aq)} + ¼\ O_{2(g)} + H^+_{(aq)} \longrightarrow Fe^{3+}_{(aq)} + ½\ H_2O_{(l)} + \text{energy} \quad \textbf{(1.4)}$$

$$FeS_{2(s)} + 7\ Fe_2(SO_4)_{3(aq)} + 8\ H_2O_{(l)} \longrightarrow 15\ FeSO_{4(aq)} + 8\ H_2SO_{4(aq)} + \text{energy} \quad \textbf{(1.5)}$$

or,

$$FeS_{2(s)} + 14\ Fe^{3+}_{(aq)} + 8\ H_2O_{(l)} \longrightarrow 15\ Fe^{2+}_{(aq)} + 2\ SO_4^{2-} + 16\ H^+ + \text{energy} \quad \textbf{(1.6)}$$

Acid mine drainage resulted from the pyrite oxidation facilitates secondary ferric iron oxide, oxyhydroxide hydrates and hydroxysulfate precipitation, which is defined as “orange-hued flocs of ferric iron” and called as “ochre”, as the pH of the drainage starts to increase (Kelly, 1988; Lottermoser, 2010). Besides the floc formation, ferric iron salts may also promote the generation of suspended colloids or fine suspended precipitates due to increasing pH (Kelly, 1988). Ferric iron precipitation in the various forms mentioned above results in lower amounts of dissolved oxygen, which is necessary of aerobic organisms. Ochre precipitation resulted from pyrite oxidation is summarized in equations **(1.7)** and **(1.8)**.

$$Fe^{3+}_{(aq)} + 3\ H_2O_{(l)} \longrightarrow Fe(OH)_{3(s)} + 3\ H^+_{(aq)} \quad \textbf{(1.7)}$$

$$Fe^{3+}_{(aq)} + 2\ H_2O_{(l)} \longrightarrow FeOOH_{(s)} + 3\ H^+_{(aq)} \quad \textbf{(1.8)}$$

Acid generating pathways classified due to the metal sulfide’s solubility in acids. Numerous metal sulfides are soluble in acids (ZnS, PbS, CuFeS2, FeS, etc.), whereas a few are insoluble (FeS2, MoS2 and WS2) (Sand et al., 2001). Whether being acid soluble or acid insoluble, metal sulfides are oxidized in multiple steps, due to the number of electrons that have to be transferred to promote oxidation (Moses et al., 1987; Luther, 1987, 1990). Two different metal oxidation mechanisms have been introduced to literature as thiosulfate mechanism and polysulfide mechanism, which

are used to define acid generating pathways (Schippers and Sand, 1999; Sand et al., 2001).

1.3.1.1 Thiosulfate mechanism

Thiosulfate mechanism is used to explain acid-insoluble oxidation of metal sulfides, which consist of FeS_2 (pyrite), MoS_2 (molybdenite) and WS_2 (tungstenite) (Sand et al., 2001). The most distinctive property of acid insoluble metal sulfides is being resistant to proton attacks. This phenomenon can be explained by molecular orbital and valence bond theory, which suggests that electron bands are generated by the orbitals of single atoms or molecules, with different energy levels (Schippers, 2004; Luther, 1987).

Sulfur atom pairs of acid insoluble metal sulfides form nonbonding orbitals, so that metal atoms are the only source of valance orbitals of metal sulfides (Vaughan and Craig, 1978; Borg and Dienes, 1992). Therefore, bonding between the metal and sulfur has nothing to do with the valence bands of acid insoluble metal sulfides. This is why a strong oxidant like Fe(III) is required to brake the bonds between metal and sulfur, by multi-step electron transfers causing a cleavage of the bonds (Singer and Stumm, 1970; Sand et al., 2001).

Besides molecular oxygen, ferric iron acts as a strong oxidizing agent (Akçıl and Çiftçi, 2003). Between hydrated Fe^{3+} ions and the pyrite surface, σ-bonds take place that can promote an electron transfer from the sulfur content of pyrite to the Fe^{3+} ions (Luther, 1987). The most effective oxidizers for pyrite oxidation, Fe^{3+} ions, are produced by the oxidation of ferrous iron (Fe^{2+}) by molecular oxygen (Schippers, 2004). Fe^{3+} ions attack to the pyrite surface again, thus the bonds between Fe and S are cleaved (Luther, 1987). For anoxic conditions, Schippers and Jørgensen (2001) suggested MnO_2 as an oxidizing agent. As a result, molecular oxygen and other oxidants can be evaluated as the source of Fe (III) generation.

Due to being the most widespread metal sulfide on Earth, thiosulfate mechanism is generally explained by the step-wise oxidation of pyrite. The thiosulfate mechanism that will be presented below also represents tungsenite and molybdenite oxidation. Overall reactions of the oxidation of FeS_2 have been proposed by Schippers (2004), representing the thiosulfate mechanism:

$$FeS_2 + 6\,Fe^{3+} + 3\,H_2O \longrightarrow S_2O_3^{2-} + 7\,Fe^{2+} + 6\,H^+ \qquad \textbf{(1.9)}$$

$$S_2O_3^{2-} + 8\ Fe^{3+} + 5\ H_2O \longrightarrow 2\ SO_4^{2-} + 7\ Fe^{2+} + 10\ H^+ \quad \textbf{(1.10)}$$

The first attack of ferric iron and formation of thiosulfate is summarized by Luther (1987) by the following equation:

$$FeS_2 + 6\ [Fe(H_2O)_6]^{3+} + 9\ H_2O \longrightarrow S_2O_3^{2-} + 7\ [Fe(H_2O)_6]^{2+} + 6\ H^+ \quad \textbf{(1.11)}$$

With Fe (III) as an oxidizer, the dominant products were detected as sulfate, high amounts of elemental sulfur with low amounts of tetrathionate and pentathionate, at pH 2 (Schippers et al., 1996). The following equation shows thiosulfate oxidation and tetrathionate formation in the presence of molecular oxygen at pH 2.9 – 8.6 (Xu and Schoonen, 1995):

$$S_2O_3^{2-} + 2\ Fe^{3+} \longrightarrow S_4O_6^{2-} + 2\ Fe^{3+} \quad \textbf{(1.12)}$$

The degradation of tetrathionate is a more different process as it is favored by alkaline conditions and is nearly stable in acid solutions (Schippers et al., 1996). Tetrathionate degradation is followed by disulfane-monosulfonic acid, trithionate and again thiosulfate formation, completing a whole cycle and giving the thiosulfate mechanism its name (Schippers, 2004). Pentathionate, sulfite and elemental sulfur are also generated as side reactions, by disulfane-monosulfonic acid oxidation (Schippers et al., 1996).

Rest of the thiosulfate reaction pathway is given in order, as following:

$$S_4O_6^{2-} + H_2O \longrightarrow HS_3O_3^- + SO_4^{2-} + H^+ \quad \textbf{(1.13)}$$

$$S_3O_3^{2-} + 1.5\ O_2 \longrightarrow S_3O_6^{2-} \quad \textbf{(1.14)}$$

$$S_3O_3^{2-} + S_2O_3^{2-} + 0.5\ O_2 + 2\ H^+ \longrightarrow S_5O_6^{2-} + H_2O \quad \textbf{(1.15)}$$

$$S_3O_3^{2-} + S_4O_6^{2-} \longrightarrow S_2O_3^{2-} + S_5O_6^{2-} \quad \textbf{(1.16)}$$

$$4\ S_3O_3^{2-} \longrightarrow S_8 + 4\ SO_3^{2-} \quad \textbf{(1.17)}$$

$$S_3O_6^{2-} + H_2O \longrightarrow S_2O_3^{2-} + SO_4^{2-} + 2\ H^+ \quad \textbf{(1.18)}$$

1.3.1.2 Polysulfide mechanism

Polysulfide mechanism is used to explain acid soluble oxidation of metal sulfides, which consist of ZnS (sphalerite), PbS (galena), $CuFeS_2$ (chalcopyrite), FeS (troilite), Fe_7S_8 (pyrrhotite), MnS_2 (hauerite), As_2S_3 (orpiment), As_4S_4 (realgar) and many others (Sand et al., 2001). Contrarily to acid insoluble oxidation mechanisms, initial

oxidation of sulfur is not required for the cleavage of the bonds between the metal and the sulfur moiety in acid soluble oxidation mechanisms (Luther, 1987; Schippers, 2004).

Polysulfide mechanism also depends on the geochemical conditions of the environment. Elemental sulfur is the main product at low pH conditions (pH 2), when Fe(III) is used as an oxidizer (Dutrizac and McDonald, 1974) and also at nearly neutral pH, in the presence of MnO_2 (Schippers and Jørgensen, 2001).

Sulfite, thiosulfate, sulfate and non-elemental sulfur are the dominant products of aqueous sulfide oxidation in marine environments, in the presence of molecular oxygen (Zhang and Millero, 1993).

Schippers (2004) suggested a first step reaction of acid soluble metal sulfides' oxidation:

$$MS + 2\ H^+ \longrightarrow M^{2+} + H_2S \qquad \textbf{(1.19)}$$

Steudel (1996) proposed a reaction that can be evaluated as a second step of acid soluble metal sulfide oxidation mechanisms:

$$H_2S + Fe^{3+} \longrightarrow H_2S^{*+} + Fe^{2+} \qquad \textbf{(1.20)}$$

Schippers and Sand (1999) brought a new perspective to the H_2S^{*+} generation, by suggesting the following reaction, where MS stands for metal sulfide and M stands for metal:

$$MS + Fe^{3+} + 2\ H^+ \longrightarrow M^{2+} + H_2S^{*+} + Fe^{2+} \qquad \textbf{(1.21)}$$

Step-wise oxidation of acid soluble metal sulfides can be continued by following equations, acting as a chain (Schippers, 2004):

$$H_2S^{*+} + H_2O \longrightarrow H_3O^+ + HS^* \qquad \textbf{(1.22)}$$

$$2\ HS^* \longrightarrow HS_2^- + H^+ \qquad \textbf{(1.23)}$$

$$HS_2^- + HS^* \longrightarrow HS_2^* + HS^- \qquad \textbf{(1.24)}$$

In the presence of various oxidants like molecular oxygen and ferric iron (Zhang and Millero, 1993), elemental sulfur can be generated from polysulfides:

$$HS_9^- \longrightarrow HS^- + S_8 \qquad \textbf{(1.25)}$$

Schippers and Sand (1999) proposed an overall reaction set summarizing the acid soluble oxidation mechanism, which they have named as polysulfide mechanism:

$$MS + Fe^{3+} + H^{+} \longrightarrow M^{2+} + 0.5\ H_2S_n + Fe^{2+},\ (n \geq 2) \quad \textbf{(1.26)}$$

$$0.5\ H_2S_n + Fe^{3+} \longrightarrow 0.125\ S_8 + Fe^{2+} + H^{+} \quad \textbf{(1.27)}$$

$$0.125\ S_8 + 1.5\ O_2 + H_2O \longrightarrow SO_4^{2-} + 2\ H^{+} \quad \textbf{(1.28)}$$

Equation **(1.28)** is an example of biological oxidation and acid generation, as elemental sulfur is chemically inert. Some of the elemental sulfur may also be a source for thiosulfate formation, as in the following reaction (Schippers, 2004):

$$0.125\ S_8 + HSO_3^{-} \longrightarrow HS_2O_3^{-} \quad \textbf{(1.29)}$$

1.3.2 Role of microbial activity

Metal sulfide oxidation is generally known as bacterially catalyzed, which is known as bioleaching in acidic and oxic aquatic environments. Great majority of the bacteria playing an active role in metal sulfide oxidation consist of acidolphilic Fe(II) and S oxidizers (Baker and Banfield, 2003; Schippers, 2004). Among acidophilics, *Acidithiobacillus ferrooxidans* and *Acidithiobacillus thiooxidans* are strongly involved with metal sulfide oxidation processes (Nordstrom and Southam, 1997; Sand et al., 2001; Baker and Banfield, 2003; Schippers, 2004; Sand and Gehrke, 2006), with a considerable contribution of *Leptospirillum ferroxidans* (Sand et al., 2001; Rohwerder et al., 2003; Schippers, 2004). Moreover, achaea was also detected in extremely acidic envrionments (i.e. Edwards et al., 2000).

Conventionally, microbes were believed to mediate oxidation of sulfidic material by two elementary mechanisms as “direct” or “indirect” oxidation (Silverman and Ehrlich, 1964; Nordstrom and Southam, 1997). Indirect oxidation is described as the oxidation of free Fe(II) ions in the aqueous environment by bacteria and the attack of resulting Fe(III) ions to the mineral surface due to its qualifications as a strong oxidizer (Schhippers, 2004). Thus, the role of the bacteria is to produce an agent which in turn is capable of oxidizing and deteriorating surface of the metal sulfide (Ehrlich and Newman, 2009). Direct oxidation was believed to be a result of attachment of bacterial cells to sulfidic mineral surface and enzymes attacking to the mineral sulfide (Ehrlich, 1996; Sand et al., 2001). However, later studies on bio-oxidation mechanisms showed that the attachment of bacteria was due to

electrochemical forces promoted by EPS (Rohwerder et al., 2003) and oxidation was as a result of Fe(III) ions of EPS (Sand et al., 2001; Sand and Gehrke, 2006). Therefore, "direct oxidation mechanism" was outdated and left its place to "contact mechanism", which refers to the attachment of cells to the mineral surface (Tributsch, 2001), is now regarded as a subclass of indirect mechanism (Rawlings, 2002; Rohwerder et al., 2003). Another subclass of indirect mechanism is now used as "non-contact mechanism" (Tributsch, 2001), which represents bacterial production of Fe(III) ions previously described by others as indirect oxidation mechanism (Silverman and Ehrlich, 1964; Schippers and Sand, 1999; Sand et al., 2001; Schippers, 2004). There is also a side mechanism called "cooperative leaching" (Rojas-Chapana et al., 1997) that describes the bacteria attached to the sulfide mineral surface providing energy source for other cultures or communities by contact leaching (Tributsh, 2001).

1.3.3 Characterization and prediction of acid mine drainage

A complete understanding of predicting or revealing the environmental impacts of AMD in a site requires various steps of applications. As a first step, classifying the type of the ore deposit may give a preliminary idea on the possibility of AMD generation but, since the characteristics of AMD is site specific even among the same type of ore deposits, prediction studies should cover a comprehensive basis, starting with the geochemical and mineralogical characterization of the ore and related wastes (Paktunç, 1998). Initial investigations on the ore mineral and host rocks should include whole rock chemistry, mineral content and abundance and paragenetic relations among the ore minerals and gangues. As associated wall rocks and surrounding lithology have some chemical signatures on stream waters and sediments, geological investigations in the field have also a specific importance (Lottermoser, 2010). Those analyses provide data about the potential acid generating or neutralizing constituents in the waste material and the potential contamination that might be naturally occurring in the surrounding environment. Likewise, similar investigations on waste material of any phase would build up a case on potential anthropogenic contamination, related to the mining activities.

For a successful prediction or characterization, several laboratory experiments are used to simulate how those rocks affect contamination and AMD generation. Ores

and wastes are generally subjected to static tests like Acid-Base Accounting (ABA), Net Acid Production (NAP) and paste pH to assess acid generation and neutralization capacity of them, based on their extraction ability in different solvents and mostly their sulfur content as it is the source of sulphuric acid (Sobek et al., 1978; Duncan and Bruynesteyn, 1979; Caruccio et al., 1981; Lawrence et al., 1989; Brodie et al., 1991; Wong et al., 1998). Since oxidation of metal sulfides leading to AMD is mostly catalyzed by bacteria (Nordstrom and Southam, 1997; Schippers and Sand, 1999; Schippers, 2004), kinetic tests in the presence of different acidophiles under different simulated environmental conditions are performed, in order to elucidate the bacterial oxidation mechanisms and the role of bacteria in acid production and heavy metal release (i.e. Baker and Wilshire, 1970; Third et al., 2000; Stott et al., 2003; Akçıl and Çiftçi, 2003; Akçıl et al., 2007; Balcı et al., 2007, 2012; Zhao et al., 2013a, 2013b).

2. STUDY AREA

Küre is located 60 km north of the Kastamonu city center in Western Black Sea region, Northern Turkey, between the geographic coordinates 41°42' N / 33°42' E. Küre is surrounded by Doğanyurt and İnebolu at North, Ağlı and Azdavay at West, Seydiler at South and Devrekani at West, which are provinces and major settlement areas of Kastamonu. Transportation from İstanbul is provided by E-80 highway (586 km) and from Kastamonu (60 km) or İnebolu (30 km) is provided by Kastamonu-İnebolu main road, to Küre. Figure 2.1, which was plotted using ArcMap 10.1 of ArcGIS software, displays the location of the study area in Kastamonu and in northern Turkey.

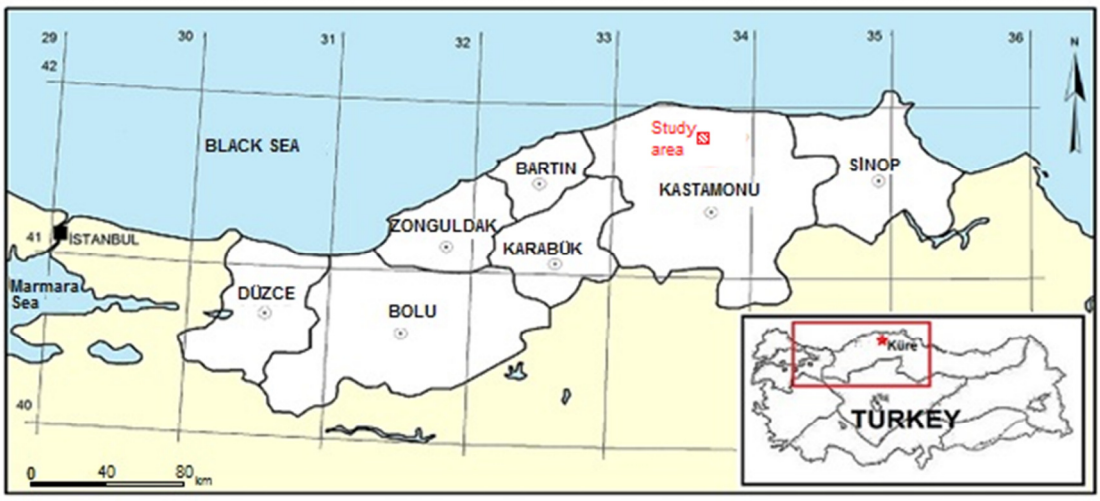


Figure 2.1 : Location map of the study area, marked (with a red square) on Western Black Sea Region (yellow plotted cities) map of Turkey. Units of the geological coordinates are in degrees. Map at the lower right (unscaled) displays the position of the base map (by a red rectangle), which is focused on Western Black Sea Region and Küre (by a red star) in Turkey.

2.1 Geographical Features

Küre (İsfendiyar) Mountains, which run parallel along the coastline, were formed during Alpine orogenesis, and constitute the main morphological feature of the area. Having high elevation summits, locally plateaus, canyons, steep slopes and deeply

carved valleys by high-energy rivers, region hosts a complicated morphology similar to Western Black Sea region topography, which is a part of Central Pontides tectonic unit. Most important morphological features of the Küre mountains include Harami Mountain (1559 m) at East, Sallama Mountain (1493 m) running through South, İmreşe Mountain (1265 m) at South, Dikmen Mountain (1514 m) at West, and Kurt Mountain (1250 m) and Göl Mountain (1379 m) at North (İbret, 2007).

Drainage network of the area had a great influence on the embodiment of the morphology. For instance, Karadonu Creek that is located in the West of the Küre city center, opened the approximately 300 m deep Ersizlerdere Canyon, which runs along 2 km through NW-SE direction between Karadonu and Ersizlerdere Villages. Located in the North of Küre city center, Küre Creek, which is one of the biggest tuributaries of Zarbana Creek, opened Karacehennemboğazı Canyon that has an approximate depth of >350m. Other surface waters that had a big influence on the regional morphology can be listed as İkizciler Creek, Uzunöz Creek and Karaman Creek. Those creeks, which are mostly shaping the dentritic drainage network of the area with their tributaries, have irregular flow rates that can be suddenly increased due to precipitation creating risk for floods.

Despite having a wide range of surface drainage network, Küre is poor in groundwater budget due to having mostly impermeable river beds, leading the precipitation travelling through the river system as runoff and discharges into Black Sea, resulting in poor levels of infiltration. Cold freshwater springs of Küre can sometimes be encountered in steep slopes, which are known as the origins of Zarbana Creek. Some of those springs are used as irrigation waters, that are collected by simple catchments and some of them cannot be used. There are also some rare karstic springs that are formed in Upper Jurassic – Lower Cretaceous İnaltı limestones (Bailey et al., 1966), associated with karstic gaps around Taşdelen region (İbret, 2007). Çatak Dam is the only dam around Küre, other than the waste effluent dam of mining operations.

Figure 2.2 illustrates the drainage network and topographical features of the study area, using 1:25000 scaled Kastamonu E31-a3 sheet topography map in ArcMap 10.1 in ArcGIS software, and using ASTER-GDEM images, which are products of NASA and METI.

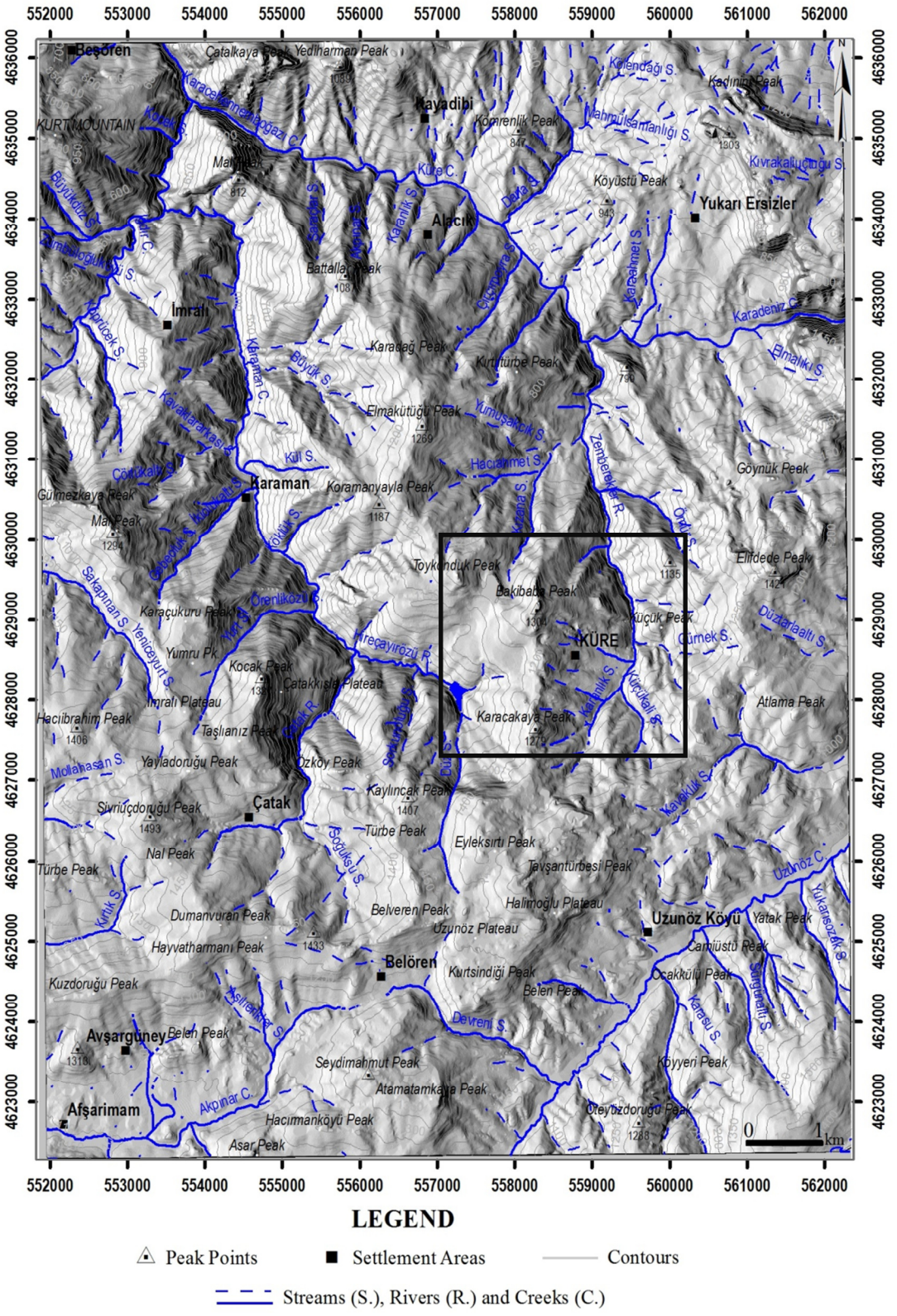


Figure 2.2 : Topography and drainage network map of Kastamonu E31-a3 sheet. Coordinates are in UTM (European Datum 1950 36N) and black rectangle defines the study area.

Climatologically, study area is under the influence of Black Sea climatic features, which suggest having precipitation every season and cold snowy winters at high

altitudes. However, Küre Mountains block the wet air mass coming from the coastline that leaves precipitation on higher altitudes. Resulting climatic features display a transition between continental climate and the Black Sea climate. Küre has the dampest season in the winter. In November, snow precipitation starts and in December, soil cover is supersaturated with water. Spring is generaly defined as the wettest season around Kastamonu. Lowest temperature is encountered in January. Snowy weather can even last until April. In May, due to increased temperature, soil starts to loose moisture because of evaporation. As typical of the climatic fetures of the Black Sea region, Küre also receives summer rains. However, July is the hottest and driest month of the area and due to lost moist content of soil; semi-arid conditions are reached in August. The above-described period between May and September is known as warm term around Küre (İbret, 2007). Due to suitable climatic conditions, area is mostly covered by pine, fir and hornbeam forests, providing a great habitat for wild life and regional ecology.

Küre district of the Kastamonu province is a preferred settlement area since the Paleolithic times, due to its suitable geographic environmental conditions. One of the main reasons that Küre was preferred among other distrticts was the copper mines in the area (Güner, 1980). The first population records of the area heads back to Ottoman Empire, stating 3581 locals used to live in Küre in 1478 (İbret, 2007). According to the most recent data obtained from Kastamonu Governorship's official website (http://www.kastamonu.gov.tr/sayfa.asp?id=3), Küre has a population of 6588 in 2014.

2.2 Geological and Tectonic Setting

Geology of the area around Küre first took interest for evaluation of the VMS deposits (Nikitin, 1926; Kovenko, 1944; Pehlivanoğlu, 1985). Later on, new geological maps were plotted (Bailey et al., 1966) and along with economic geology of the ore deposits (Çağatay et al., 1980), the focal point became a closer look to the origin of stratigraphic units (Güner, 1980). Moreover, the strategic tectonic location of the area led to debates on the Paleotethys Ocean, which resulted in contradicting models on the origin of the Triassic ophiolitic Küre complex (Yılmaz and Boztuğ, 1986; Ustaömer and Robertson, 1994; Okay et al., 2006). Küre is located in the area between the İzmir-Ankara suture and Black Sea, which corresponds to the central

part of the Pontides mountain chain (Okay et al., 2006; 2014). The stratigraphic units of Central Pontides around Küre vary from a Triassic ophiolitic complex with deep-sea sediments and ultramafic rocks with basaltic lava flows (Boztuğ, 1992) locally cut by Middle Jurassic granitoids (Boztuğ et al., 1984; Yılmaz and Boztuğ, 1986) to the Upper Jurassic reddish conglomerate bed (Ustaömer and Robertson, 1994), Upper Jurassic – Lower Cretaceous limestones and Lower Cretaceous turbidite sequence (Okay et al., 2014). Geological map and the crossection in Figure 2.3 displays the distribution and relationship of geological formations around Küre, which was published by Okay et al. (2014).

The oldest stratigraphic unit which covers a wide range in Küre is called the Akgöl Formation (Ketin and Gümüş, 1962), which is also called the Küre Complex (Ustaömer and Robertson, 1994; Boztuğ et al., 1995; Okay et al., 2006). The Triassic basement of the Küre Complex is formed of ultramafic rocks (wherlite, serpentinized ultramafics and serpentinites) at the lower levels, having tectonic contacts with massive and pillow lavas, and lava breccias at the top (Ustaömer and Robertson, 1994; Boztuğ et al., 1995; Çakır, 1995; Koç et al., 1995). Also known as the Küre Ophiolites (Boztuğ, 1992; Güner, 1980), this unit have some sheeted dykes, dacitic and gabrroic intrusive rocks and locally intruded by the Karaman Pluton, Ağlı Porphry, and Sallamandağ members (Okay et al., 2014) of the Jurassic Kastamonu granitoid belt (Boztuğ et al., 1984). Deep-sea sediments that are also known as the Börümce Formation depositionally cover Küre ophiolites, which consist of folded and well bedded gray- dark gray sand stones or greywackes and black shales that are highly deformed, having locally interbedded limestones (Ketin and Gümüş, 1963; Bailey et al., 1966; Güner, 1980). Along the contact zones of black shales and pillow lavas, Cyprus-type Küre VMS ores are localized via mineral rich hydrothermal fluids travelling through fault cracks and depositing the ores (Bailey et al., 1966; Güner, 1980; Ustaömer and Robertson, 1994; Çakır, 1995; Koç et al., 1995; Kuşçu and Erler, 2002). A further hypothesis was suggested on the formation of the massive sulfides by Çakır (1995), stating the generation of hydrothermal fluids due to sea water-basalt interaction that travel through cracks and post-depositional remobilization due to Dogger aged intrusions.

Akgöl Formation is unconformably overlain by the conglomerates, limestones and flysch sequence of the Yaralıgöz Group. Bürnük Formation (Ketin and Gümüş,

1962) builds up the Upper Jurassic (Altun et al., 1990) reddish conglomerate, conglomeratic sandstone and locally interbedded limestone basement.

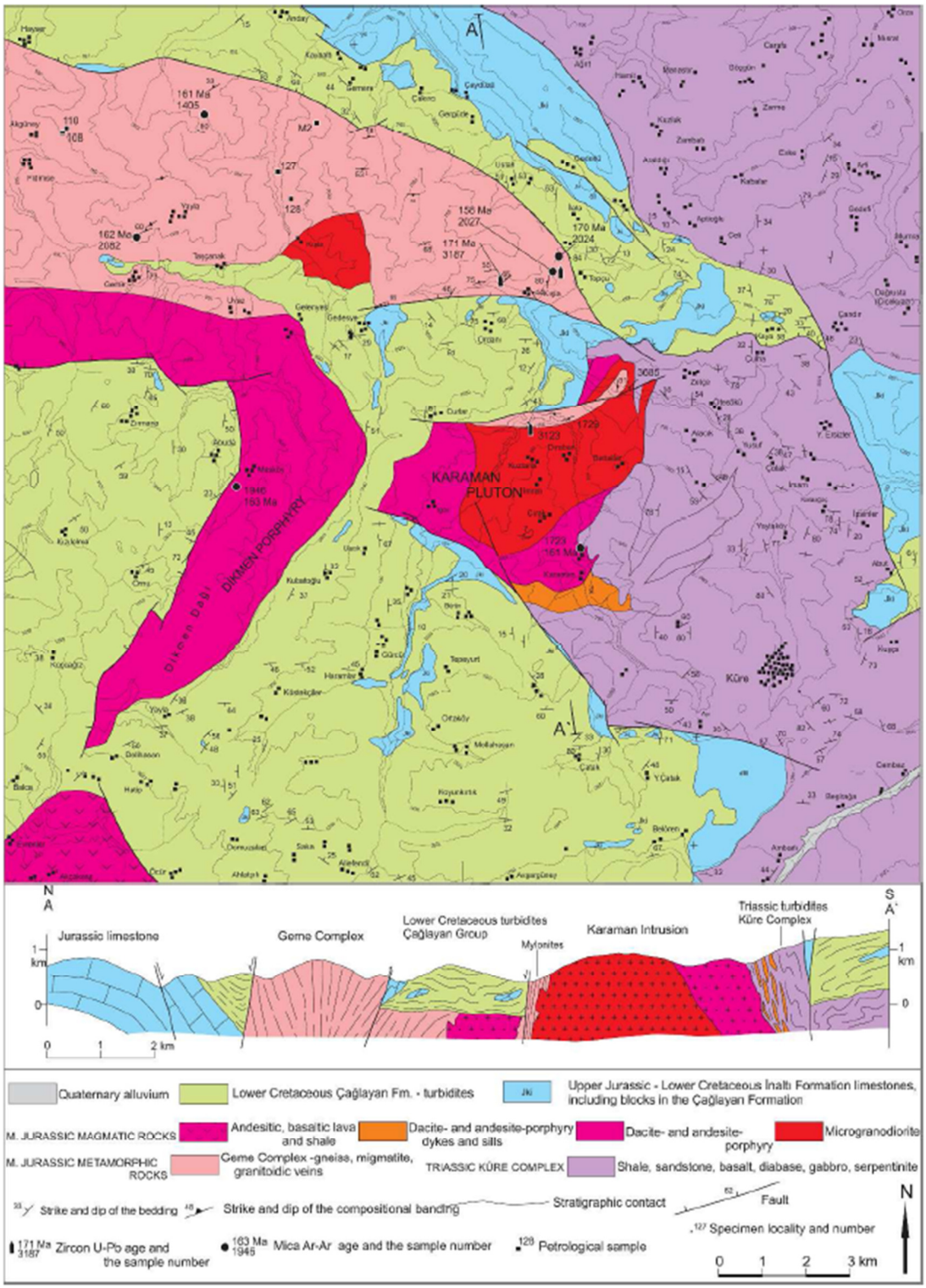


Figure 2.3 : General geology map and geological cross-section of the area around Küre (in Okay et al., 2014).

Upper Jurassic-Lower Cretaceous limestones are named as İnaltı Formation (Ketin and Gümüş, 1962), which unconformably overlays the underlying units of the Central Pontides (Tüysüz, 1990) or have transitions. İnaltı limestones that are rich in fossil content (foraminifera and algae) mostly massive around Küre displaying wide slickensides but, also layers and karstic voids can be observed (Bailey et al., 1966; Güner, 1980). Upper part of the Yaralıgöz Group that unconformably overlies the shallow marine limestones, consists of the Lower Cretaceous Çağlayan Formation flysch sequence which is also called as Ulus Formation (Tüysüz, 1999; Okay et al., 2006). This upper flysch of 2000-3000 m thickness displays a sequence of dark colored shales interbedded with brown-gray turbiditic thin to medium bedded turbiditic sandstones (Okay et al., 2006). Locally green-gray colored siltstone layers and sandstones with paleocurrent structures (flute casts, groove marks), fault grooves and thick layers can be observed.

In the study area covering 12 km^2 around Küre city center and the mining sites, ophiolitic Küre Complex is widely distributed. İnaltı Limestones and Çağlayan Formation are located in close proximity at the North, South and West of the study area. In-situ geological observations related to those formations are described in Chapter 4.1 supported with location photograps.

2.3 Mining Operations on the Study Area

Study area covers a 12 km^2 area in the vicinity of the mining operations in Küre, which have been providing a living for most of the locals for a long time. History of mining on VMS ore deposits of the region heads back to Greek or Roman occupation (Kovenko, 1944), which later came under the Ottoman Empire's control (Güner, 1980). The oldest mine that was also operated by several other countries via tunnels (Figure 2.4) is Bakibaba, which was reported to have 1,7 million tons of 1-2,5% copper in sum, back in time (Bailey et al., 1966). Ore deposits of Bakibaba was also reported to be containing 3,4% Cu of 1,5 million tons reserve (Demirbaş and Ağaoğlu, 1980) and the production was reported to be 90000 tons per year at grade of 6% Cu. Another important ore deposit of Küre is Aşıköy ore body, in which annual production was reported to be 155000 tons of ore containing 3% Cu (Güner, 1980). More recently, open-pit and underground mines of Aşıköy was believed to contain 1,61-2,73% Cu bearing ore with 10,23 million tons of proved reserve in total.

There are also Toykondu and Kızılsu mineralizations at northwest and south of Aşıköy, which were reported to have 175954 tons of ore containing 4,03% Cu (Çakır, 1995) and just a relatively small ore body which was believed to have 9% Cu (Bailey et al., 1966), respectively. Küre mining site was claimed by MTA in 1939, started to be operated by the name Eti Bakır A.Ş. and being operated by Cengiz Holding since 2004.



Figure 2.4 : Entrance to ancient underground adits of Küre copper mines.

Higher grade ores of those Cyprus type copper deposits are observed as massive sulfide bodies in shape of lenses of pyrite and chalcopyrite at higher levels, which can be vein or stockwork type at lower elevations, whereas lower grade ores are disseminated in pillow lava (Kuşçu and Erler, 2002). Main ore minerals are chalcopyrite and pyrite, along with lower amounts of marcacite, sphalerite, covellite, bravoite, linneite and trace amounts of hematite, chromite, rutile, anatase, chalcosite, magnetite, pyrrhotite, bornite and gold (Çağatay et al., 1980).

Currently, only underground tunnels of Aşıköy and Bakibaba are being exploited by Cengiz Holding for massive pyritic chalcopyrtite and Aşıköy is about to be run short. Ores are converted into concentrates containing 17% Cu and wastes are deposited in a waste effluent dam. Approximate annual production is 110000 metric tons of copper concentrate and 400000 metric tons of pyrite concentrate. Open-pit mine of Aşıköy is covered with excavated earth and open-pit mine of Bakibaba is left for further applications besides the Gossan outcropping nearby which is currently being processed. Figure 2.5 illustrates different locations around Küre mining operations.



Figure 2.5 : General views from the Küre mining sites: (a) Bakibaba open-cut mine (inactive). (b) Gossan outcrop near Bakibaba open-cut mine. (c) Waste effluent dam. (d) New tunnel boring operation at 512 m elevation in Bakibaba underground mining tunnels. (e) Ancient slag heaps. (f) Processed product storage area.

Even though, only waste dump areas were specified as the waste effluent dam or the ancient slag heap dumping places; field exploration of this study revealed mining wastes dumped from the slopes of Karanlık Stream (Figure 2.6a) and Zemberekler River (Figure 2.6b). Karanlık Stream displays characteristic AMD colors (yellow, orange, red) both in water and precipitates; whereas, Zemberekler River is greenish, pointing to copper contamination also considering its flow path starting from the underground mining site and taking in account the previous reports of the CENTO group (Bailey et al., 1966; James, 1966).



Figure 2.6 : Waste dumping areas in the field (black arrows represent flow directions). (a) Ancient slags and relatively recent mining and gossan waste heaps dumped on the slopes of AMD impacted Karanlık Stream (location AMD-5 in Figure 3.1). (b) Mining waste, core and core case dumping into green colored Zemberekler River (location PRW in Figure 3.1).

3. MATERIALS AND METHODS

In order to fulfill the objectives of this study, comprehensive field and laboratory studies were carried out. This chapter describes materials and methods used in the study in detail.

3.1 Field Studies

The study area is located in the 1:25000 scaled topographical map of Kastamonu E31-a3 sheet, which covers the province of Küre and the close vicinity. Sampling and field investigations were mostly concentrated in a 12 km^2 area around the ETİBAKIR Aşıköy and Bakibaba mining operations (see Figure 2.2).

3.1.1 Field exploration and geological investigations

Geological investigations were mostly carried out on the roadside outcrops of the section of Kastamonu-İnebolu main road and some crossroads, located in or around the Kastamonu E31-a3 sheet. Considering the field studies mostly aimed at geochemical sampling, geological investigations were only superficial, which consisted of basically defining and photographing the lithological units on the way to the mining sites and collecting hand specimens for further analyses in case for future applications. Outcrop investigations with GPS locations were used to check the accuracy of previous lithology maps of the area. Moreover, by overlapping existing maps with georeferenced Google Earth images combined with our GPS locations, a new digital lithological map was created using ArcMap 10.1 (ArcGIS), which contributed to the literature as being the first UTM coordinated 1:25000 scaled lithology map of the area. Streams were plotted in colors to take attention to the variety of lithological units that they are flowing through. Results of geological investigations are presented in Chapter 4.1.

Field exploration studies consisted of the observations around the ETİBAKIR mining operation site, in order to obtain information about current operations and detect any mining related environmental problems, which are described in Chapter 2.3.

3.1.2 Sampling and in-situ applications

Two years of sampling were carried out in the summer period, each having diverse goals regarding the characterization of Küre AMD environment. Figure 3.1 shows the sampling locations, plotted on the 3D hill-shade model (ASTER-GDEM data) used for topography mapping using ArcGIS (as described in Chapter 2).

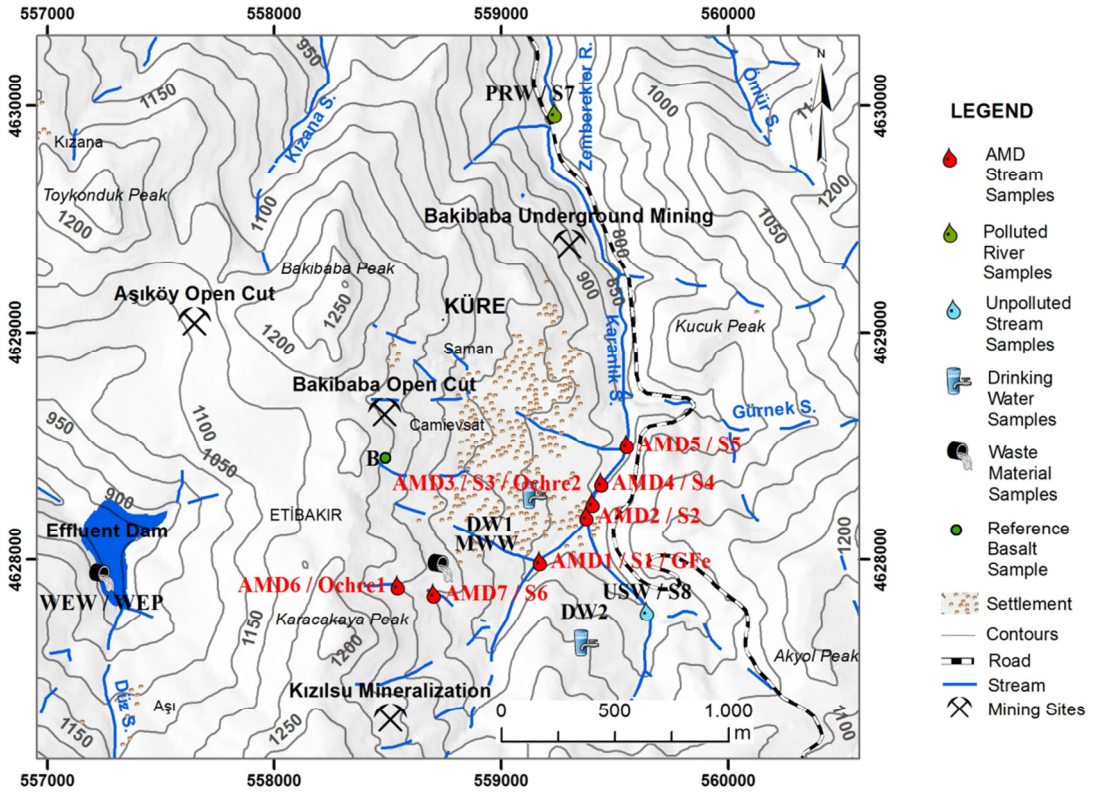


Figure 3.1 : Sampling location map plotted on the topography model (Coordinate system (UTM): European Datum 1950 36N).

During the first field study in in July-2013; massive pyritic copper ore (n=1; O), ore bearing wall rocks (n=3; OBR1-3; basalts and serpentinized basalts with chalcopyrite, pyrite, magnetite and specularite content) and leakage waters from the adit walls (n=5; GW1-5; groundwaters) were sampled from different elevation levels (between 780-512 m above sea level) of Bakibaba underground mining tunnels (Figure 3.2d,e). Water (n=1; WEW) and precipitate (n=1; WEP) (flotation tailing) samples were collected from the effluent dam as waste materials, where mining wastes and flotation effluents are being stored currently (Figure 3.2f), within the

open-cut mining area. Basalt sample (B) was collected to represent surface basalts from an outcrop near the road entering to Bakibaba open-cut mining site. A reddish-brown (Karanlık Stream) (Figure 3.2a,b) and a greenish river (Zemberekler River) (Figure 3.2c) were discovered and exploratory samples were taken from the water (n=3; SWE1-3) and stream-bed sediments (n=3; SE1-3).



Figure 3.2 : Sampling and in-situ measurement locationts of 2013 field study: (a) pH measurements on Karanlık Stream (SWE-1 or AMD-2). (b) Water sampling from Karanlık Stream and filtering (SWE-2 or AMD-7). (c) Sediment sampling from Zemberekler River (SWE-3 or PRW). (d) Water sampling from boreholes (GW) in Bakibaba underground mining tunnels. (e) Water sampling from sidewall leakages (GW) in Bakibaba underground mining tunnels. (f) Illustration of effluent input to the waste dam by piping system and WEW sampling location.

Second sampling campaign was carried out in June-2014, which was arranged for characterizing AMD impacted or uncontaminated streams and drinking water sources. Water (n=5; AMD1-5), sediment (n=5; S1-5) and ochre (Ochre2) and ochre coated gravel (n=1; GFe) samples were taken along the AMD impacted Karanlık Stream. Another AMD impacted stream (unnamed) flowing downslope in a close proximity to open-cut mining facilities, which probably drains through mineralization, was located for two water (AMD6-7), sediment (S6) and iron oxy/hydroxide rich ochre (Ochre1) samples (Figure 3.3a). Moreover, at the same location, municipal waste water (MWW) that had greenish color and looked like contaminated with detergent-like chemicals was sampled, because of its mixing with the acidic drainage (Figure 3.3b). A water (PRW) and sediment (S7) sample was taken from heavy-metal polluted Zemberekler River. A water (USW) and sediment (S8) sample was taken from Küçükali Stream, which was relatively un-contaminated (colorless water with no visible turbidity) and two fountain waters (DW1: Müderris Çeşmesi; DW-2: Halil İbrahim Kes Hayratı) which are used for drinking and irrigation.



Figure 3.3 : In-situ pH measurements of the unnamed mine drainage (black arrows point to flow directions): (a) AMD-6. (b) AMD-7, just above the mixing zone with MWW.

All waters were sampled in clean HDPE bottles that were rinsed with the sample and solid samples were kept in two layers of zip-locked plastic sampling bags, minimizing air contact as much as possible. Water samples were taken in duplicate, one being un-processed and one being filtered in-situ through 0,2 µm membrane or syringe tip Sartorius filters using Nagel Bottle or syringes and acidified with 1/10 diluted Merck research-grade HNO_3. Figure 3.4 illustrates sampling locations and Figure 3.5 illustrates in-situ applications like pH measurements and filtering.



Figure 3.4 : 2014 field geochemistry locations (black arrows point to flow directions): (a) Uncontaminated Küçükali Stream (USW). (b) Section of Karanlık Stream (AMD-1) before mixing with Küçükali Stream. (c) General view from Karanlık Stream (AMD-4). (d) Ochre sample (Ochre2) collection (AMD-4) from Karanlık Stream.

In-situ pH measurements were made with WTW 3110 portable pH meter using SenTix 41 probe, at each sampling location. Prior to measurements at every different stream or water body, probe was calibrated with pH 4.01, pH 7 and pH 9.12 standards.

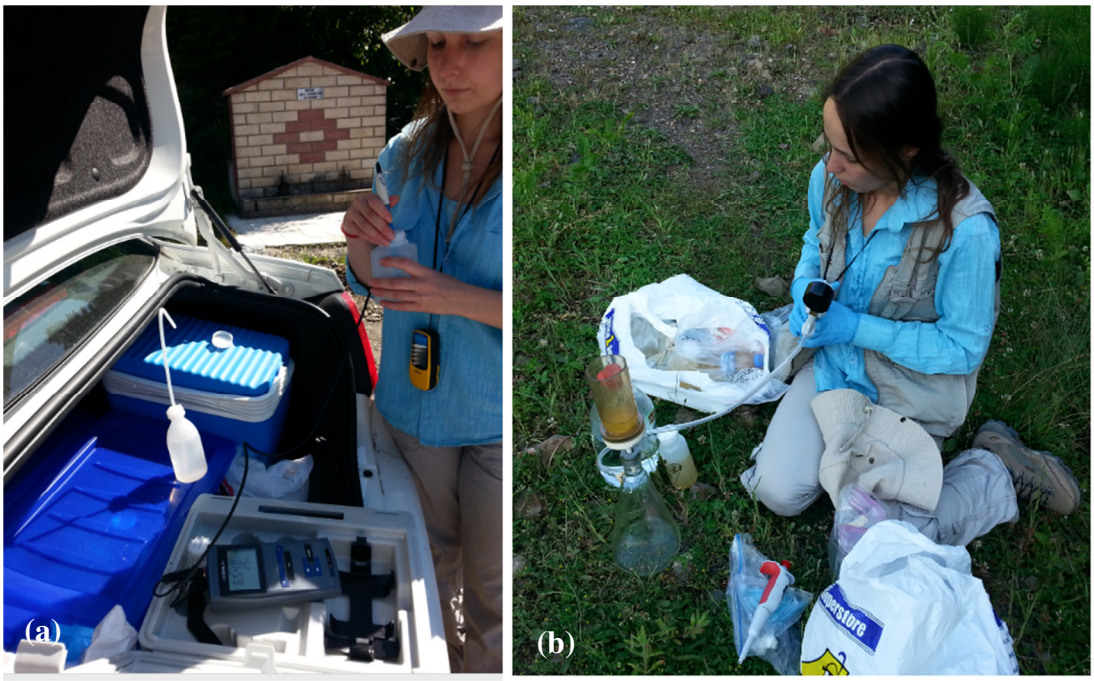


Figure 3.5 : In-situ geochemical applications of 2014 field trip: (a) Fountain (drinking) water (DW) sampling and pH measurement. (b) In-situ water filtering with Nagel bottle.

All samples were kept in portable cold case during transportation to the laboratory. Water samples were kept at +4^{o}C and sediment samples were kept at -20^{o}C for further analysis at the laboratory.

3.2 Laboratory Studies

Küre VMS deposits and surrounding aquatic environment (AMD or uncontaminated drainages) were characterized using geochemical and mineralogical laboratory techniques.

3.2.1 Water analyses

Filtered and acidified water samples were analyzed with inductively coupled plasma-mass spectrometry (ICP-MS) for their metal content (by MEİTAM; Mersin University, Advanced Technology Education Research and Application Center). Sulfate and ferrous iron and total iron measurements of the water samples were made

with HACH Lange DR 2800 Spectrophotometry (Figure 3.6), using powder pillow reagents with SulfaVer 4; 1, 10-Pheanthroline and FerroVer methods respectively. Instrument was auto-calibrated after every startup. Ferric iron values were calculated via deducting ferrous iron values from ferrover iron results. Eh and pH values were measured with WTW Multi 9310 bench-top multi-parameter instrument using the probes SenTix ORP 900 and SenTix 940 respectively. EC values of the waters were analyzed with Crison CM 35 conductivity-meter, using the Pt 1000 sensor probe 56 00. Eh, pH and EC-meters were calibrated prior to first use and every week, following manufacturers' instructions.

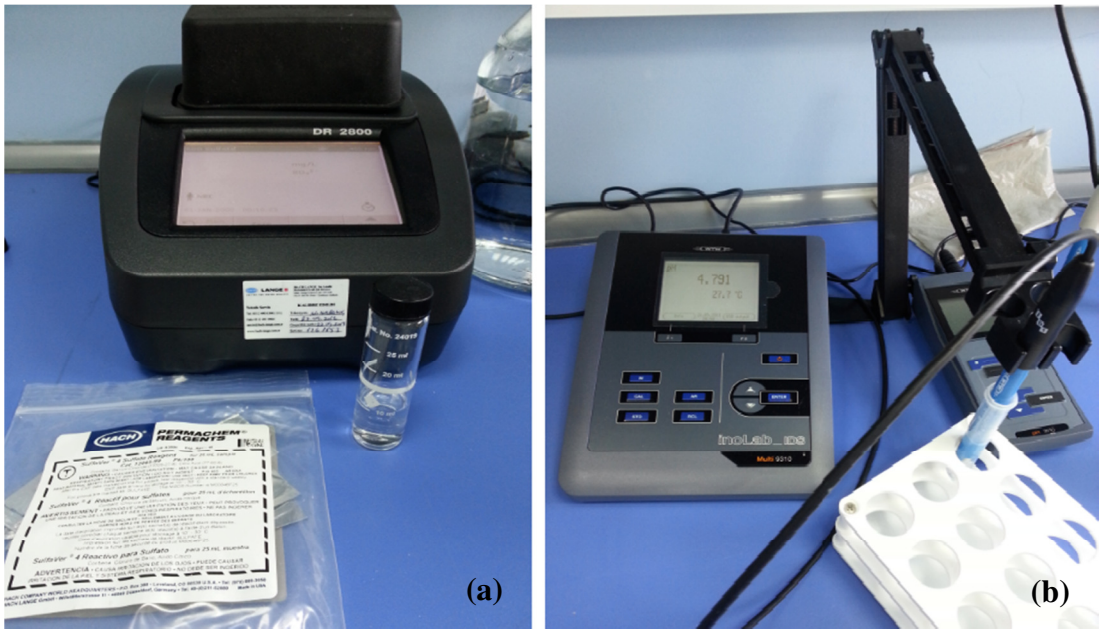


Figure 3.6 : Examples from water chemistry analyses: (a) Spectrophotometry. (b) Laboratory pH measurements.

3.2.2 Solid phase analyses

Sediment, gravel and iron oxy/hydroxide samples were dried at 30^{o}C for sample preparation. Iron coating over gravels were collected using a clean brush. All samples were sieved through 1 mm mesh opening and samples < 1 mm grain size were grinded and collected for analysis. Ore and ore bearing rock samples were crushed and grinded to obtain 45 µm grain size. Polished slides were prepared (by Geology Thin Section Laboratory of ITU) from the ore bearing rocks and investigated with ore microscopy.

Whole rock chemistry of selected sediment, ore and ore bearing rock samples were analyzed with X-ray fluorescence (XRF; by X-Ray Laboratory of ITU Metallurgical

& Materials Engineering). Mineralogical compositions were detected using a Bruker D8 Advance X-ray Diffraction (XRD) instrument (Figure 3.7a) between 2 and 70^{o} theta angles with Cu target (X-Ray Laboratory of ITU Faculty of Mines). Evaluations of detected peaks, background corrections and x/y displacements of diffractograms were made using Diffrac Suite EVA software. Polished slides were investigated with ore microscopy using a Nikon LV100 ore microscope. Additionally, collected iron dusts over gravels and iron oxy/hydroxide rich sediments were analyzed with scanning electron microscope (SEM) (Figure 3.7b) coupled with an Energy Dispersive X-ray Spectroscopy (EDS) instrument (by Boğaziçi University Advanced Technologies R&D Center).

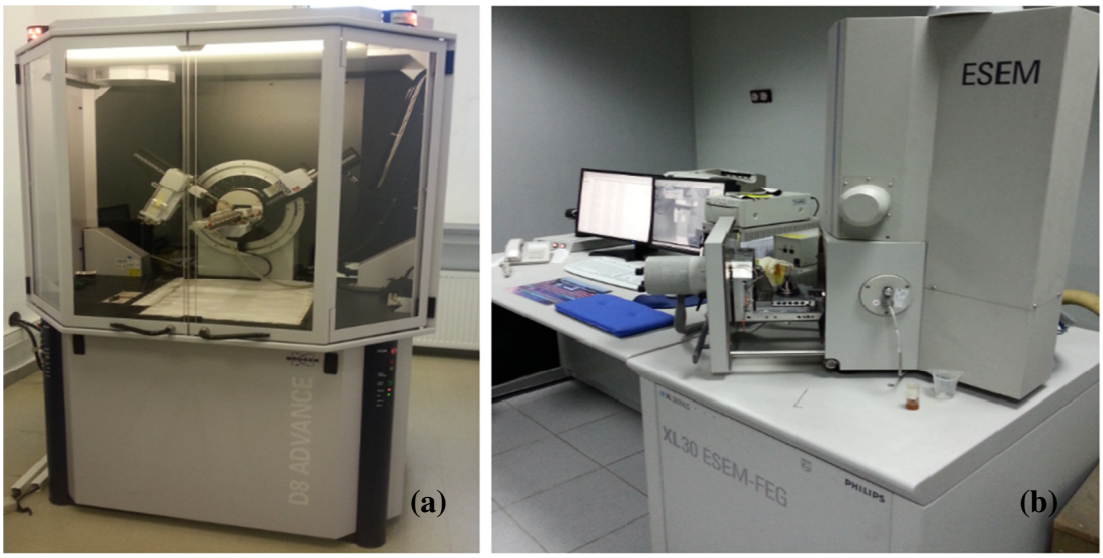


Figure 3.7 : Examples of instrumentations used for geochemical and mineralogical characterization of the solid phases: (a) Bruker D8 XRD instrument. (b) Philips XL30 ESEM-FEG SEM instrument coupled with EDS.

3.2.3 Mixing zone chemistry simulation titrations

Titration experiments were conducted on the stream waters taken from three different locations using three different titrants, in order to have insights on how the water chemistry changes on the mixing zones or after the precipitation of oxy/hydroxide forms of heavy metals. 150 ml of water sample from the Karanlık Stream (AMD-1) was titrated with 95 ml of the neutral water sample of Küçükali Stream (USW) for 3 hours and 40 minutes, in order to simulate their mixing (Figure 3.8a). Moreover, in order to simulate mixing with other contaminant input to AMD waters, 150 ml of AMD water sample (AMD-7) was titrated with 50 ml of the waste seepage sample (MWW) for 3 hours (Figure 3.8a). Furthermore, 400 ml of the heavy metal-rich

Karanlık Stream AMD water (AMD-1) was titrated with 0,1M NaOH (prepared with ultrapure water and MERCK NaOH pellets) for 2 hours and 30 minutes, in order simulate the fate of metals during secondary mineral precipitation (Figure 3.8b). During all of the titrations, pH was monitored (WTW Multi 9310) and experiments were ended between the pH ranges that may represent the AMD water pH values in the field. Resulting liquid media were filtered with 0,2 µm Sartorius filters using Nagel Bottle and acidified with 1/10 diluted Merck research-grade HNO_3. Filtered samples (AMD-1+USW, AMD-7+MWW and AMD-1+NaOH, respectively) were analyzed with ICP-MS for their metal concentrations (by MEİTAM).

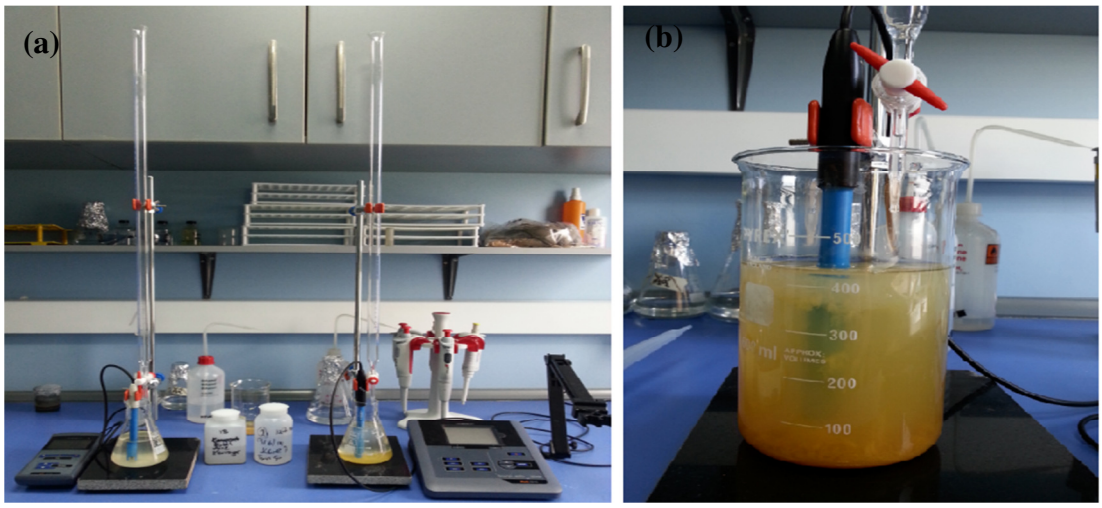


Figure 3.8 : Mixing zone chemistry simulations: (a) Titration experiments (AMD-7+MWW, AMD-1+USW). (b) Freshly forming precipitates from NaOH titration experiment (AMD-1+NaOH).

3.2.4 Geochemical static AMD prediction tests

Ore (O), ore bearing rocks (OBR1, OBR2, OBR3), waste effluent dam precipitate (WEP) and the representative basalt sample (B) of various grain sizes were solubilized in different solvents (ultrapure water or research grade Merck chemicals) and their capacity for acid generation or neutralization were investigated using different procedures. Volume and molarity or normality of acids and/or bases used in the experiments are presented in Table 3.1 and formulas used for calculations are listed in Table 3.2.

3.2.4.1 Paste pH

20 g of all samples with < 1 mm grain size were put in different beakers with 100 ml volume. Ultrapure water was added to obtain 100% w/vol ratio (pulp density) and

mixed with a glass stirrer (Sobek et al., 1978; Page et al., 1982). Eh, pH, EC, salinity and temperature values were frequently monitored for three weeks. After each measurement, mixtures were stirred with the glass stirrer and beakers were sealed with Parafilm M bands (Figure 3.9).



Figure 3.9 : Illustration of paste pH experiments.

3.2.4.2 Initial neutralization potential

Initial neutralization potential test (INP) uses Lapakko (1994) modified procedure of the British Columbia Research Initial Test (Duncan and Walden 1975; Bruynesteyn and Hackl 1984). 10 g of samples with < 45 µm grain size were mixed with 100 ml ultrapure water (10% pulp density) in 400 ml beakers, using a magnetic stirrer for 15 minutes (Figure 3.10a). After the settlement of grains, samples were back-titrated with 1N H_2SO_4 to pH 6 (Bruynesteyn and Hackl, 1984; Lapakko, 1994) (Figure 3.10b).

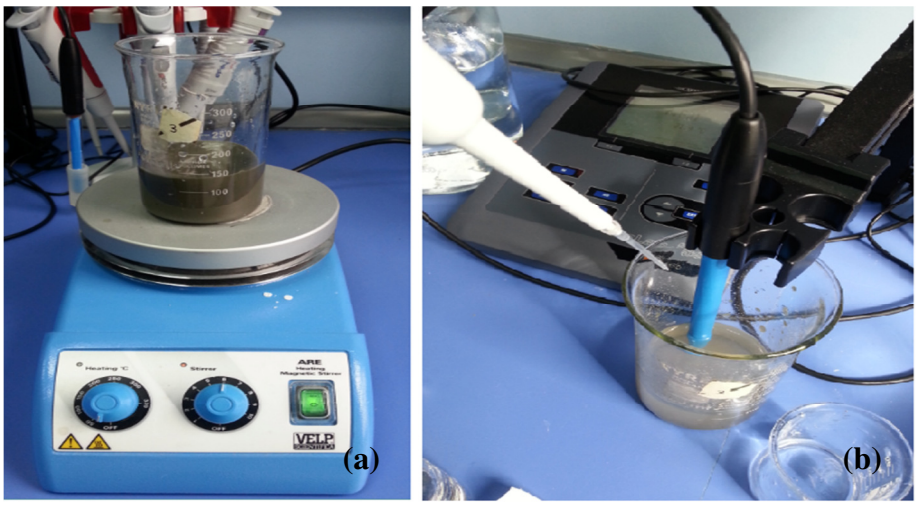


Figure 3.10 : Illustration of INP experiments: (a) Sample stirring using magnetic stirrer. (b) Back titration of the experiment.

3.2.4.3 Standard acid-base accounting

Standard acid-base accounting (SABA) test involves initial treatment of samples of 250 µm grain size with 25% HCl solution in order to determine the volume and molarity of HCl to be used in the accounting for each sample, using the visible fizz intensities of samples. After the fizz rating (Figure 3.11a), 2 g of samples were placed into 250 ml flasks, treated with HCl solution of determined qualifications and placed into pre-heated water bath at 85°C until reactions were completed, for at least two hours (Figure 3.11b). Pure water was added to obtain a total volume of 125 ml and experiments were kept in water bath for another minute. After heated-acid extraction, flasks were sealed and left for cooling and then, titrated with NaOH of the same molarity as the acid, until a final pH of 7 was reached (Sobek et al., 1978; MEND, 1991).

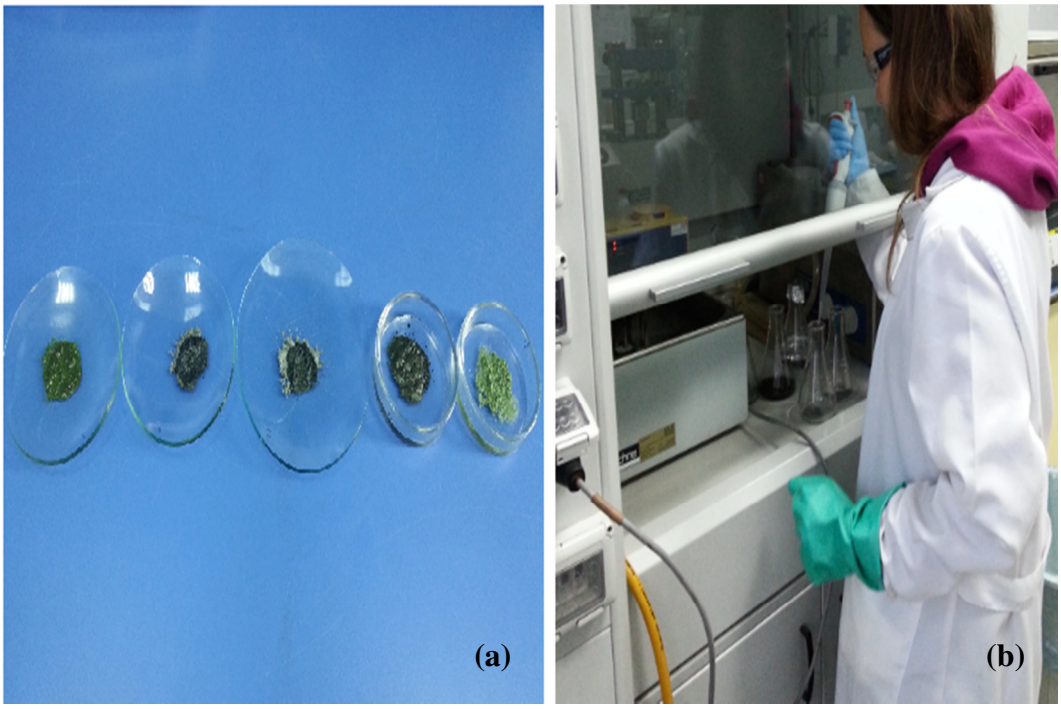


Figure 3.11 : Illustration of SABA experiments: (a) Samples subjected to fizz rating. (b) Acid addition to flasks before heat treatment in water bath.

3.2.4.4 Net acid generation

For net acid generation (NAG) experiments, 2,5 g of samples with < 75 µm grain size were placed in flasks with the addition of 15% H_2O_2 solution, which has a pH value between 4 and 7. Flasks were left under a flow chamber until reactions were finished and they were placed in a pre-heated water bath at 70°C (Figure 3.12a), right after. After two hours of reactions, flasks were cooled down to room temperature and

titrated with 0,1 M NaOH (for experiment pH>2,5) or 0,5 M NaOH (for experiment pH<2,5), to pH 7 (Lawrence et al., 1989) (Figure 3.12b).

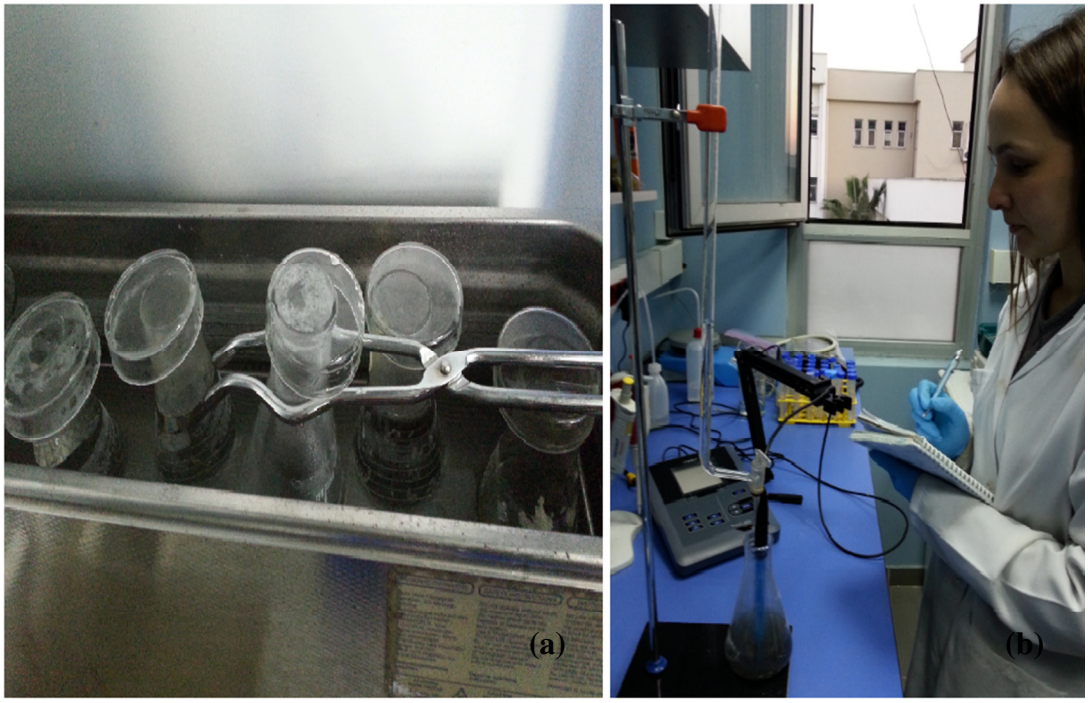


Figure 3.12 : Illustration of NAG experiments: (a) Heat treatment in water bath. (b) Titrations after heat treatment.

3.2.5 Biological and chemical leaching of the massive ore

3.2.5.1 Bacterial culture growth

The pure *Acidithiobacillus ferrooxidans* strain (Af) was obtained from an actively growing culture, previously purchased from the German Collection of Microorganisms and Cell Cultures (DSMZ). Mixed culture (E) mainly dominated by *Acidithiobacillus ferrooxidans* and *Acidithiobacillus thiooxidans* was enriched from a bacteria rich water sample (with visual bacterial mat), initially obtained from an AMD environment caused by Pb-Zn mining in Balya, Turkey (Çelik-Balcı et al., 2014).

A growth medium was prepared containing NH_4Cl (3 g/L), KH_2PO_4 (0,5 g/L), $MgSO_4.7H_2O$ (0,5 g/L) and $CaCl_2$ (0,25 g/L) and pH was adjusted to 2,5 using 1N H_2SO_4 solution. The liquid growth medium and laboratory equipment were autoclaved for 15 min at 121^{o}C. As the energy source, ethanol rinsed and UV sterilized elemental sulfur and 0,2 µm Sartorius syringe filter sterilized $FeSO_4.7H_2O$ solution was used with final concentrations of 10 g/L and 50 g/L, respectively.

Cultures were activated with 25% inoculation to the sterile growth medium in sterile flasks on a rotary shaker that was set to 180 rpm at 26^{o}C. Subcultures were grown with 10% inoculation ratio from the activated cultures at same shaking conditions. Inoculations were made under sterile conditions provided by ethanol rinsed and UV sterilized laminar flow chamber. All chemical reagents used were research grade Merck products and ultrapure water was obtained from MilliQ system.

3.2.5.2 Experimental setup

Bioleaching experiments were carried out in 500 ml sterile flasks using the growth medium specified above with an initial pH of 2,5 on ethanol rinsed and UV sterilized grinded ore sample (O), providing 4% pulp density. After the addition of 10 g/L UV sterilized elemental sulfur, cultures were inoculated to the experimental media with a 25% volume ratio and experiments (B1-Af and B1-E) were set up on a rotary shaker which was set to 180 rpm at 26^{o}C. A bacteria-free control (B1-C) experiment was also set up to investigate the effect of chemical oxidation under same experimental conditions. Chemical compositions of experiments were monitored for 115 days and two other sets of bioleaching experiments were set up using bacteria in heavy metal rich leaching solutions, in order to assess their leaching capability under shifted conditions. Considering groundwaters might reach higher temperatures travelling through lower elevations, cultures were also introduced to a higher temperature environment. Initial tests were left on the shaker for six months to obtain secondary precipitates. Leaching solutions of B1-Af and B1-E were inoculated to sterile growth medium with 25% volume ratios on UV sterilized ore samples that provide 5% pulp density. One set of experiments were placed on a shaker set to 180 rpm at 26^{o}C (B2/26-Af and B2/26-E) and the other set to 40^{o}C (B2/40-Af and B2/40-E). No other chemical controls were set up as the behavior of bacteria were to be investigated. New sets were continuously monitored for 57and 55 days, respectively. Experimental setup is illustrated in Figure 3.13.

3.2.5.3 Sampling and analytical techniques

During the experiments, 10 ml supernatants were frequently withdrawn and sampled in sterile conditions. Decreased volume was immediately replaced with the sterile growth medium. Samples were filtered through 0,2 µm Sartorius syringe filters; 7 ml aliquots were immediately acidified with 1/10 diluted HNO_3 and analyzed for their

metal content with Inductively Coupled Plasma Mass Spectrometry (ICP-MS). Sulfate, ferrous iron and total iron measurements of the remaining aliquots were made with HACH Lange DR 2800 Spectrophotometry, using powder pillow reagents with SulfaVer 4; 1, 10-Pheanthroline and FerroVer methods respectively. Ferric iron values were calculated from the difference ferrover iron and ferrous iron values.



Figure 3.13: Illustration of the steps of bioleaching experiments: (a) Laminar flow (Biosafety Cabinet) used as sterile environment. (b) Bacterial culture growth on shaker. (c) Elemental sulfur sterilization under UV light in laminar flow. (d) Chemical control and bioleaching flasks after four months of experiments.

Eh and pH values were measured with WTW Multi 9310 bench-top multi-parameter instrument using the probes SenTix ORP 900 and SenTix 940 respectively. EC values were analyzed with Crison CM 35 conductivity-meter, using the Pt 1000 sensor probe 56 00. Eh, pH and EC-meters were calibrated prior to first use and every week, following manufacturers' instructions. After the end of experiments, all

experimental media were filtered through 0,2 µm Sartorius filters using Nagel Bottle (Figure 3.14) and filtrates were acidified with 1/10 diluted HNO_3 for ICP-MS analysis. Solid residues of the B1 and B2/40 experimental sets obtained on the filters were freeze-dried and grinded to obtain <45 µm grain size for XRF, XRD and SEM analysis to identify the resulting ore chemistry and secondary mineral phases.

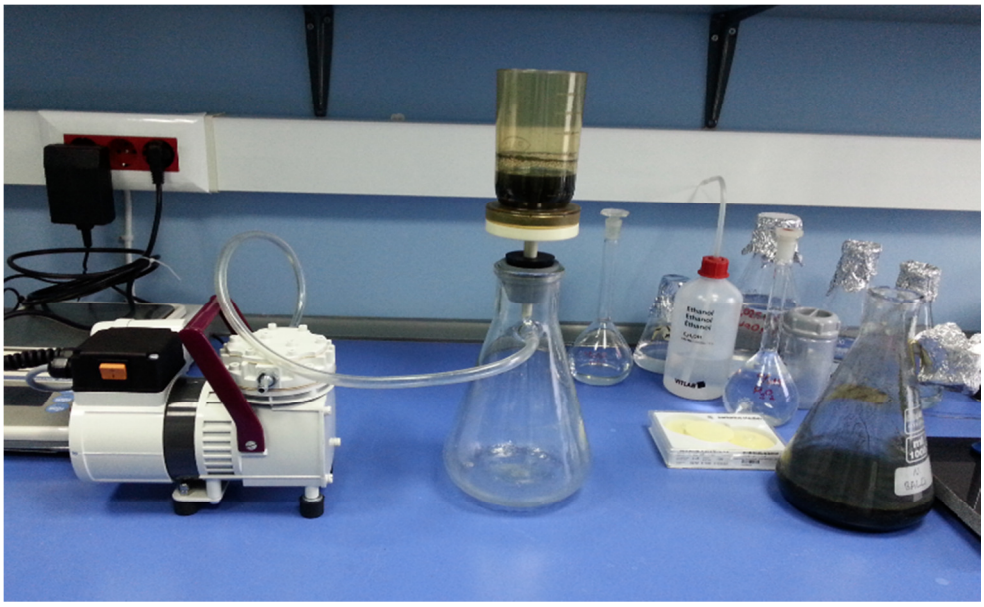


Figure 3.14 : Filtering system with Nagel bottle and automated pump.

4. RESULTS AND DISCUSSION

4.1 Simplified Geology of the Area Around Mining Operations

Detailed lithological features of the units are described by other authors (i.e. Bailey et al., 1966; Güner, 1980; Okay et al., 2014). In this section, only light observations will be described and illustrated. Studies were mostly concentrated in 1:25000 scaled Kastamonu E31-a3 sheet, while a few locations fell into Kastomonu E31-a4 and E31-d2 sheets (UTM, 36T region).

Triassic aged Küre Complex starts at the bottom with Akgöl Formation (Okay et al., 2014). Akgöl Formation consists of a flysch-like subgraywacke-shale sequence, which is known to be unconformably covered by the Yaralıgöz Group (Ketin and Gümüş, 1962). Subgreywackes of the formation, that can be observed on Kastamonu-İnebolu road cut outcrops at the South of the study area (UTM: 559721/4625535 – 559984/4626515 in E31-a3 sheet), display deformed, gray colored coarse grained sandstone (Figure 4.1a) characteristics with plant remains and local sequencing of dark colored shales. Generally, shales are described as organic rich black shales (Güner, 1980), that are extesively deformed leading to cleavage (Figure 4.1b) and alterated (UTM: 560142/4626703).



Figure 4.1 : Akgöl Formation: (a) Subgreywacke. (b) Alterated black shale.

Contacts of lithological units can be observed on Kastamonu-İnebolu road. Most clear contact zone can be observed at the contacts between black shales and greenish basalts (pillow lavas), as presented in Figure 4.2 (UTM: 560304/4626900).



Figure 4.2 : Tectonic contact of basalt and black shale on a roadcut on Kastamonu-İnebolu main road. Red line depicts the contact between two lithological units; whereas the yellow line indicates a fault plane, which obviously generated a deformation zone.

Pillow lavas of the Küre Complex can be observed in various shapes and sizes, which are well distributed on the roadcuts of Kastamonu-İnebolu road. Fresh inner surfaces display green-gray color, whereas having outer surfaces displaying metallic luster and brownish alteration color. Pillow lavas are either elliptical with longer y axises of dimensions extending up to 2 meters (Figure 4.3a) (UTM: 559514/4629410), or spherical with relatively small diameters (Figure 4.3b) (UTM: 559241/4629953). Chalcopyrite and sphalerite are visible on the surfaces of pillow lavas (Figure 4.3c) or in pillow lavas broken in half, displaying a radial crack structure like shrapnel (Figure 4.3d) (UTM: 559514/4629410).

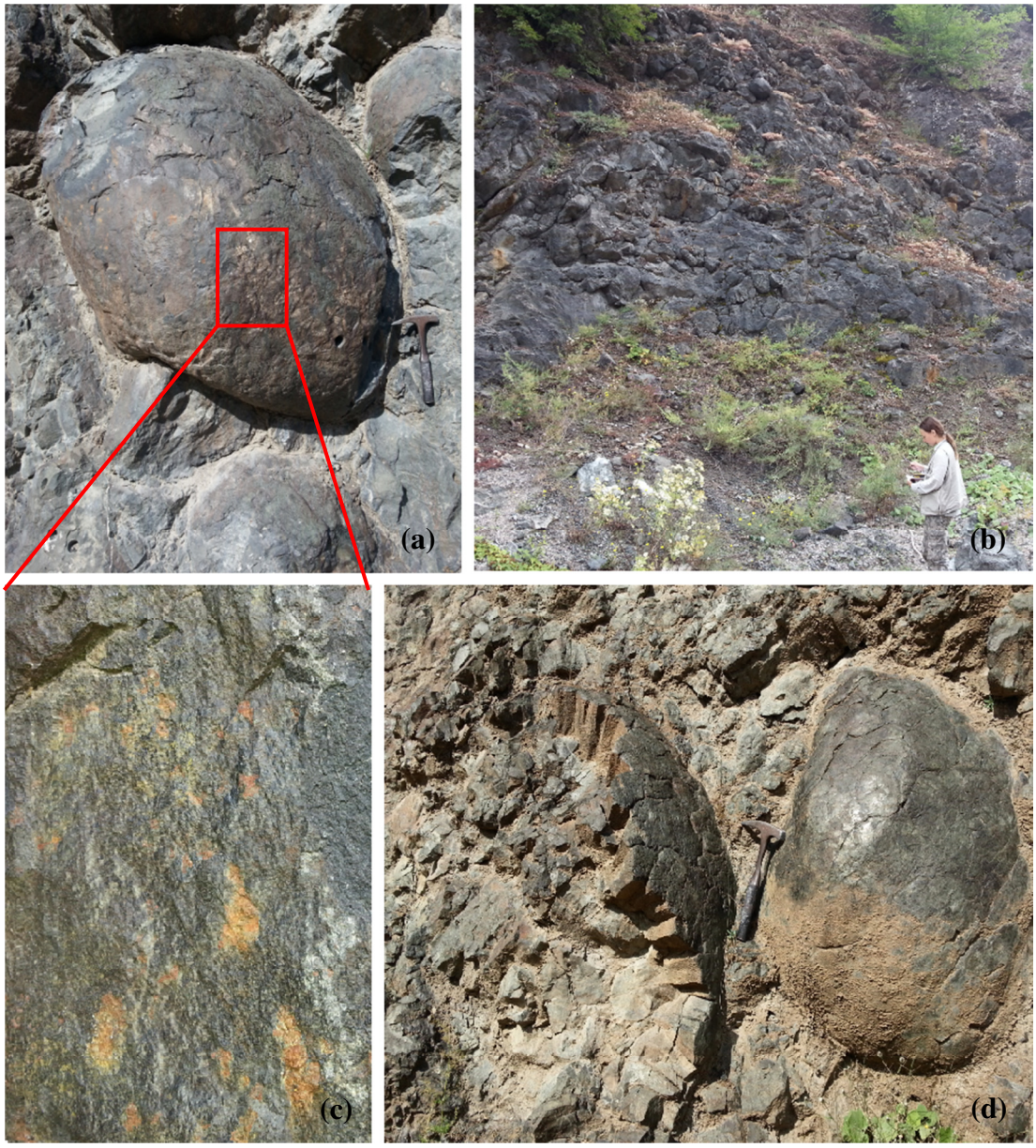


Figure 4.3 : Different features of pillow lavas from Küre Complex: (a) 2 meter long elliptical shape. (b) Spherical, relatively small pillow lava. (c) Chalcopyrite content visible on pillow lava displayed in Figure 4.3a. (d) Internal structure of pillow lava.

Upper Jurassic – Lower Cretaceous İnaltı Limestones overlay lithological units of Central Pontides beneath, unconformably (Tüysüz, 1990). İnaltı Limestones are known as massive or thickly bedded, having karstic gaps, light gray color and rich foraminifera content (Ketin and Gümüş, 1962; Güner, 1980). İnaltı Formation was observed as massive, light gray colored and with fault planes at the North (UTM: 559186/4632559 in E31-a3 sheet) (Figure 4.4a) and Northwest (UTM: 549186/4632559 in E31-a4) (Figure 4.4b) of the study area or as biomicritic blocks (Figure 4.4c) at the South (UTM: 554844/4618264 in E31-d2 sheet).

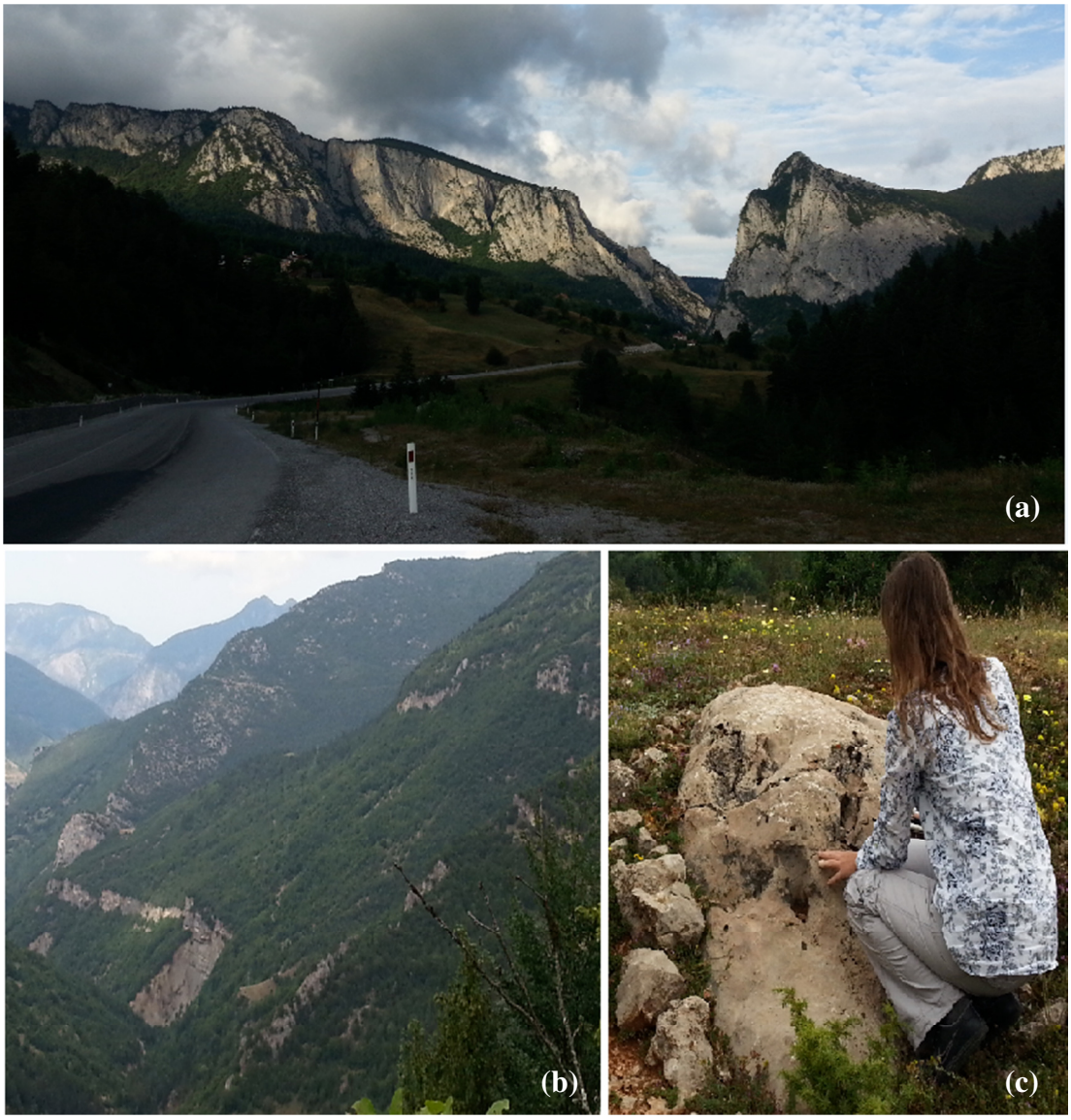


Figure 4.4 : İnaltı Formation: (a) Fault scarps at North of the city center. (b) Fault scarps at Northwest. (c) Biomicritic blocks at South.

Lower Cretaceous Çağlayan Formation (or Ulus Formation) is known as a turbiditic sandstone-shale sequence or a flysch that has a wide range of spatial distribution in Central Pontides (Karabük to Sinop), which has lateral or vertical transition with the İnaltı Formation (Okay et al., 2014). Çağlayan formation was only observed within the boundaries of E31-a4 sheet, with its characteristic features of laminated to very thick bedded layers, local cross-beddings, medium to coarse grain size, high quartz content, plant remains and bioturbiditic marks, paleocurrent structures (grooves marks, flute casts and asymmetrical ripple marks), and light brownish-yellow fresh surface color with brown alteration color (Figure 4.5). Moreover, a rake angle (42^{o}) was measured on a slickenside (UTM: 550619/4623603) and strike/dip angle (22/40

NW and 77/44 NW) measurements were made by a Silva compass in two different locations (UTM: 551115/4623269 and 550619/4623603).



Figure 4.5 : Field views of Çağlayan Formation (note that photos of Çağlayan Formation were taken from different localities in Central Pontides, in scope of a structural geology project coordinated by Prof. Dr. Aral Okay): (a) A typical outcrop view. (b) Illustration of rake angle measurement in the study area. (c) Typical, well-preserved flute cast of Çağlayan Formation.

Combining with the field observations and GPS locations of this study, a new geological map of the area was plotted (using ArcGIS), overlapping on the topography map displayed in Figure 2.2, Google Earth images of the area and previous maps (by Bailey et al., 1966; Güner, 1980; Kuşçu and Erler, 2002; Okay et

al., 2014) of the area. The new geology map of approximately a 16 km^2 area includes UTM coordinates different than the others, which is displayed in Figure 4.6. Çağlayan Formation is not present in the map. Note that only the formations and features mentioned above were observed in the field and others plotted from the previous maps (Bailey et al., 1966; Güner, 1980; Kuşçu and Erler, 2002).

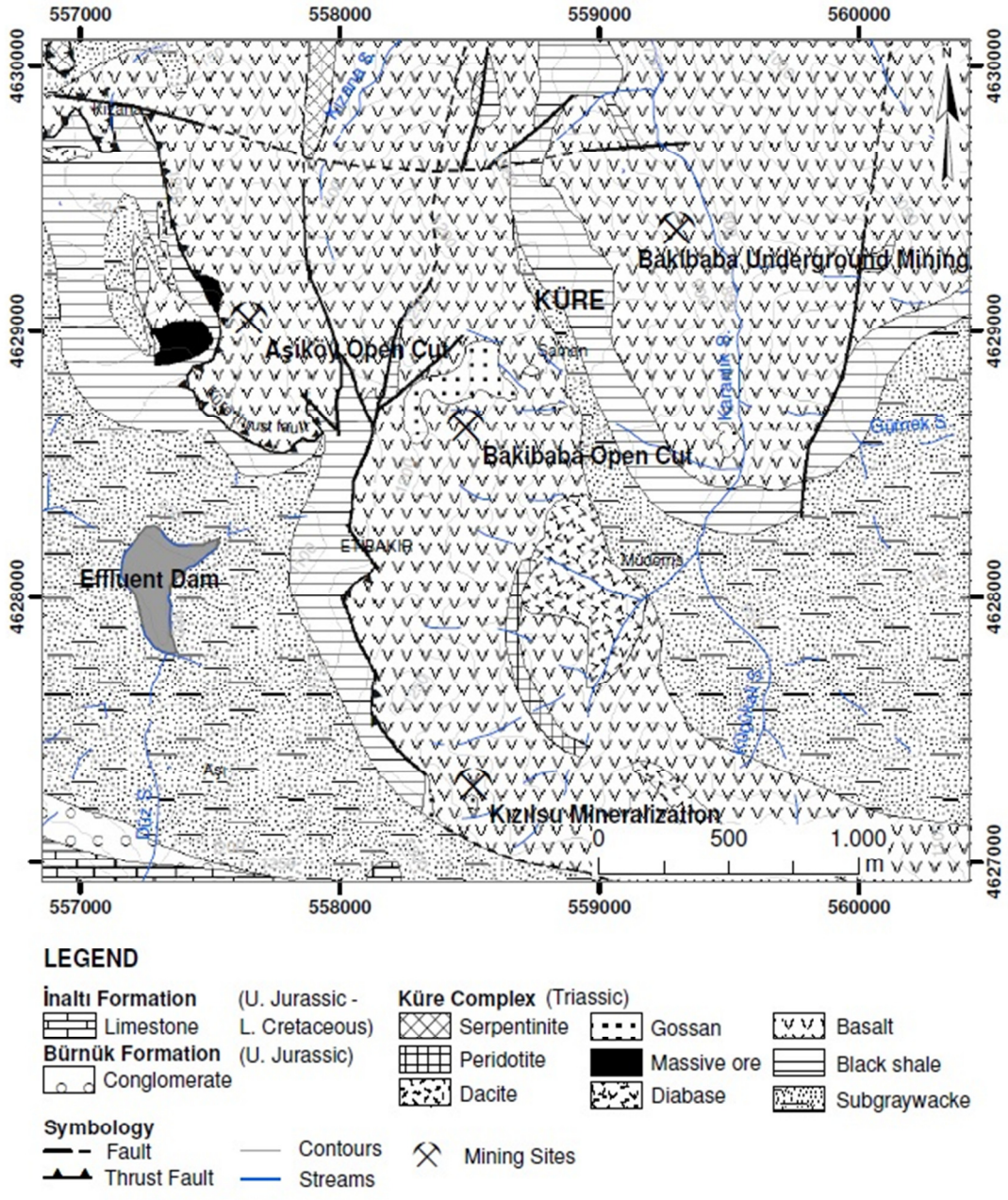


Figure 4.6 : UTM coordinated new geological map of the study area (after Bailey et al., 1966).

4.2 Geochemical and Mineralogical Features of the Ore and Wastes

4.2.1 Bulk chemistry

Selected element and major oxide compositions determined with XRF analysis of the ore, ore bearing rocks, representative basalt and waste effluent dam are listed in Table 4.1. Listed elements were chosen according to highest concentrations in samples and their relations to VMS deposits. According to the results, ore sample that is used for static experiments contain high concentrations of copper (5,43%), iron (28,95%), sulfur (44,81%) and zinc (3,42%), along with considerable amounts of cobalt, nickel, manganese, arsenic, lead and vanadium and trace amounts of zirconium. Ore bearing wall rocks show a similar composition with decreasing concentrations relative to the ore mineral as expected. Trace concentrations of Pb and As point out enrichment in the ore, associated with ore minerals. However, high concentrations of Cr and Ti were detected, suggesting the abundance of Cr and Ti bearing minerals like chromite ($FeCr_2O_4$), rutile (TiO_2) and anatase (TiO_2). Reference basalt sample showed trace concentrations relative to other samples except S (4,12%) and Zn (0,02%) exceeding some OBR's and, Zr (56 ppm), Mn (0,22%) and TiO_2 (0,76%) even exceeding the concentrations in the ore mineral.

Waste effluent precipitate also displays similar composition with ore and ore bearing rocks. Concentrations of Cu, Fe and S suggest the presence of ore minerals that could not be recovered by processing, leading to a potential source of acid generation if subjected to oxidation. High concentrations of As in the precipitate sample is attributed to selected recovery of metals in ores, resulting in a As rich sludge. Different than the other samples, high CaO, Na_2O and K_2O concentrations may represent additional chemicals that could be used as neutralizing and settlement agents. Considering that mine tailings containing low grade ores can be recycled (Schippers et al., 2014), overall metal concentrations of the effluent precipitate can be regarded as good candidates for metal recovery.

Due to its chemical composition, the massive sulfide ore is the main source of potential environmental contamination and acid generation resulting from the high heavy metal and sulfur content.

Table 4.1 : Bulk chemical composition of the rock samples.

Sample	O	OBR-1	OBR-2	OBR-3	WEP	B
Fe	28,95%	22,01%	33,63%	32,91%	24,85%	8,76%
Cu	5,43%	0,03%	0,04%	85 ppm	0,44%	4 ppm
S	44,81%	2,43%	0,45%	0,03%	31,17%	4,20%
Zn	3,42%	0,05%	27 ppm	84 ppm	0,52%	0,02%
Co	0,23%	0,04%	0,08%	0,05%	0,05%	78 ppm
Ni	0,06%	0,06%	0,06%	0,06%	0,05%	0,02%
Ti	ND	0,45%	0,38%	0,46%	0,13%	0,33%
Mn	0,01%	0,02%	0,01%	0,03%	0,04%	0,22%
Cr	ND	0,05%	0,05%	0,03%	0,06%	0,06%
Pb	0,04%	ND	1 ppm	ND	225 ppm	5 ppm
As	0,05%	5 ppm	11 ppm	2 ppm	0,03%	1 pmm
Zr	13 ppm	69 ppm	49 ppm	67 ppm	40 ppm	56 ppm
V	0,08%	ND	20 ppm	0,07%	0,06%	0,02%
SiO_2	ND	24,36%	15,29%	16,17%	16,62%	47,81%
Al_2O_3	ND	19,59%	14,41%	15,65%	6,04%	14,94%
Fe_2O_3	62,24%	29,84%	36,02%	35,31%	36,21%	11,26%
Cr_2O_3	ND	0,07%	0,46%	0,04%	0,04%	0,07%
MgO	ND	13,42%	7,38%	10,62%	2,37%	12,21%
CaO	ND	0,16%	1,75%	0,75%	2,83%	3,83%
Na_2O	ND	ND	ND	ND	0,38%	1,49%
K_2O	ND	ND	ND	ND	0,43%	0,79%
TiO_2	0,01%	0,68%	0,60%	0,79%	0,19%	0,76%
P_2O5	ND	ND	ND	ND	0,05%	0,07%
MnO	0,01%	0,03%	0,22%	0,03%	0,05%	0,24%

4.2.2 Mineralogical investigations

Major mineral compositions of the ore, ore bearing rocks and the effluent precipitate were determined with XRD between 2^o-70^o theta angles with steps of $0{,}019^o$ and a step time of 32 seconds at room temperature and evaluations made by DIFFRAC.SUIT EVA software are displayed in Figure 4.7. Ore and ore bearing rocks were collected from 675, 645, 630 and 512m elevation levels of Bakibaba underground tunnels, respectively. Mineralogical composition of the ore revealed major moiety of the ore minerals as cubic pyrite and tetragonal chalcopyrite. Sphalerite was also present as a minor sulphide phase. However, we were not able identify other ore minerals like bornite or Co and/or Ni bearing phases indicated by

other authors (i.e. Çağatay et al., 1980). This may be because of very low amounts hindering detection.

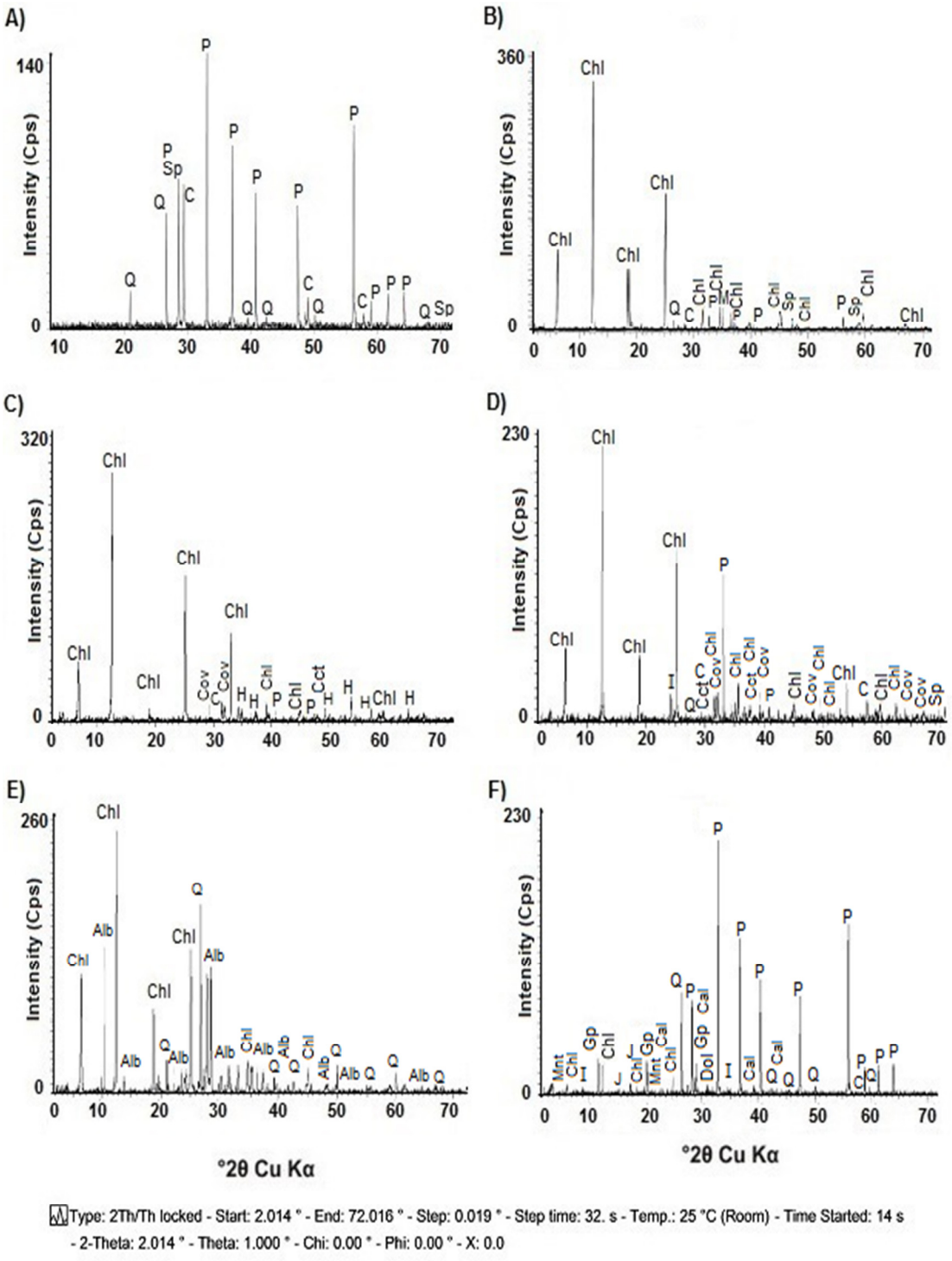


Figure 4.7 : X-ray diffractograms of samples subjected to static tests experiments (Alb: Albite, C: Chalcopyrite, Cal: Calcite, Cct: Chalcocite, Chl: Chlorite, Cov: Covellite, Dol: Dolomite, Gp: Gypsum, H: Hematite, I: Illite, J: Jarosite, M: Magnetite, Mnt: Montmorillonite, P: Pyrite, Q: Quartz, Sp: Sphalerite): (A) Massive sulfide ore. (B) OBR-1. (C) OBR-2. (D) OBR-3. (E) B. (F) WEP.

Quartz is detected as the abundant gangue phase. Quantitative analyses were not carried on; nevertheless, values can be found in previously reports on the ore mineral as chalcopyrite between 1-10% (Bailey et al., 1966), pyrite between 80-85% and quartz between 1,9-5,7% (Bailey et al., 1966; Güner, 1980). Ore bearing wall rocks commonly contained pyrite and chalcopyrite as ore minerals with secondary iron oxides as hematite and/or magnetite. Presence of chalcocite and covellite were also detected. Gangue phases are mainly composed of chlorite, quartz and illite. Reference basalt sample was mainly composed of quartz, albite and chlorite. Flotation tailings contained both of the ore minerals, mostly pyrite, and gangue phases of quartz and clay minerals. Gypsum and jarosite were detected as secondary sulfates and presence of carbonate minerals are attributed to possible anthropogenic input of settlement reagents.

Microscopic investigations of polished ore bearing rock slides showed the paragenetic relationships between pyrite, chalcopyrite, hematite and magnetite (Figure 4.8). Majority of the pyrite grains in the ore bearing rocks have deformed anhedral morphology, along with some subhedral and locally euhedral cubic grains. They are either observed as big grains containing chalcopyrite and specularite within or in their fractures, or as relatively small grains disseminated in a matrix. Also reported by Kuşçu and Erler (2002), three type of deformation structures can be observed on pyrite grains as cataclastic fractures, annealing and fracture filling structures. Annealing structures are rarely observed as triple junction of fractures with 120^{o} angles (Kuşçu and Erler, 2002). Moreover, calcite can be observed as vein fillings. Chalcopyrite mostly substitutes the edges of pyrite grains, which may also result in fracture filling structures. Chalcopyrite can also be observed as separate large anhedral grains, locally containing fracture fillings of specularite. Morphology of hematite crystals were mostly observed as acicular, which can also be named as specularite. They either display vein fillings, stock work structures or they are in the form of clusters. Specularite is present within pyrite and chalcopyrite grains or filled the fractures of the ore minerals suggesting either simultaneous mineralization or mineralization at a later stage, respectively. Locally, deformed pyrite or chalcopyrite particles can be observed within specularite. Moreover, rarely prismatic magnetite grains are present surrounded by specularite.

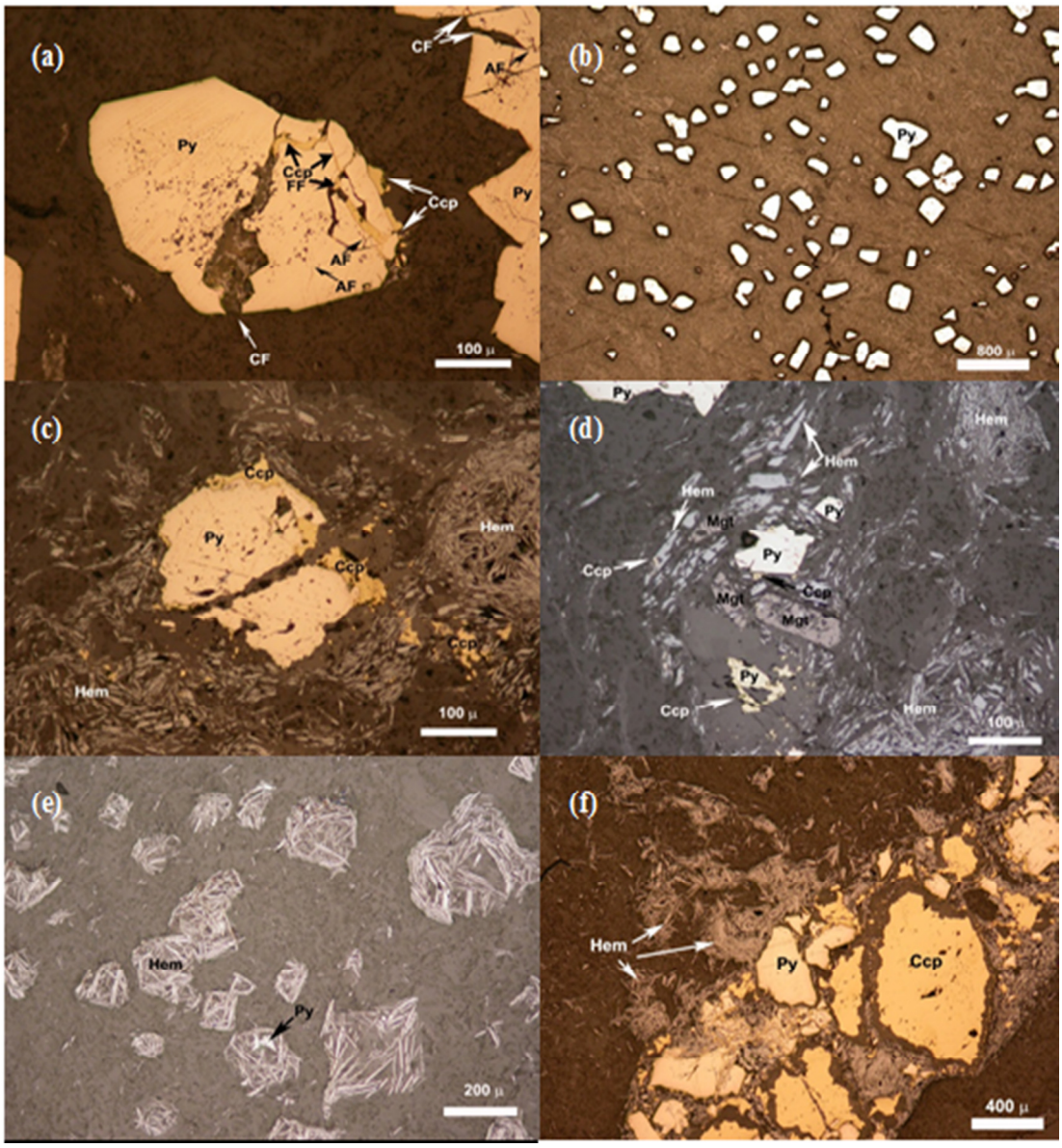


Figure 4.8 : Microscopic imaging of OBR's (Ccp: Chalcopyrite, Hem: Hematite, Mgt: Magnetite, Py: Pyrite; AF: Annealing fracture, CF: Cataclastic fracture, FF: Fracture filling): (A) Pyrite grains having chalcopyrite fracture fillings, cataclastic and annealing fractures in OBR-1. (B) Disseminated pyrite grains in the matrix in OBR-1. (C) Pyrite grain being substituted by chalcopyrite and surrounded by specularite in OBR-2. (D) Pyrite, chalcopyrite, specularite and prismatic magnetite in OBR-2. (E) Specularite clusters in OBR-2. (F) Paragenetetic relationship between pyrite, chalcopyrite and specularite in OBR-3.

4.2.3 Evaluation of static AMD prediction test results

Results of all of the calculated values using the parameters presented in Table 4.2 and formulations in Table 4.3 regarding static test are listed in Table 4.4

Table 4.2 : Amounts and concentrations of acid or base used in the experiments.

	V_a (ml)		M_a	V_b (ml)		M_b	
Sample	**INP**	**SABA**	**SABA**	**SABA**	**NAG**	**SABA**	**NAG**
O	*	40	0,1	127	21,1	0,1	0,5
OBR-1	0,005	40	0,1	25	51	0,1	0,1
OBR-2	0,005	40	0,5	18	0,7	0,5	0,1
OBR-3	0,002	40	0,5	17	*	0,5	*
WEP	*	40	0,1	21	15	0,1	0,5
B	0,004	20	0,1	4,9	0,01	0,1	0,1

Table 4.3 : Formulations and parameters used in static test calculations.

Tests	**Formulations**	**References**	**Parameters**
SABA	AP = S (%) x 31,25	Lawrence et al. (1989)	S (%) = Percentage of sulfur content of the sample
INP	MPA = S (%) x 30,6	Miller and Jeffery (1995)	V_a = Consumed volume of acid
INP	AC = (49 x V_a x N_a) / W	Bruynesteyn and Hackl (1984)	V_b = Consumed volume of base
SABA	NP = (50 x M_a x (V_a - (M_b/M_a) x V_b) / W	Sobek et al. (1978)	M_a = Molarity of the acid
SABA	NNP = NP - AP	Lottermoser (2010)	M_b = Molarity of the base
INP; SABA	NPR_{INP} = NP/MPA; NPR_{SABA} = NP/AP	Brodie et al. (1991); MEND (1991)	N_a = Normality of the acid
NAG	NAG = (49 x V_b x M_b) / W	Miller et al. (1997)	W = Sample weight

4.2.3.1 Paste pH

Paste pH results give an idea about the possible production of acidity and toxicity of fine grained wastes, when they interact with water forming slurry and the sulfur moiety is oxidized in time (Sobek et al., 1978). Electrical conductivity with pH values below 4 is either used as an indicator of high concentrations of total dissolved solids (TDS) in the solution if EC>20 µS/cm (Lottermoser, 2010) or acid generation with EC values above 2000 µS/cm (Environmental Australia, 1997). For all samples, increase in EC values is evident correlated with slight drops in the pH values in the first 24 hours (Figure 4.9). After 504 hours of monitoring, results revealed that interaction with OBR's and basalt with ultrapure water did not cause any acidity, considering the final pH values between 7,85 and 8,20. Final electrical conductivity values of the OBR's varied between 440 and 1501 µS/cm, where representative basalt sample (B) caused the lowest EC value of 228 µS/cm. Ore and the WEP sample's final leachate pH value stayed below 4, while excessive EC values were reached starting with first measurement which resulted in 6620 and 9650 µS/cm, respectively. According to Environmental Australia (1997) classification, our results show that only samples O and WEP are acid generating. However, due to high sulfur concentration of the OBR's, other static tests should be combined for evaluation (Price and Errington, 1995).

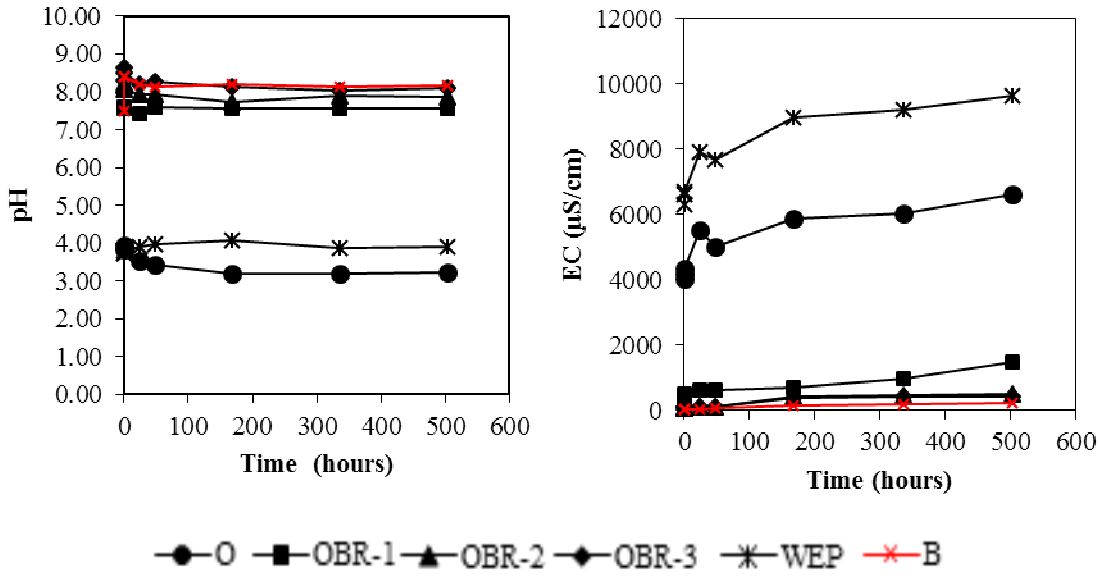


Figure 4.9 : Shifts in the pH and EC values of the solution during paste pH tests.

4.2.3.2 Initial neutralization potential

INP method tests the acid consumption (which corresponds to neutralization potential) via sulfuric acid titration to the sample mixed with deionized water, in order to evaluate the balance between the acid consumption (AC) or in other words neutralization potential and maximum potential acidity (MPA), which is calculated from the sulfur content of the sample multiplied with a factor of 30,6 (Bruynesteyn and Hackl, 1984; MEND, 1991; Miller and Jeffry, 1995). Brodie et al. (1991) proposed neutralization potential ratio (NPR) NP/APP limits that are used for evaluating SABA results, which suggest acid production if NP/APP<1 or neutralization if NP/APP>3 and the interval between them refers to uncertainty; and where APP refers to acid production potential. In this study, NP/MPA ratio is regarded as NPR_{INP}, in order to correlate with NPR values derived from SABA tests (NPR_{SABA}). Samples O and WEP were not subjected to the test because of their acidic paste pH being lower than the back-titration limit (pH 6). Our results showed that the samples producing acid to be OBR-1, OBR-2 and B due to the test, while the character of OBR-3 was uncertain (Figure 4.10).

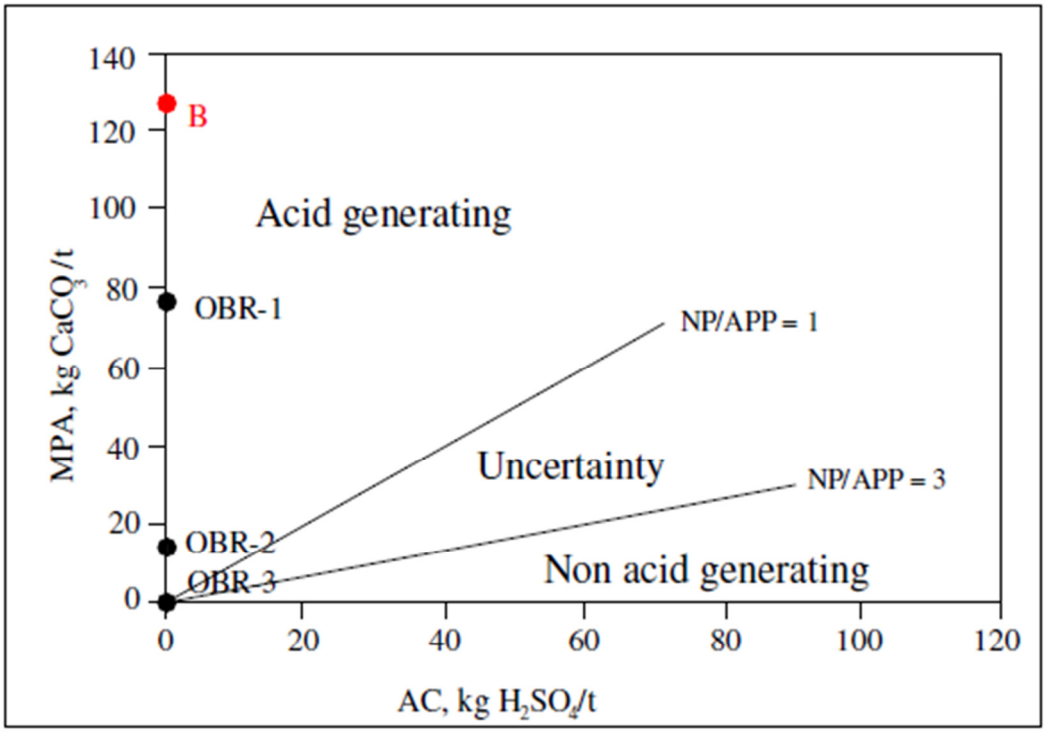


Figure 4.10 : Evaluation of initial neutralization potential test results.

4.2.3.3 Standard acid-base accounting

Unlike the paste pH and INP tests, acid generating and neutralizing contents of the samples are extracted with heated HCl and a NP is calculated as kg $CaCO_3$/t as a result of SABA tests (Sobek et al., 1978). Generally, a net neutralization potential (NNP) is calculated from the deduction of AP from NP for evaluation (EPA, 1994; Skousen et al., 2002; Lottermoser, 2010). However, NNP evaluation is limited to tresholds (NNP > -20 ppt = acid producing and NNP > 20 ppt = alkalinity producing) and interpretation of results between the limit values are challenging (EPA, 1994). Therefore, NP/APP ratio of Brodie et al. (1991) was used instead for evaluation (see Table 4.2 for NNP calculations). The value corresponding to APP in SABA calculations is acid potential (AP), which is calculated by multiplying the total amount of sulfur in the sample with a factor of 31,25 (MEND, 1991). Thus, here, NPR_{SABA} value corresponds to the ratio of NP/AP. Our results indicate that samples O, OBR-1 and WEP samples that displayed slight fizz rating, with the sample B that displayed no fizz have acid producing characters; whereas OBR-2 and OBR-3 samples having moderate fizz rating act as neutralizing agents (Figure 4.11).

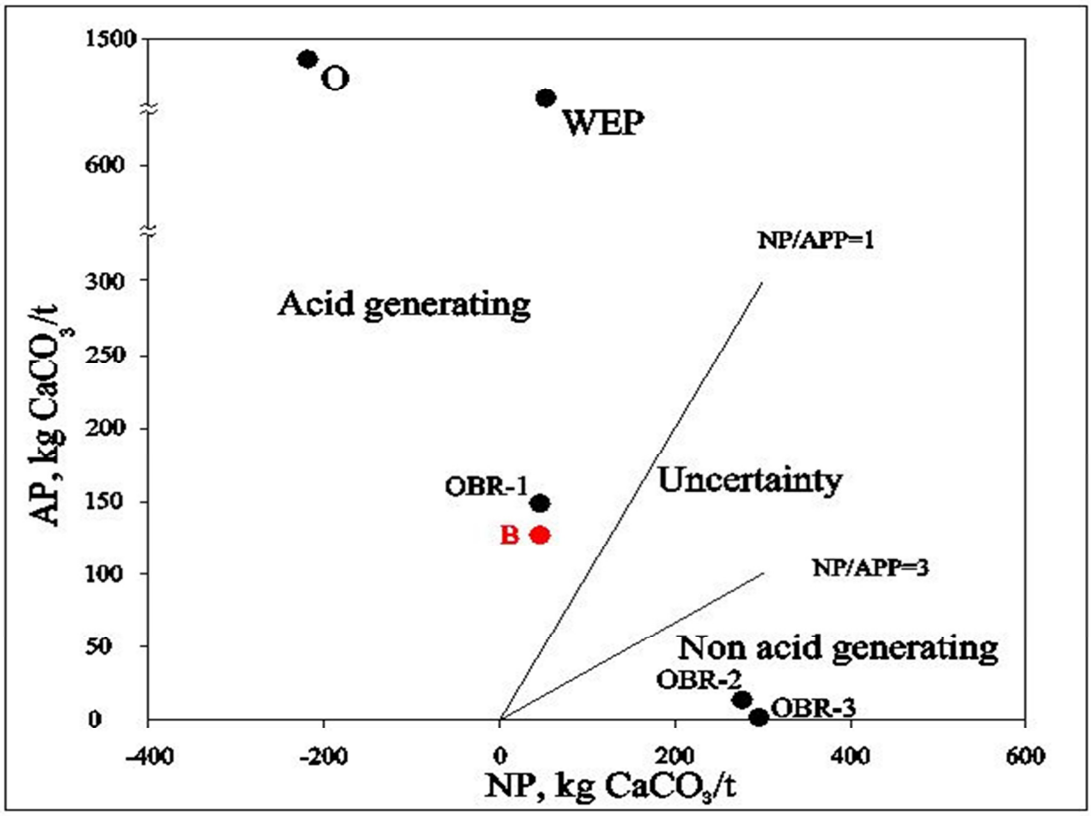


Figure 4.11 : Evaluation of standard acid-base accounting test results.

4.2.3.4 Net acid generation

Net acid generation tests aim to oxidize the fine grained mine wastes quickly with hydrogen peroxide, which is a strong oxidizing agent (Miller et al., 1990). Different than the other methods, NAG does not take in account the S content for the calculations and the amount of sulfuric acid that can be generated after a complete oxidation (assumption) is calculated as kg H_2SO_4/t (Sobek et al., 1978; Miller et al., 1997). OBR-3 sample was not subjected to the test due to neutral initial leachate. Our results show that samples O, OBR-1 and WEP have acid producing characters (Figure 4.12).

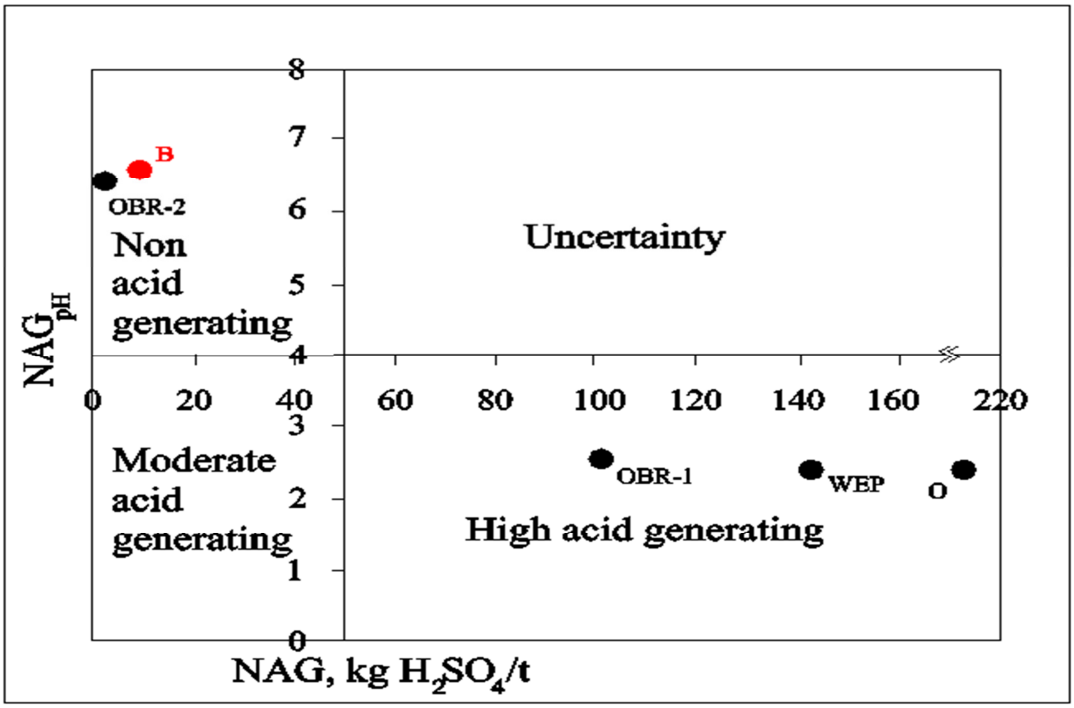


Figure 4.12 : Evaluation of net acid generation test results.

4.2.4 Neutralizing and Acid Generating Potential of Küre VMS Deposits

As expected, massive pyritic chalcopyrite ore of Küre VMS deposits is the major source of acid generation with the highest sulfur content and acid production potential (1400 tons of potential acidity per ton of ore) that can produce a net acidity about 206,5 kg H_2SO_4 per a ton of ore. This is supported by the highest pyrite and chalcopyrite content in mineralogical composition and lowest final paste pH value of 3,24. However, paste pH test are generally monitored about three weeks, which may not be the time that equilibrium is reached. Therefore, sample was not disposed until a last measurement at the end of two months, revealing lower pH values can be

reached on surface waters around Küre, about pH 2,6. High EC values also indicate that the heavy metal content as dissolved solids in predicted AMD waters can reach toxic levels for the environment (Environmental Australia, 1997).

Table 4.4 : Results of the geochemical static AMD prediction tests.

Sample	**O**	**OBR-1**	**OBR-2**	**OBR-3**	**WEP**	**B**
Elevation	675	645	630	512	-	-
Sulfur	44,8	2,43	0,45	0,03	31,17	4,2
AP (ppt)	1400	75,94	14,03	1,07	974,03	129,6
MPA (ppt)	1371	74,358	13,77	0,918	953,802	126,9
Paste pH	3,24	7,55	7,85	8,1	3,89	8,17
Paste EC (µS/cm)	6620	1501	515	440	9650	228
AC (kg H_2SO_4/t)	*	0,0245	0,0245	0,0098	*	0,0196
NP (kg $CaCO_3$/t)	-217,5	37,5	275	287,5	47,5	37,75
NNP (ppt)	-1618	-38,44	260,97	286,43	-926,53	-91,85
NPR_{INC}	-0,159	0,50432	19,971	313,181	0,0498	0,29748
NPR_{SABA}	-0,16	0,49	19,6	270,4	0,05	0,3
NAG (kg H_2SO_4/t)	206,5	100	1,4	*	147	7,06
NAG_{pH}	2,39	2,52	6,46	*	2,39	6,5

Waste effluent precipitates of the copper deposits have the second highest potential of acid production regarding the high sulfur content, which is consistent with low final paste pH of 3,89. Potential production of acidity is calculated as 974,1 ppt, whereas net acidity that can be produced is 147 kg H_2SO_4 per a ton of waste, consistent with the high sulfur value of the waste material . Moreover, the carbonate and silicate bearing mineral content derived from settlement chemicals (Lawrence and Scheske, 1997), are consistent with the NP (47,5 kg $CaCO_3$/t) detected for the WEP sample. Combined with the high EC values, overall results suggest that WEP can produce acidity and toxicity when its exposed to an aqueous environment outside the effluent dam, if high pulp density is provided. Considering their high paste pH, OBR's are insignificant in AMD production around Küre. This can be attributed to the short period of oxidation resulting in slow rates of acid generating reactions and high NP of the serpentinized host basalts. However, up to 1500 µS/cm EC values may suggest the production of contaminated waters, and their pyrite and chalcopyrite (sulfur) content still might produce some acidity (Miller and Murray, 1988; Lottermoser, 2010). Inconsistent with the paste pH values OBR-1 showed acid

production potential as a result of INP, SABA and NAG tests, which might produce 100 kg H_2SO_4 per a ton of OBR-1, may suggest minor contribution to AMD generation. OBR-2 was also regarded as acid producing due to INP tests but, this can be attributed to the overestimation resulting from the total sulfur content in the calculations, which is assumed to be 100% deriving from pyrite (Perry, 1998). Reference basalt sample revealed unexpected results from INP an SABA tests displaying an acid producing character, which is inconsistent with the high paste pH and non acid generating character due to NAG tests. This could be attributed to S(%) value accounted in INP and SABA calculations. Considering the high paste pH, sample B is evaluated as non-acid generating.

4.2.4.1 Limitations of the static test methods

In order to assess the acid generation and neutralization potentials of coal mining related ore or waste materials, static test methods were developed like acid-base accounting (Sobek et al., 1978) and modified in time to apply to other type of mining sites or enhance the effectivity for applications (Lapakko, 1994; Morin and Hutt, 1997; Jambor et al., 2007). Static test are widely applied to predict AMD for sulfidic ore deposit sites around the world, due to its simplicity (Lottermoser, 2010). However, those test methods have some limitations that may cause under or overestimation of the results (MEND, 1991; Lapakko, 2002; Karadeniz, 2008; Sahoo et al., 2014) that can be listed as artificially increased reactive surface area by grinding (Paktunç, 1998); neglected origin of the sulfur which can be non-acid generating (Casagrande, 1989; Perry, 1998); oxidized carbon content by chemical treatments (Lottermoser, 2010); neglected form, size or crystal structure of minerals and slow dissolution and oxidation rates of some neutralizing constituents (Sverdrup, 1990; Kwong, 1993; Lawrence and Scheske, 1997; Paktunç, 1999; Weber et al., 2004). Moreover, besides the inconsistency between different static test methods, differences between the measured neutralization potentials and computed or calculated neutralization potentials based on the stoichiometry of neutralization reactions, abundance of the mineral and/or relative reactivity of minerals with normalized abundances relative to calcite were reviewed by several authors (Kwong, 1993; Lawrence and Scheske, 1997; Paktunç, 1999; Jambor et al., 2007; Bouzahzah et al., 2014). Therefore, predicted mine drainage characteristics may lead to inaccurate evaluations, as well as not totally representing the field conditions. Test

results that were obtained for the reference basalt sample set a great example for the limitations. Sample B should have represented an end value of neutralization for current samples; on the contrary, INP and SABA test results indicated an acid-producing character. However, due to the mineralogical analysis, basalt sample did not contain any ore mineral that could produce acidity. This case shows the overestimation of determined sulfur values accounted in INP and SABA tests, which is assumed to be totally deriving from pyrite.

4.3 Bacterial and Chemical Leaching of the Massive Ore

AMD processes were divided into two stages as AMD generation and post AMD, considering the distinctive shifts in the solution chemistry at mixing zones of waters with different physicochemical and geochemical characteristics.

AMD generation in the presence of *Acidithibacillus ferrooxidans* was initially acid-consuming, probably due to acid dissolution of chalcopyrite and the oxidation of released ferrous iron in the solution (Dutrizac, 1989; Bevilaqua et al., 2002; Stott et al, 2003; Xia et al., 2012; Zhao et al., 2013a). A peak value of 3,3 was obtained after 3 days of bioleaching and pH generally decreased through the rest of the bioleaching, until a final pH of 2,4 was reached (Figure 4.13a). Abiotic chemical control followed a similar pattern with a maximum pH value of 4,3 and final pH value of 3,3; at the end of the first week and 119 days, respectively. However, mixed enrichment cultures did not display a regular pattern. On the contrary, pH decreased and constant stages were evident, resulted with a final value of pH 1,3. Eh values tend to increase in the presence of bacteria and decrease in the abiotic experiment at the first 20 days of experiments. For the rest of the process, *Acidithiobacillus ferrooxidans* continuously raised the redox potential up to 423 mV, whereas enrichment caused a peak of 510 mV and provided a final redox potential of 447 mV. Chemical control Eh dropped from 455 to 324 mV and displayed a slightly increasing trend, which ended with a final redox potential value of 390 mV (Figure 4.13a).

Solution chemistry significantly changed after the early phase of AMD generation (first 34 days), with decreasing pH and excessively elevated Cu, Co and Zn concentrations. A rapid release of metals is evident between 55 and 87 days suggesting an exponential phase for all experiments. Between 87 and 115 days, concentrations in the presence of bacteria start to decrease leading to a stationary

phase and possibly elevated rates of chemical oxidation in return. Cu, Zn and Co concentrations showed a similar trend at all experiments, while fluctuations were observed for Fe and SO_4^{2-} values in the presence of bacteria. At the end of AMD simulation experiments, highest final Cu (864 ppm) and Co (7 ppm); Zn (307 ppm); SO_4^{2-} (11750 mg/L) and Fe (1124 ppm) concentrations were obtained by the pure culture, chemical control experiment and the mixed cultures, respectively (Figure 4.14).

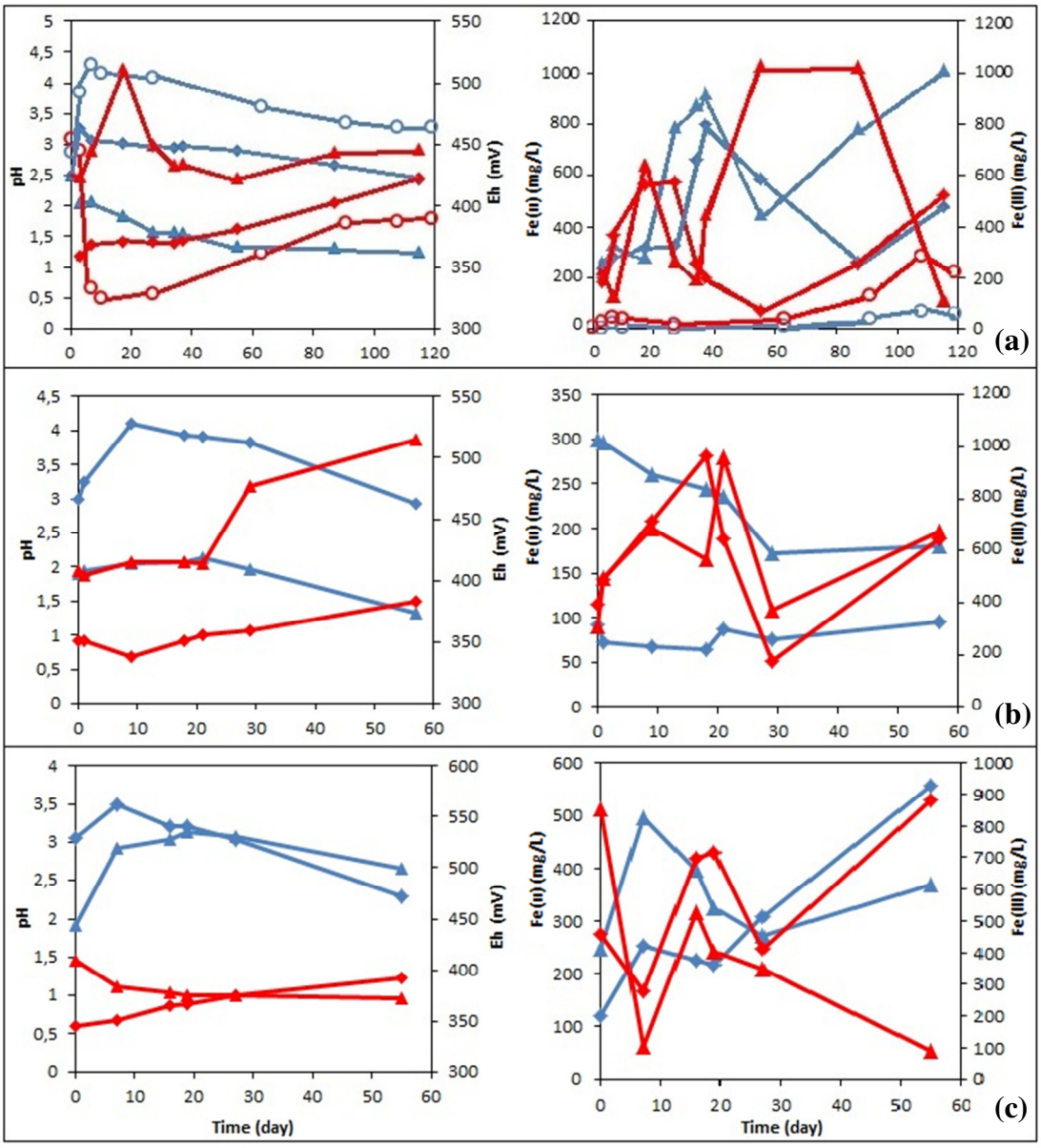


Figure 4.13 : Shifts in pH with Eh (mV) and Fe(II) with Fe(III) of the solution during B1/26 (A), B2/26 (B) and B2/40 (C) experiments; where diamonds, triangles and hollow circles refer to *Acidithibacillus ferrooxidans*, mixed enrichment cultures and abiotic control experiments, respectively. Blue colors are representing pH or Fe(II), while red colors are representing Eh or Fe(III) shifts, respectively.

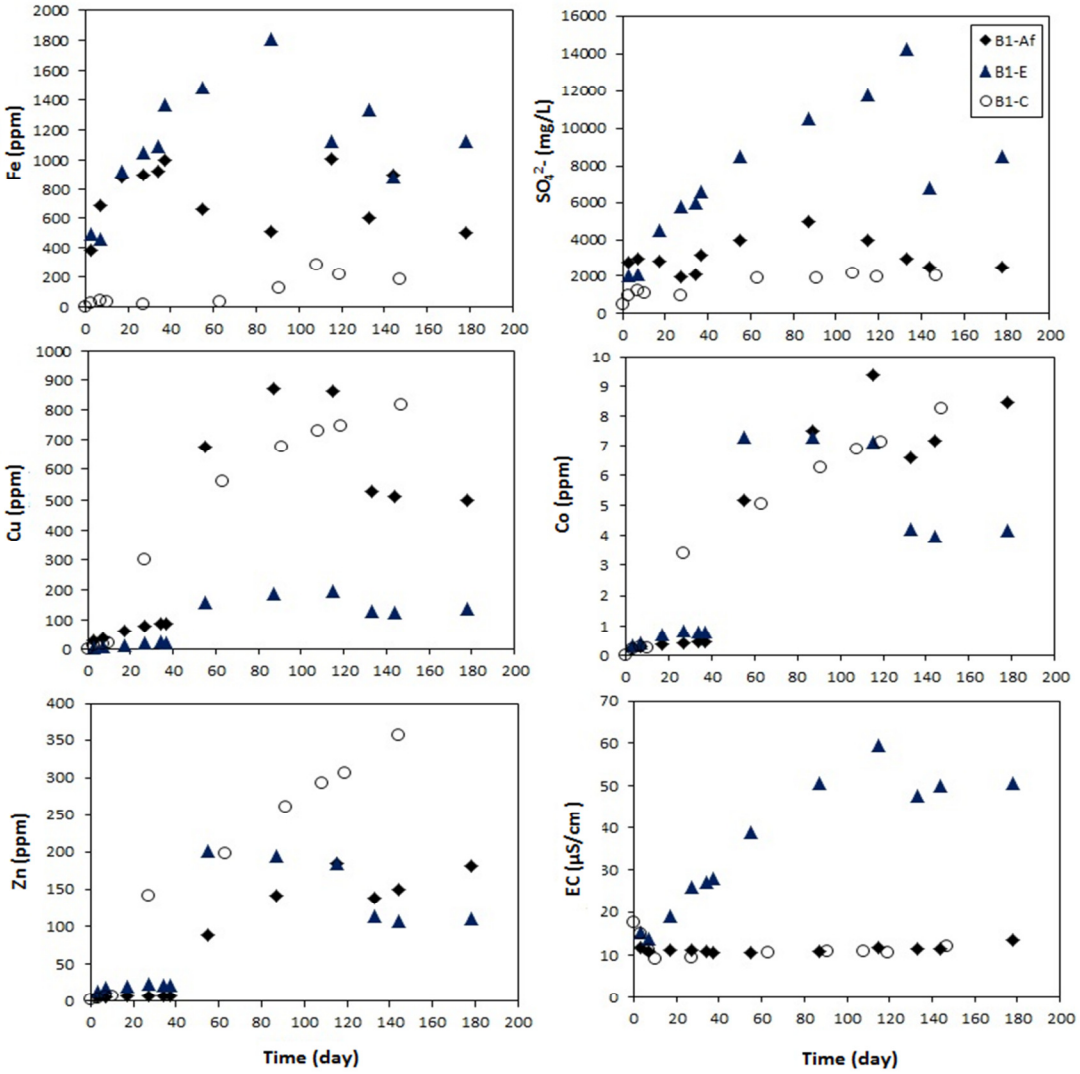


Figure 4.14 : Shifts in total Fe, SO_4^{2-}, Cu, Co and Zn concentrations and EC, during B1/26 experiments.

At the post AMD stage, bacteria that were adapted to elevated heavy metal concentrations were introduced to a non-AMD-affected environment with unleached new ore, in order to simulate mixing zones. As expected, initial pH values were elevated relative to the AMD generation stage due to dilution by fresh medium and increasing trends were evident for both cultures due to acid consumption mentioned above (Dutrizac, 1989). In the presence of pure *A. ferrooxidans* culture, pH was increased to 4,1 and 3,2; which later decreased to 2,9 and 2,3 at 26°C and 40°C, respectively (Figure 4.13b and Figure 4.13c). Mixed enrichment culture displayed slightly lower pH values that peaked at 2,1 and 3,1 at 26°C and 40°C, respectively. However, final pH values were observed as 1,3 and 2,7 at the end of 55-57 days. At lower temperatures, Eh varied between 337-383 mV and 405-515 mV with averagely increasing trends for pure and mixed cultures, respectively. Nevertheless, lower Eh

values were observed at higher temperatures and redox potential resulted from mixed cultures displayed a decreasing trend.

Pure culture still efficiently leached Cu (resulting in a final concentration of 759 ppm), whereas mixed cultures promoted the release of the highest concentrations of Fe, SO_4^{2-}, and Zn, with final concentrations of 256 ppm 7250 mg/L and 214 ppm, respectively, at 26°C (Figure 4.15).

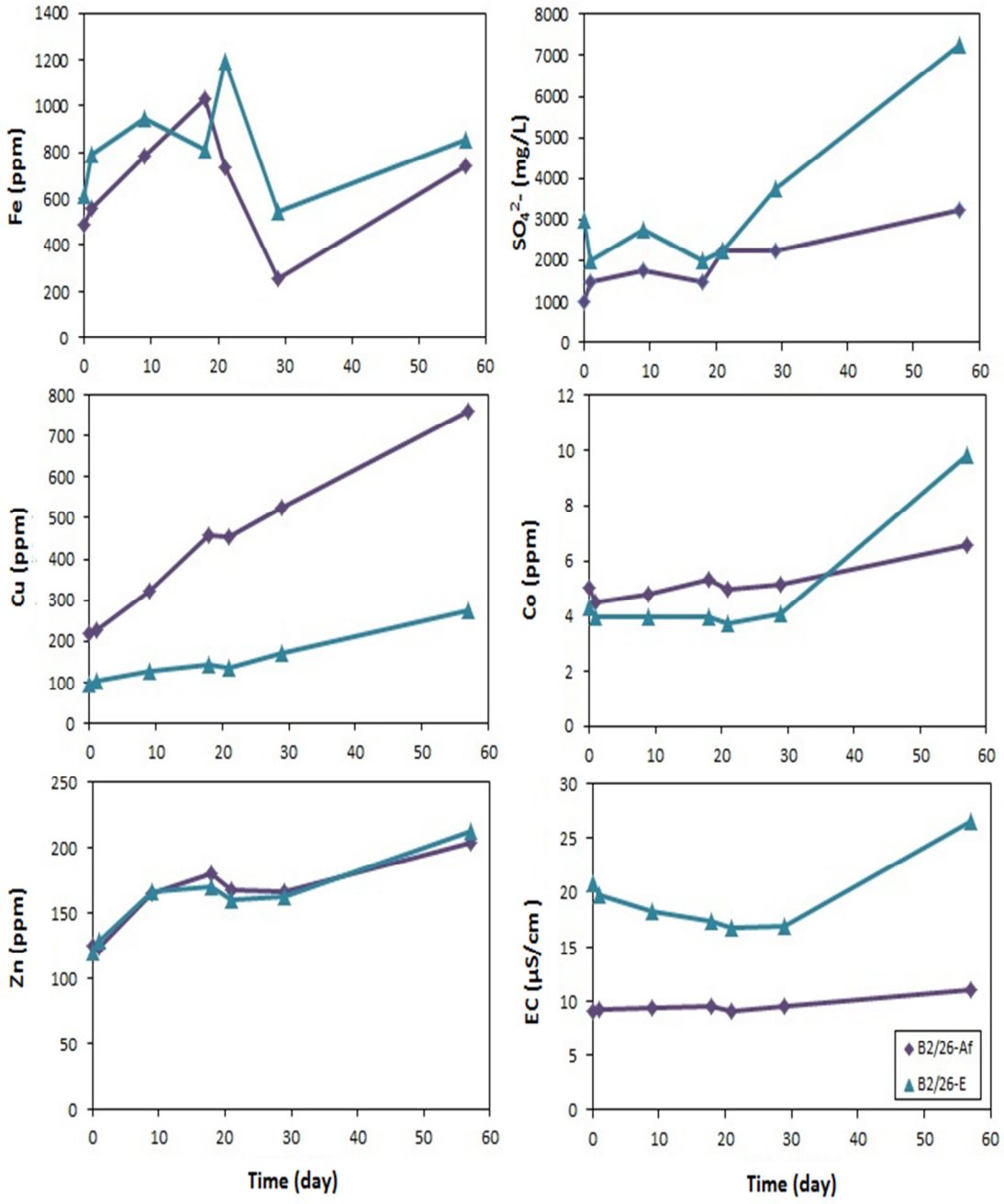


Figure 4.15 : Shifts in total Fe, SO_4^{2-}, Cu, Co and Zn concentrations and EC, during B2/26 experiments.

However, leaching of Co changed trends and turned out to be released more by mixed cultures at later stages, having a final concentration of 10 ppm (Figure 4.15). When bacteria were introduced to 40°C environment, only Zn and SO_4^{2-} were detected as highest final concentrations (337 ppm and 3500 mg/L, respectively) with mixed cultures. On the contrary, highest final concentrations of Fe (1440 ppm), Co (11 ppm) and Cu (1041 ppm) were obtained in the presence of pure *A. ferrooxidans* culture (Figure 4.16). Increase in temperature also increased the heavy metal concentrations in solution, probably due to increased chemical oxidation rates versus temperature.

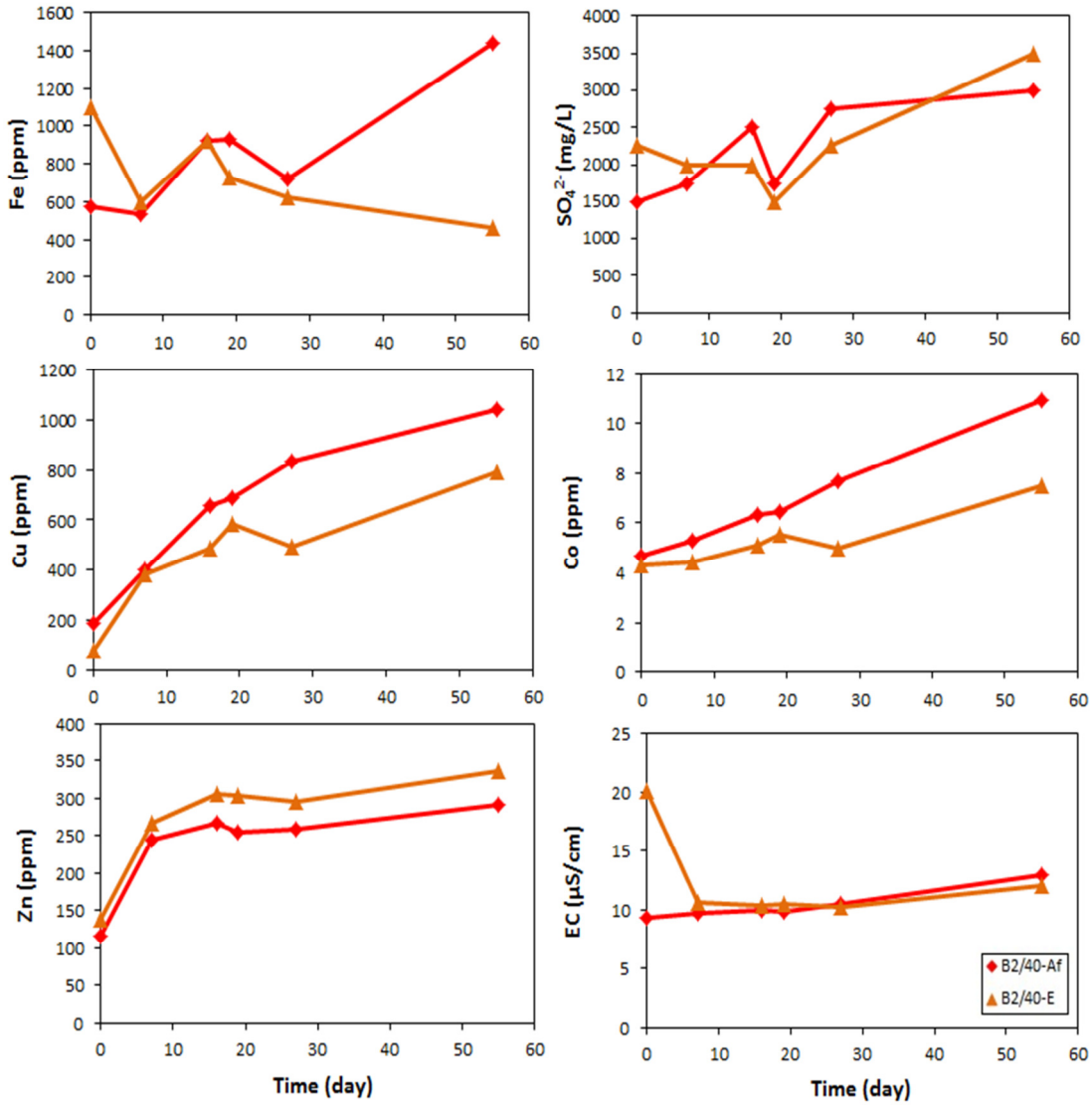


Figure 4.16 : Shifts in total Fe, SO_4^{2-}, Cu, Co and Zn concentrations and EC, during B2/40 experiments.

4.3.1 Chemical and mineralogical features of the ore after leaching

Mineralogical compositions of nearly all samples revealed quartz, pyrite and sulfur with secondary precipitation of jarosite at different levels. Some samples also contained schwertmannite. We were not able to identify the main ore mineral chalcopyrite in every leached sample, as most of the Cu was dissolved and wt% fell under the detection limit. This could be explained by the high content of pyrite stimulating and accelerating copper leaching (Dutrizac, 1989; Mo et al., 2012). Sphalerite was also detected as a minor sulfide phase. X-ray diffractograms of the untreated ore sample and residual precipitates of B1 (after 6 months of leaching) and B2/40 (after 2 months of leaching) experiments are displayed at Figure 4.17.

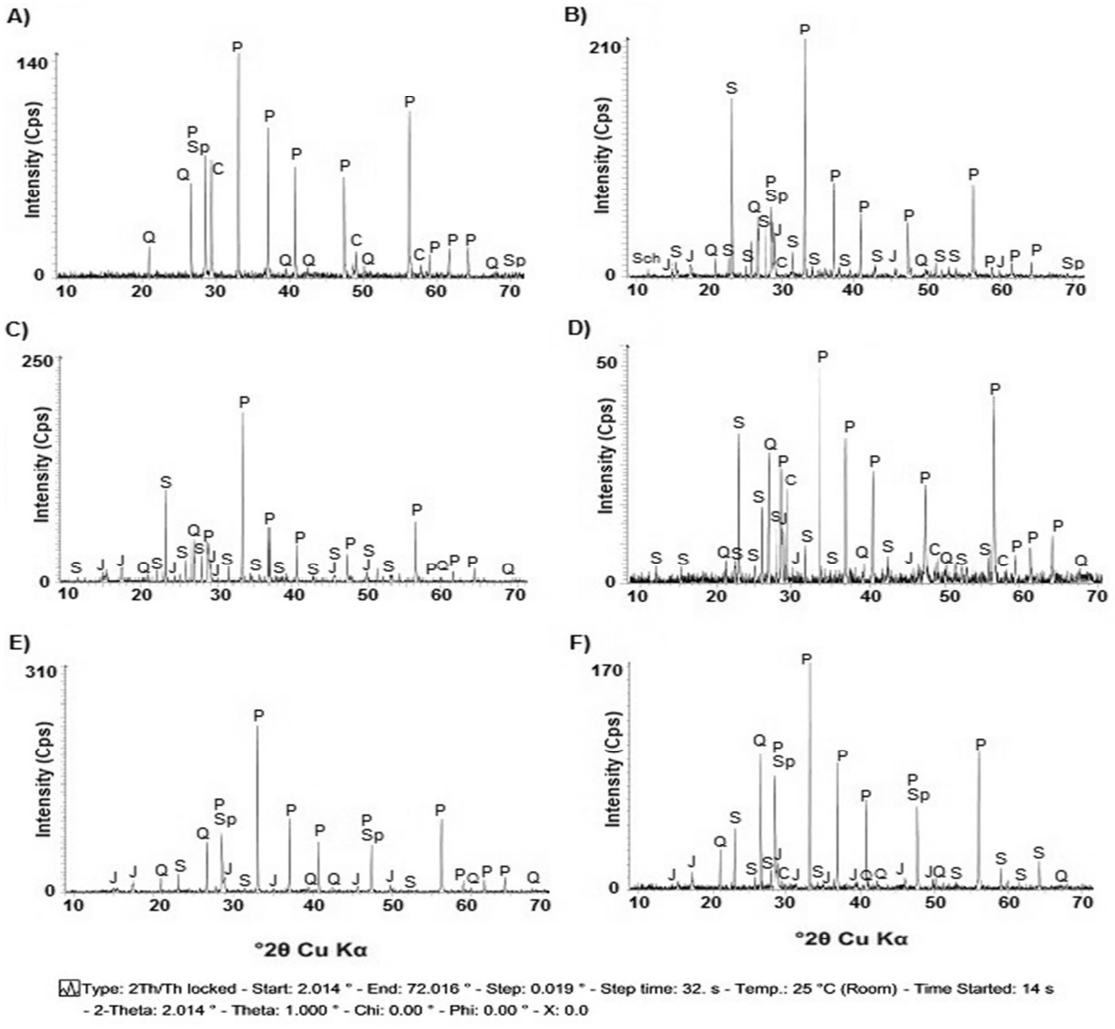


Figure 4.17 : X-ray diffractograms of (A) Untreated massive sulfide ore and leached residue after six months of (B) B1-C, (C) B1-Af, (D) B1-E; and two months of (E) B2/40-Af and (F) B2/40-E experiments (C: Chalcopyrite, J: Jarosite, P: Pyrite, Q: Quartz, S: Sulfur, Sch: Schwertmannite, Sp: Sphalerite).

Various morphological features are observed on mineral surfaces by SEM imaging, regardless some relatively intact surfaces. Figure. 4.18A shows a spherical morphology and an euhedral cubic grain with secondary precipitation in close proximity, resulted from chemical leaching. Semihedral pyrite grain with secondary precipitates above has a relatively smooth surface, probably due to its resistance to proton attack (Sand et al., 2001).

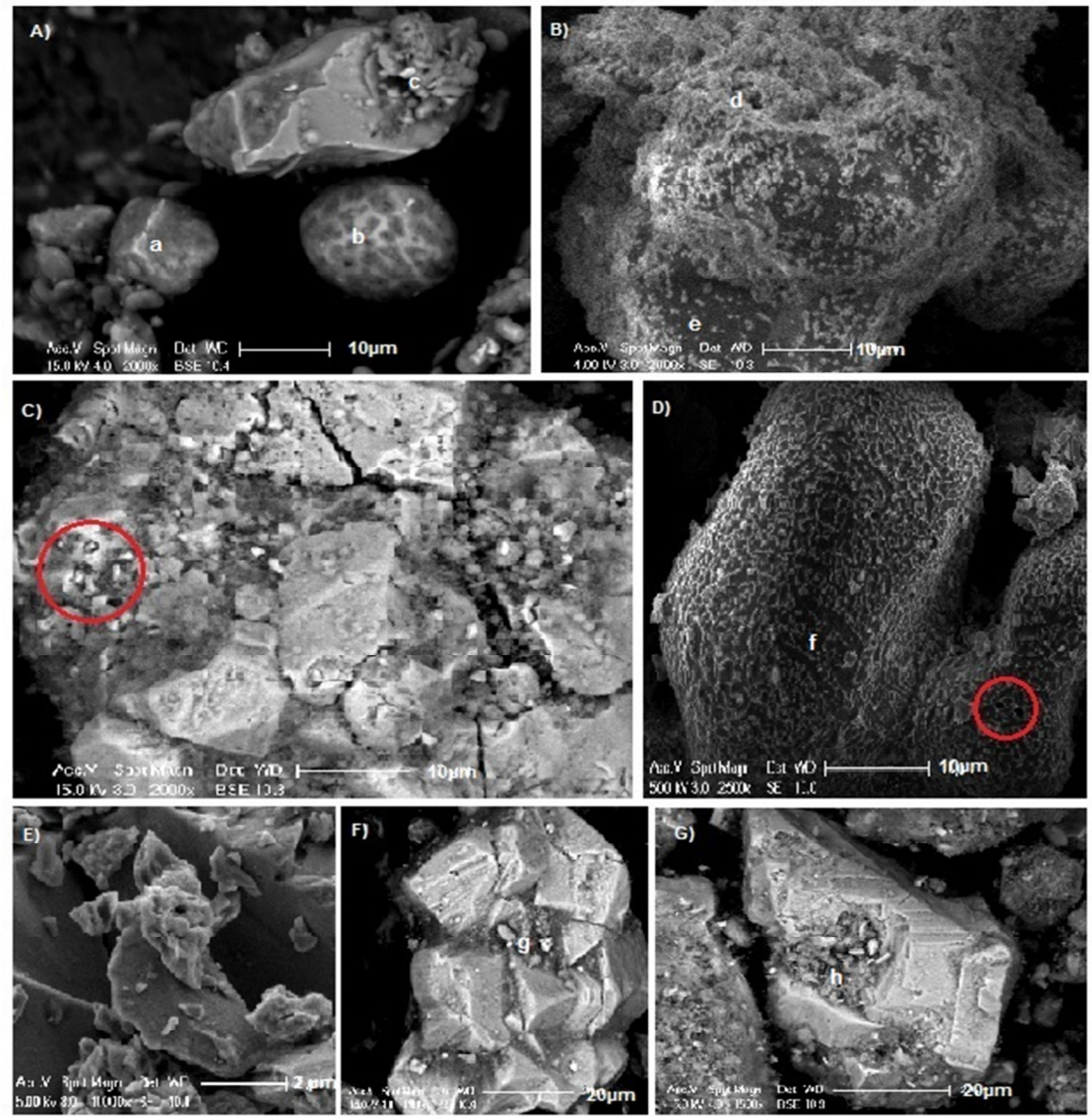


Figure 4.18 : SEM imaging of the surface of leached residue after six months of B1 and two months of B2/40 experiments: (A) Morphologies formed after chemical leaching. (B) Secondary precipitation in the presence of *A. ferrooxidans* in B1-Af experiment. (C) Rod shaped *A. ferrooxidans* in red circled area. (D) Deep holes (red circled) and irregular etched surface formed by mixed acidophiles in B1-E experiments. (E) Rose shaped secondary precipitate. (F) Relatively intact pyrite in B2/40-Af experiments. (G) Secondary precipitates (left), newly being oxidized surface (middle) and hexagonal quartz (top right) in B2/40-E experiments.

Figure 4.18B clearly demonstrates a secondary precipitate cover on leached minerals, produced after 180 days of bioleaching by *A. ferrooxidans* at 26^{o}C. Morphology of the precipitates are mostly globular with the exception of some cubic grains. It should be noted surface of chalcopyrite can become granular after some time (Zhao et al., 2013a) and this should not be mixed up with fresh precipitates. Regular or irregular fractures are also observed on pyrites (Figure 4.18C), while chalcopyrite surfaces are corroded by acidic conditions. Rod shaped and about a micron long bacteria are observed in bright color (white) and pits in the vicinity of them are probably due to bacterial activity (Figure 4.18C). The fact that no more bacterial cells were imaged via SEM can be attributed to the preference of bacteria to be attached to mineral right after inoculation (Harneit et al., 2006) and due to the long period between sampling and imaging, cells could be eliminated. At the same conditions, mixed culture of Fe and S oxidizers caused irregular grain shapes with etched surfaces; on which honeycomb like morphology and deep holes can also be observed (Figure 4.18D). Moreover, rose shaped and globular secondary precipitates are detected (Figure 4.18E).

A jump in the temperature to 40^{o}C did not cause any distinctive changes in the surface morphology. Such case is observed in Figure 4.18F as a pyrite twin still is intact in the presence of *A. ferrooxidans.* This could be attributed to a shorter period of leaching or longer period of bacterial adaptation to higher temperatures with decreasing leaching efficiencies (Chen and Shakhnovich, 2010; Karimi et al., 2010). However, extent of secondary precipitation increased with thicker layers of surface covers and more corroded chalcopyrite surfaces occurred. Figure 4.18G displays the morphological features in the presence of mixed acidophiles at higher temperatures. Thick layers of secondary precipitates (at left), most currently started to be oxidized grain (at middle with bright color) and a euhedral hexagonal quartz grain (upper left with darker color) can be observed.

EDS measurements coupled with SEM images revealed the chemical composition of secondary precipitates and changes in the massive sulfide chemistry after bioleaching (Table 4.5), also proving the presence of Cu sulfide phases which could not be detected by XRD analysis. Consistent with the XRD measurements, most of the precipitates are iron hydroxy-sulfates, pointing to the composition of jarosite. Some Zn rich composition with high amounts of Na and O is present along with rarely high

composition of Zn with S, indicating the presence of secondary Zn precipitates and sphalerite, respectively. Some measurements show co-precipitation of Al, Zn, Cu and Fe with a little extent of oxidation. Moreover, a Cr rich composition with high S content is detected, pointing to enrichment of Cr in a secondary chromium-sulfide phase.

Table 4.5 : EDS analysis (% concentration)of selected surfaces that were subjected to SEM imaging. Lower case letters represent analyzed surfaces displayed in Figure 4.18.

SEM image	Section	C	N	O	Cr	Na	Mg	Al	Si	P	S	K	Fe	Cu	Zn
4A	a	7,2	0,5	4,8	ND	1,2	0,2	6,0	0,3	0,7	8,1	0,3	65,8	3,2	1,9
4A	b	4,9	0,9	12,2	ND	0,2	0,3	0,5	0,5	2,3	67,1	0,7	7,6	1,6	1,2
4A	c	7,8	2,4	29,1	ND	0,6	0,3	1,2	0,7	2,4	15,2	3,6	33,4	1,7	1,7
4B	d	3,5	1,7	11,6	ND	0,7	ND	0,7	0,7	2,0	57,5	0,7	17,9	1,6	1,4
4B	e	0,4	0,4	3,3	ND	0,2	ND	0,4	0,6	1,4	42,5	0,5	47,4	1,1	1,8
4D	f	2,0	0,7	0,0	26,4	0,8	ND	ND	0,7	2,0	63,6	ND	1,5	1,5	1,1
4F	g	3,0	4,9	27,5	ND	0,7	0,8	0,5	0,8	2,5	19,9	3,0	34,3	1,7	0,5
4G	h	0,7	1,2	11,6	ND	0,4	0,4	0,4	0,9	2,0	24,0	2,4	49,7	3,3	3,0
6	İ	4,2	0,6	10,6	ND	0,2	ND	ND	14,0	1,0	30,3	ND	34,1	2,7	2,3

Overall chemistry of residue samples were determined using XRF and selected elemental compositions are listed in Table 4.6.

Table 4.6 : Selected elemental composition (%) of experimental residues collected after 6 months for B1 experiments and 2 months for B2 experiments, determined by XRF analysis.

Experiment	Fe	Cu	Zn	Co	S	Al	Pb	Ti	As	Mn	Ni	Mo	Cd	Sb
B1-Af	629	543	224	10,1	10,8	3,8	0,03	0,4	0,7	0,8	0,2	0,05	0,3	0,04
B1-E	1040	171	123	4,6	11,2	7,7	2,1	0,7	2,4	0,7	0,1	0,1	0,2	0,3
B1-C	162	985	462	10,8	10,8	2,4	0,04	0,4	0,03	0,3	0,1	0,05	0,6	0,3
B2/26-Af	141	1176	392	10,8	11,2	4,6	0,02	0,4	0,02	0,4	0,1	0,05	0,5	0,03
B2/26-E	1738	385	247	11,8	10,1	33,9	1,3	0,6	6,3	0,4	0,1	0,2	0,3	0,6
B2/40-Af	860	1236	483	16,2	11,4	8,2	0,03	0,5	0,7	0,4	0,2	0,05	0,6	0,05
B2/40-E	579	1166	412	11,7	9,2	12,3	0,04	0,4	0,2	0,5	0,1	0,05	0,5	0,05

4.3.2 Comparative leaching characteristics

Metal release ratios were calculated based on selected metals' prospective aqueous concentration per a liter medium and metal release in the aqueous media relative to

initial chemistry of each experimental set. Comparative metal release (%) for each condition is represented in Figure 4.19. Comparing all seven experiments, highest Cu release was about 31% via bacterial oxidation with *A. ferrooxidans* at 40°C, whereas Fe (13%), Co (8%) and Zn (15%) were released more efficiently by the Balya enrichment culture at 26°C. Moreover, negative values of Fe, Co and Zn were obtained from the post AMD stage (B2/26 and B2/40) experiments, indication temporary inhibition at the leaching abilities of pure and mixed cultures.

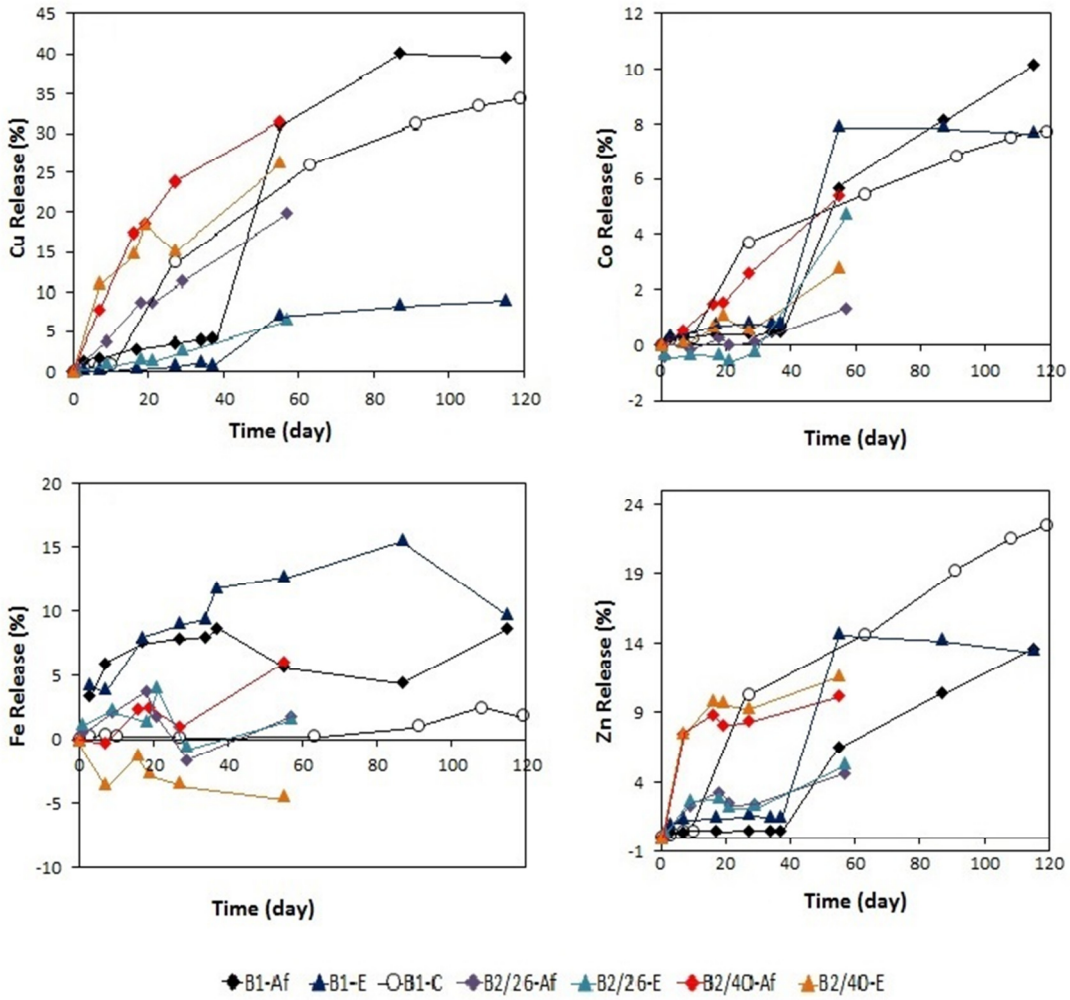


Figure 4.19 : Comparative metal release efficiencies of all experiments, in terms of heavy metal release ratio (%) calculated from metal concentrations in the solution relative to initial metal concentrations in the massive sulfide ore.

On the other hand, longer term biological and chemical AMD generation (B1) experiments revealed that the maximum Fe (16%) was released also by the enrichment culture at 26°C. However, the highest release ratio of Cu (40%) was obtained in the presence of *A. ferrooxidans*, which showed a great increment after the

first 34th day of the acid generation stage. This could explain why we could not catch any XRD peaks of chalcopyrite in the presence of pure cultures of the iron oxidizer. It is also noteworthy that the differences between bacterial and chemical removal ratios were not significant, as also observed by Bevilaqua et al. (2014). Decreases in Cu release ratios could be attributed to co-precipitation with jarosite, as also discussed by Zhao et al. (2013a). Furthermore, Co release (10%) peaked by *A. ferrooxidans* at the end of the experiments and it is evident that Zn tends to be released considerably more by chemical leaching in long term, which revealed an approximate release ratio of 23%.

Bioleaching is affected by several factors, which have been studied or reviewed by many authors, like pH and Eh of the solution, mineralogy of the ore mineral and presence of gangue phases, precipitation and dissolution of secondary minerals, pulp density, availability of oxidants and nutrients, temperature, presence of catalysts, amount of ferric iron and attachment of bacterial cells to the mineral surface (Stott et al.; 2003; Schippers, 2004; Watling, 2006; Dopson et al., 2006; Akçıl et al., 2007; Ahmadi et al., 2011; Feng et al., 2013; Dong et al., 2013a, 2013b, 2013c; Li et al., 2013; Bevilaqua et al., 2014; Nazari et al., 2014). One of the most important factors affecting leaching abilities of bacterial culture is the passivation effect (Hackl et al., 1995; Klauber et al., 2001). Many authors reported the precipitation of iron-hyroyxsulfate phases like potassium jarosite, elemental sulfur, covellite or copper polysulfides, which decreased the area on mineral surface to be reached by bacteria (Stott et al., 2000; Third et al., 2000; Klauber et al., 2001; Bevilaqua et al., 2002; Córdoba et al., 2009; Ahmadi et al., 2010, 2011; Nazari et al., 2014). Some cases showed a loose precipitation of secondary products, causing a little passivation effect (Gu et al., 2013). In this study, extent of passivation can be detected both from the chemical shifts in the solutions or from the mineralogy of the residue. Below zero values in metal removal ratios in Figure 4.19 is a sign of precipitation, which also indicates co-precipitation or simultaneous precipitation of Zn and Co with Fe. As evident from Figure 4.18B and Figure 4.18G, mineral surfaces are tightly covered with passivating layers, which turned out to be mostly K-jarosite according to EDS and XRD measurements of all samples. Similar results obtained from mineralogical compositions (Figure 4.17) may prove the point stated by Pan et al. (2012)'s, indicating no changes occur in the mineralogy due to increased leaching periods,

regardless some physical changes on the surface (Ohmura et al., 1993). Even was not detected in XRD diffractograms, ammonium jarosite may be present due to relatively high nitrogen levels combined with K, S and Fe, deducted from some EDS results (Table 4.5). Moreover, Parker et al. (2003) reported not detecting any copper sulfide phase from their experiments (He et al., 2012). However, intermediate copper sulfides may be present according to our EDS results but, did not have an effect on passivation due to their low abundance. Furthermore, synergistic activity of Fe and S oxidizing bacteria are noted, as sulfur oxidizers are able to remove S bearing passivating layers and leaching efficiencies are enhanced in the presence of mixed cultures (Norris, 1983; Rohwerder et al., 2003; Stott et al., 2003; Akçıl et al., 2007). Therefore, passivation inhibited mostly the activity of *A. ferrooxidans* pure cultures in our experiments. Sulfur measurements were disregarded in terms of passivation due to external addition to the system. Chemical leaching experiments showed nearly all secondary precipitates due to XRD measurements, including schwertmannite. However, no significant passivation was observed considering our SEM imaging of chemical control experiments (Figure 4.18A) that only showed loosely precipitated secondary minerals, not a continuous layer coating the mineral surface.

Iron-hydroxysulfate precipitation controls the range of pH in the solution during experiments, which is important for the stability of secondary minerals and the activity of bacteria (He et al., 2012). Likewise, highly acidic conditions may help the prevention of secondary precipitation of ferric iron to some extent (Feng et al., 2013), as precipitation is not favored at pH values around pH 1 (Stott et al., 2000). However, limited bacterial activity in low pH conditions was also noted (Deveci et al., 2004; Xia et al., 2012). Above a pH value of 2, jarosite precipitation is reported by several authors (Stott et al., 2000; Mehta and Pandey, 2013). This can be the case for passivation we observed in the presence of *A. ferrooxidans* that generated pH values between 2,3 and 4,1 (Figure 4.13a). On the contrary, more acidic conditions created by enrichment cultures (pH 1,32 – 2,13) might have hindered secondary precipitation to some extent, combining with the efficiency of metal removal. It is well-known that if AMD waters encounter an aqueous system with a higher pH value, secondary precipitation is promoted (Stumm and Morgan, 1996; Munk et al., 2002; Lottermoser, 2010). Therefore, when relatively more acidic leachates of B1 experiments were introduced to a fresh medium, an immediate increase in pH should

have stimulated ferric iron precipitation which resulted in a higher extent of passivation for B2 experiments (Figure 4.13b and Figure 4.13c).

Temperature is a well-known effect to bioleaching systems, which is generally known for enhancing the chemical leaching rates and dissolution if increasing (Stott et al., 2003; Akçıl et al., 2007; Dreisinger et al., 2007). Higher Zn and Cu release ratios (Figure 4.19) at higher temperatures (B2/40) can be attributed to increased chemical oxidation, relative to the moderate temperature experiments with same chemical conditions (B2/26). Elevated temperature is also an accelerator for secondary precipitation, thus passivation (Gomez et al., 1999). This effect can clearly be observed from Fe precipitation at higher temperatures (Figure 4.19) and SEM images of related experiments (Figuure 4.18G). It can be deducted that elevated temperature significantly inhibited Fe and Co release rates of mixed cultures. This can also be explained by lower temperatures promoting pyrite oxidation (Petersen and Dixon, 2006), which was the dominant sulfide phase in the massive ore. However, *A. ferrooxidans* seems to be relatively unaffected, besides some fluctuations in removal ratios, indicating tolerance to relatively high temperatures compared to symbiotically living mixed acidophiles.

In order to get better leaching rates, bioleaching experiments are generally set up with adapted cultures to environment or to the material to be leached. Karimi et al. (2010) noted that thermally adapted bacteria could have adjusted to higher temperatures faster than un-adapted cultures and leaching rates could have been better. It is suggested that excessive heavy metal concentrations could be toxic to bacterial cells (Li and Ke, 2001). However, cultures adapted to a specific metal are shown to be better at leaching that metal (Xia et al., 2008; Karimi et al. 2010). Studies point out differences in the proteins of adapted on un-adapted bacterial cells (i.e. Das et al., 1998; Xia et al., 2008). Xia et al. (2008) described the relationship between adaptation and cell attachment as increasing protein concentration leading to increasing positive cell-surface charges that promotes attachment in return. Mixed enrichment cultures used in our experiments being more effective in leaching Zn (Figure 4.19) can be attributed of their adaptation to a Zn rich-environment, as they were initially isolated from an AMD water resulted from Pb-Zn mining (Çelik-Balcı et al., 2014). Nevertheless, B2/26 experiments displayed a decrease in metal release ratios; even they were adapted to the temperature and metal concentrations in their

surrounding environment. Only judging by the metal releasing efficiencies, this can be explained by the secondary precipitation and simultaneous precipitation of metal species with ferric iron. It is also noteworthy that adaptations generally take place in a short period of leaching with lower pulp densities; unlikely our B1 experiments with long duration and B2 experimental media were inoculated by cultures with low bacterial activity, which is more suitable to represent the lifespan of bacteria in mixing zones of natural AMD systems.

The other fact that could have affected the efficiency of bacterial leaching is externally added elemental sulfur to the system. The idea was to create an unexpected environment for the bacteria, which may represent the contact zones of AMD and mining wastes. As there is no control experiment without additional sulfur, no judgments can be made with the existing data. However, effect of additional sulfur on leaching efficiency is one of the studied subjects by other authors. Results of Xia et al. (2012) showed that about 3 g/L of additional sulfur was beneficial for metal recovery; nonetheless, excessive portions about 6 g/L inhibited the process. It is also believed that additional sulfur was beneficial for sulfur oxidizing ability of bacteria, where iron oxidizing ability of them were limited (Dopson and Lindstrom, 2004; Xia et al., 2012). Nevertheless, *A. ferrooxidans* can still the dominant culture at the end of the leaching process (Xia et al., 2012). In our experiments, bacteria could have chosen to oxidize the elemental sulfur instead of the ore minerals; as explained by Gomez et al. (1996) for initial concentrations of Fe (II). The fact that there were still intact particles of metal sulfides may be attributed to the selective leaching behavior of the bacterial cultures, while pH was still decreasing due to the continuous production of sulfuric acid (Bevilaqua et al., 2002). Moreover, bacteria in B2 experiments could have continued to oxidize the particles that they were readily attached onto and carried by the leachate inoculum from B1 experiments. On the other hand, low pH conditions resulted from elemental sulfur oxidation may have postponed the passivation effect to later stages (Xia et al., 2012) for AMD generation experiments.

4.3.3 Implications on microbial oxidation mechanisms

This study showed the presence of “rod-shaped erosion pits” (Figure 4.20) that are compatible with bacterial cell shapes (Jiang et al., 2008), which can be interpreted as

a proof of contact leaching (Zhao et al., 2013a). “Deep holes” on mineral surfaces (Figure 4.18D) were interpreted as a sign of ferric iron attack by Zhao et al. (2013a), which they also observed on chemical controls. However, our chemical control experiments displayed broader and shallow concavities, in contrast to biologically produced nearly circular and narrow deep pits. Those deep holes from biotic experiments still could be resulted from ferric iron attack but, our results may be pointing to localization of ferric iron within the EPS of bacterial cells and affecting a relatively small area on the mineral surface. Therefore, they are interpreted as indicators for the contact bioleaching mechanism.

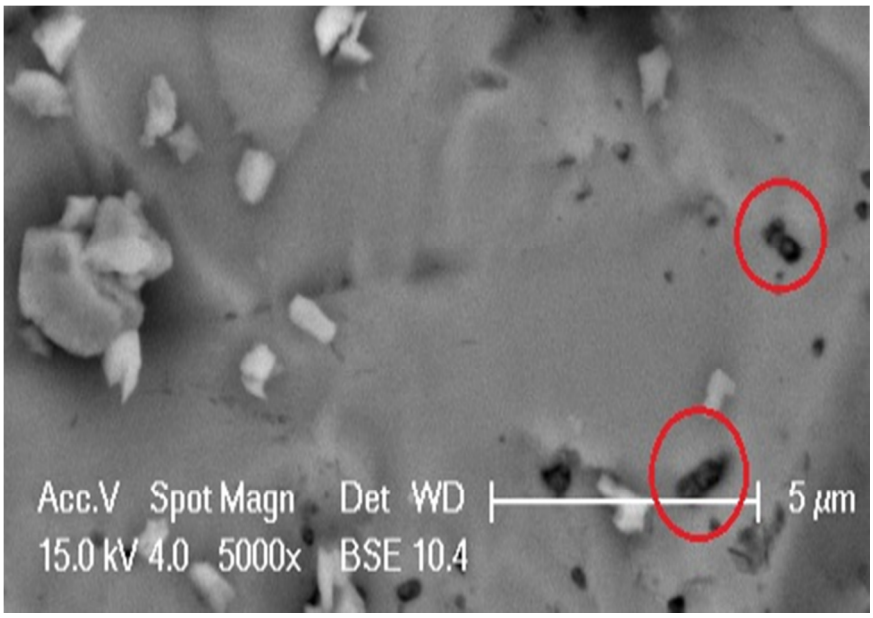


Figure 4.20 : About a micron long rod-shaped erosion pits (red circled) that were observed on the ore surface, in the presence of mixed acidophilic enrichment culture.

4.4 Geochemical and Mineralogical Features of the Küre Mining Environment

4.4.1 Water chemistry

Selected chemical and physical parameters of the groundwater samples (GW1-5), which were collected from 780 m, 725 m, 690 m, 630 m and 512 m elevations (above sea level) in Bakibaba tunnels, respectively; and drinking water samples (DW1 and DW2) are listed in Table 4.7. Concentrations of heavy metals in the groundwater samples are strictly dependant on pH values (2,9 – 8,3) and indirectly dependent on the proximity to sulfur bearing content. Groundwater samples with low pH values are enriched in Mn, Fe, Co, Cu and Zn; reaching up to 15450, 19600,

1990, 130 and 9940 ppb, respectively. Interestingly, groundwater SO_4^{2-} concentrations above 700 m elevation show positive correlation with pH, having the highest concentration of 1250 mg/l at pH 7, which may be as a consequence of bacterial processes. Below 700 m, SO_4^{2-} concentrations follow a similar trend with heavy metals. Below 650 m elevation, groundwater is neutral to alkaline and relatively uncontaminated, considering the distance to the ore and sulfur rich lithology. Waste effluent chemistry indicates that water quality can be increased to some level by neutralization, with Mn, Fe, Co, Cu and Zn concentrations decreasing down to 1840, 60, 150, 580 and 170 ppb, respectively and SO_4^{2-} concentrations to 650 mg/l. When acidic groundwater reaches to surface, Fe and Zn concentrations decrease down to 4070 and 5580 ppb, respectively. This suggests immediate precipitation of Fe with Zn, also showing those metals' sensitivity to shifting redox conditions. Fe precipitation can also be visually observed at sampling points as reddish crusts, as shown in Figure 3.2d and Figure 3.2e.

Investigated stream waters of Küre district had characteristics of moderately acidic or neutral mine drainage waters with pH values ranging from 3,7 to 8,1; redox potential (Eh) values ranging from 243 to 495 mV; and electrical conductivity (EC) values ranging from 454 to 3870 µS/cm as listed in Table 4.7. Moderately acidic mine drainage waters of Karanlık Stream and drainage from the open-cut mine have an average pH value of 3,95 (n=9) with high concentrations of SO_4^{2-} (1600-3050 mg/L), Al (99,3-325,6 ppm), Cu (21,3-40,4 ppm), Mn (13,8-30,5 ppm), Zn (5,3-9,4 ppm), Co (3,9-7,6 ppm), Fe (1,4-6 ppm) and relatively lower concentrations of Ti (576-926 ppb), Sr (467-715 ppb) and Ni (450-716 ppb). Polluted Zemberekler River (PRW) nd relatively unpolluted Küçükali Stream (USW) are characterized with pH values of 7,9 and 8,1; and chemical composition of SO_4^{2-} (650 and 100 mg/L), Al (1711 and 670 ppb), Cu (3662 and 371 ppb), Mn (4729 and 87 ppb), Zn (2308 and 175 ppb), Co (1172 and 23 ppb), Fe (280 and 163 ppb), Ti (839 and 129 ppb), Sr (707-259 ppb) and Ni (93-8 ppb) (Table 4.7).

4.4.2 Geochemical and Mineralogical Characterization of Streambeds

XRF, XRD, SEM and EDS results are presented in this chapter.

4.4.2.1 Bulk chemistry of the sediments and secondary precipitates

Selceted elements of the bulk chemistry of the sediment and ochre samples are presented in Table 4.8. Moderately acidic mine drainage streambed sediments were found to be rich in Fe, S and Cu; with Fe values ranging from 11 to 15,5%; detectable S values ranging from 1,3 to 2,1% and Cu values ranging from 0,1 to 0,25%. Detectable average Al (1,2%), Ti (0,35%), Ag (0,1%), Mn (0,1%), Cr (0,05%), Pd (0,05%), Sn (0,05%), Cd (0,04%), and Sr (0,04%) compositions exceed the values in the massive ore (Mn: 0,01%, Sr: 0,01, Sn: 3 ppm;Al, Ag, Ti, Cd, Pd and Cr were not detected in the ore composition). Lowest concentrations of heavy metals were observed in the relatively unpolluted Küçükali Stream sediments; whereas, highest concentrations were observed in the sediments of polluted and slightly alkaline Zemberekler River.

4.4.2.2 Mineralogy of the sediments and secondary precipitates

Mineralogical compoitions of AMD streambed sediments are illustrated in Figure 4.21 and XRD diffractograms of rest of the sediment (S7 and S8) and ochre samples (Ochre1, Ochre2 and GFe) are shown in Figure 4.22.

Main ore minerals pyrite and chalcopyrite were present nearly in all of the samples' mineralogical compositions with sphalerite as another sulfide phase. Jarosite, schwertmannite and goethite were the main secondary iron precipitates of AMD stream sediments. Other secondary products can be listed as gypsum, which is present in every sample, and gibbsite detectable only in samples of certain successive locations. Neutral and relatively clean Küçükali Stream (USW) only displayed ferrihydrite, considering stability limits depending on the water pH. Quartz, albite, chlorite, kaolinite, illite, fluoro-edenite and some metal bearing (Zn, Sr, Al and Fe) clay minerals were the gangue phases, probably originating from the lithological units of the drainage waters.

SEM imaging of the AMD streambed ochre (Ochre1) and the gravel crust ochre (GFe) samples (Figure 4.23 and Figure 4.24, respectively) displayed various morphologies changing from nearly intact subhedral grains to anhedral grains with completely disturbed surfaces.

Table 4.7 : Selected physicochemical parameters and chemical compositions of the surface water, groundwater and drinking water samples representing the Küre mine drainage environment.

Sample	AMD1	AMD2ave	AMD3	AMD4ave	AMD5	AMD6	AMD7	DW1	DW2	GW-1	GW-2	GW-3	GW-4	GW-5	MWW	PRWave	USW	WEW
pH	3,7	3,8	4,0	4,1	4,2	3,8	4,1	7,1	7,5	2,9	7,1	4,5	7,9	8,3	7,8	7,9	8,1	7,7
Eh (mV)	494,7	464,6	410,7	413,4	319,0	446,2	432,9	232,3	184,5	544,4	237,8	255,7	168,3	164,9	226,3	301,4	243,8	118,7
EC (µS)	3870	3385	3320	2930	2740	3200	2970	584	356	2880	2670	2280	890	342	1620	1860	454	3490
SO_4^{2-} (mg/L)	3050	2425	2200	2400	1600	1600	1950	150	200	1050	1250	700	400	300	650	650	100	650
Ti (ppb)	645	576	584	585	605	926	889	207	133	ND	ND	ND	ND	ND	652	839	129	ND
Al (ppb)	325600	261800	267600	273000	249800	111180	99300	603	717	ND	ND	ND	ND	ND	339	1711	670	ND
Cr (ppb)	18	37	14	21	14	6	4	0	0	3	1	2	2	3	0	38	0	ND
Mn (ppb)	21720	30481	18766	24592	17714	15380	13836	42	50	15450	5204	8226	168	4	4216	4729	87	1841
Fe (ppb)	6042	5408	3472	2172	4300	1419	2236	204	128	19602	193	12381	305	29	365	280	163	58
Co (ppb)	5866	7545	5052	6223	4744	4198	3850	17	17	1992	284	871	3	0	224	1172	23	150
Ni (ppb)	585	716	484	560	470	481	450	7	2	97	10	52	ND	ND	29	93	8	22
Cu (ppb)	28500	40409	22920	32149	21260	27800	26940	263	145	131	2	5	7	2	548	3662	371	578
Zn (ppb)	6924	9410	5626	7837	5292	8534	8622	405	65	9942	46	687	17	15	425	2308	175	169
Sr (ppb)	715	618	635	568	629	506	467	117	31	253	287	270	99	99	599	707	259	1275
Cd (ppb)	29	31	25	26	24	27	26	9	9	13	8	7	8	8	11	12	9	9
Pb (ppb)	29	15	14	8	11	15	12	9	10	8	2	2	3	1	10	11	8	3
As (ppb)	3	3	1	3	1	3	4	8	0	3	1	1	5	7	3	3	1	3

Table 4.8 : Selected elemental compositions (%) of the riverine sediments and ochre precipitates and the ochre crustation on gravels.

Sample	Fe	Cu	S	Zn	Co	Al	Ti	Mn	Cr	Pd	As	Zr	V	Ag	Cd
S1	13,6	0,12	2,05	0,018	0,02	1	0,31	0,1	0,06	0,06	0,004	0,004	ND	0,15	0,07
S2	12,8	0,12	2,1	0,02	0,01	1,25	0,4	0,1	0,05	0,06	0,003	0,006	0,07	0,13	ND
S3	11,8	0,1	2,3	0,01	0,009	1,2	0,3	0,1	0,04	ND	ND	0,005	0,04	0,03	0,005
S4	11,3	0,12	1,3	0,02	0,02	1,3	0,3	0,1	0,08	0,04	0,003	0,007	0,06	0,11	0,05
S5	11	0,1	ND	0,02	ND	1,5	0,4	0,1	0,04	0,02	ND	0,004	ND	0,03	0,03
S6	15,5	0,25	ND	0,03	ND	1	0,4	0,1	0,05	0,07	0,006	0,005	ND	0,16	ND
S7	15,5	0,6	11	0,13	0,17	2,5	0,3	0,15	0,03	0,05	0,01	0,004	0,06	0,2	ND
S8	4,5	ND	ND	0,01	ND	1,6	0,4	0,11	0,03	0,05	ND	0,02	0,04	0,03	0,05
Ochre1	30	0,7	4,6	0,03	0,03	ND	0	0,02	0,03	ND	0,02	ND	ND	ND	ND
Ochre2	20,9	0,3	2,5	0,02	0,03	ND	0,4	0,1	0,02	0,04	0,004	0,003	0,03	0,06	0,16
Gfe	20	0,1	3	0,02	ND	ND	0,25	0,06	0,05	ND	ND	ND	0,01	0,04	ND

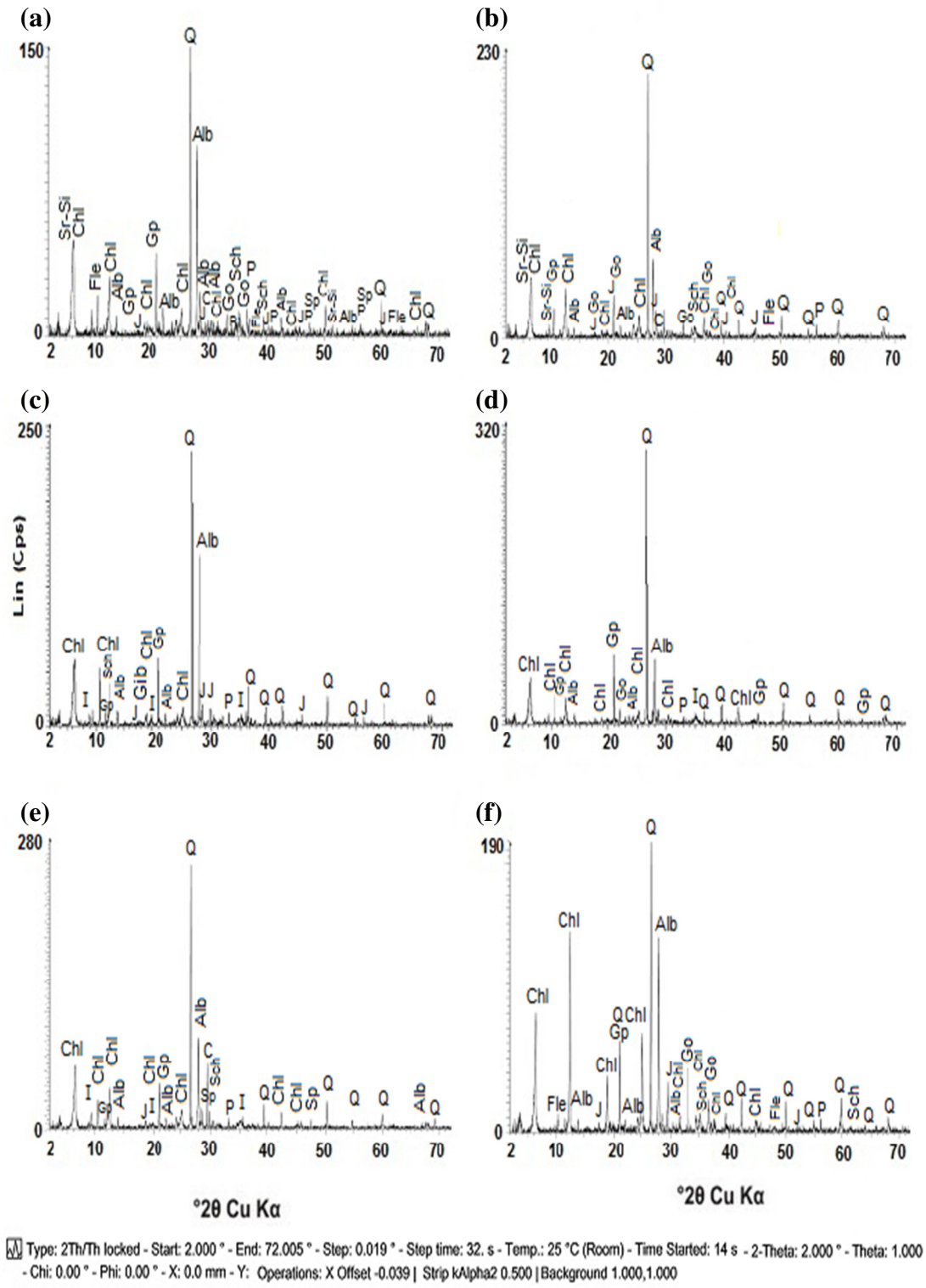


Figure 4.21 : X-ray diffractograms of AMD streambed sediments (Alb: Albite, C: Chalcopyrite, Chl: Chlorite, Fle: Fluoro-edenite, Gib: Gibbsite, Go: Goethite, Gp: Gypsum, I: Illite, J: Jarosite, P: Pyrite, Q: Quartz, Sch: Schwertmannite, Sp: Sphalerite, Sr-Si: Strontium Aluminum Ammine Silicate): (a) S1. (b) S2. (c) S3. (d) S4. (e) S5. (f) S6.

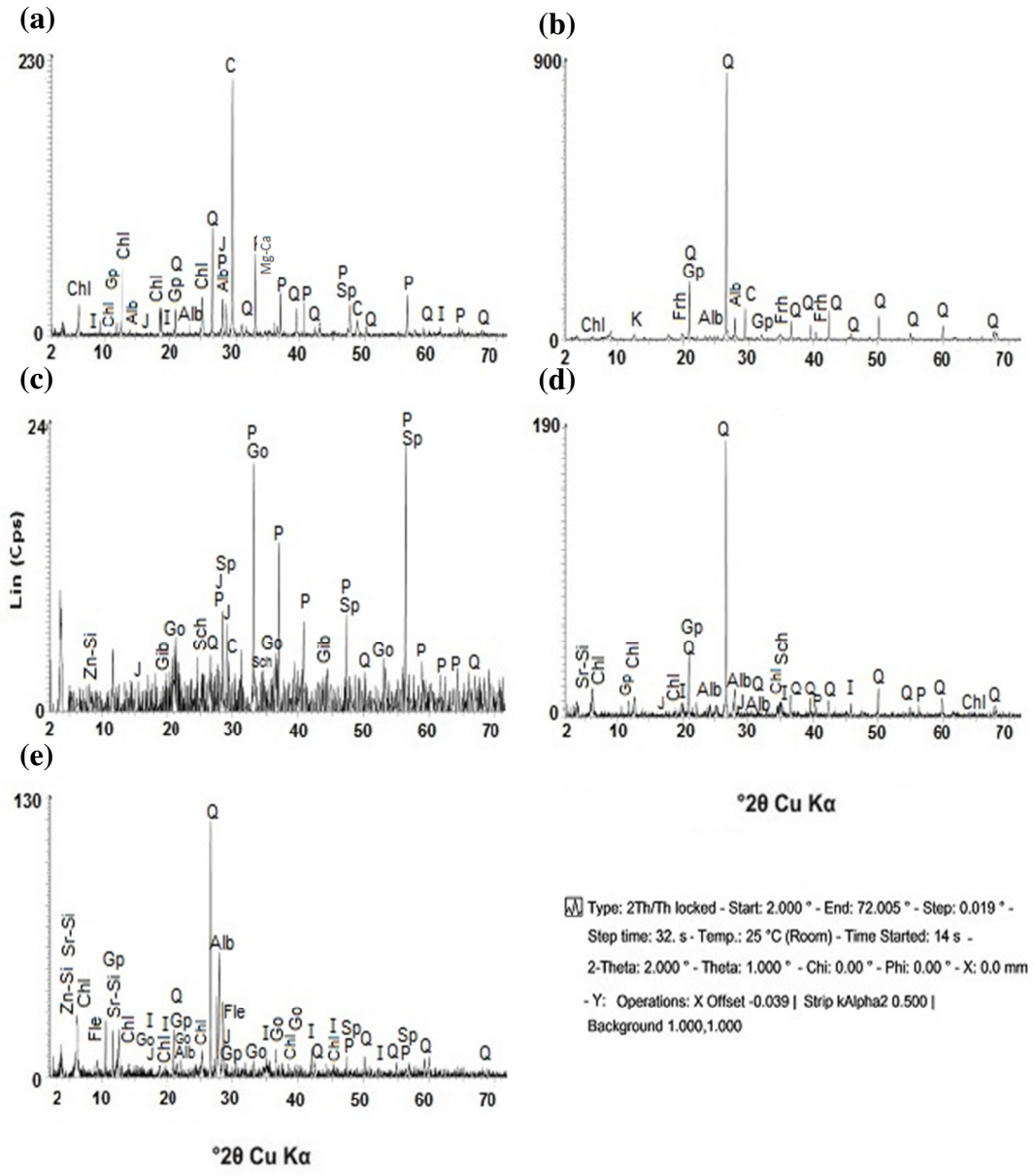


Figure 4.22 : X-ray diffractograms of neutral-alkaline streambed sediments and ochre samples (Alb: Albite, C: Chalcopyrite, Chl: Chlorite, Fle: Fluoro-edenite, Frh: Ferrihydrite, Gib: Gibbsite, Go: Goethite, Gp: Gypsum, I: Illite, J: Jarosite, K: Kaolinite, Mg-Ca: Mg-bearing calcite, P: Pyrite, Q: Quartz, Sch: Schwertmannite, Sp: Sphalerite, Sr-Si: Strontium Aluminum Ammine Silicate, Zn-Si: Zinc Hydronium Aluminum Silicate Hydroxide): (a) S7. (b) S8. (c) Ochre1. (d) Ochre2. (e) GFe.

Grain size of the samples is ranging from 1 to 100 µm, which can be approximately detected from scales of the images. Generally, mineral grains are covered with globular or cloudy secondary formations of irregular morphologies. Moreover, one akaganeite-like tubular morphology (Figure 4.23) was observed, with relatively bigger size (Richmond et al., 2006).

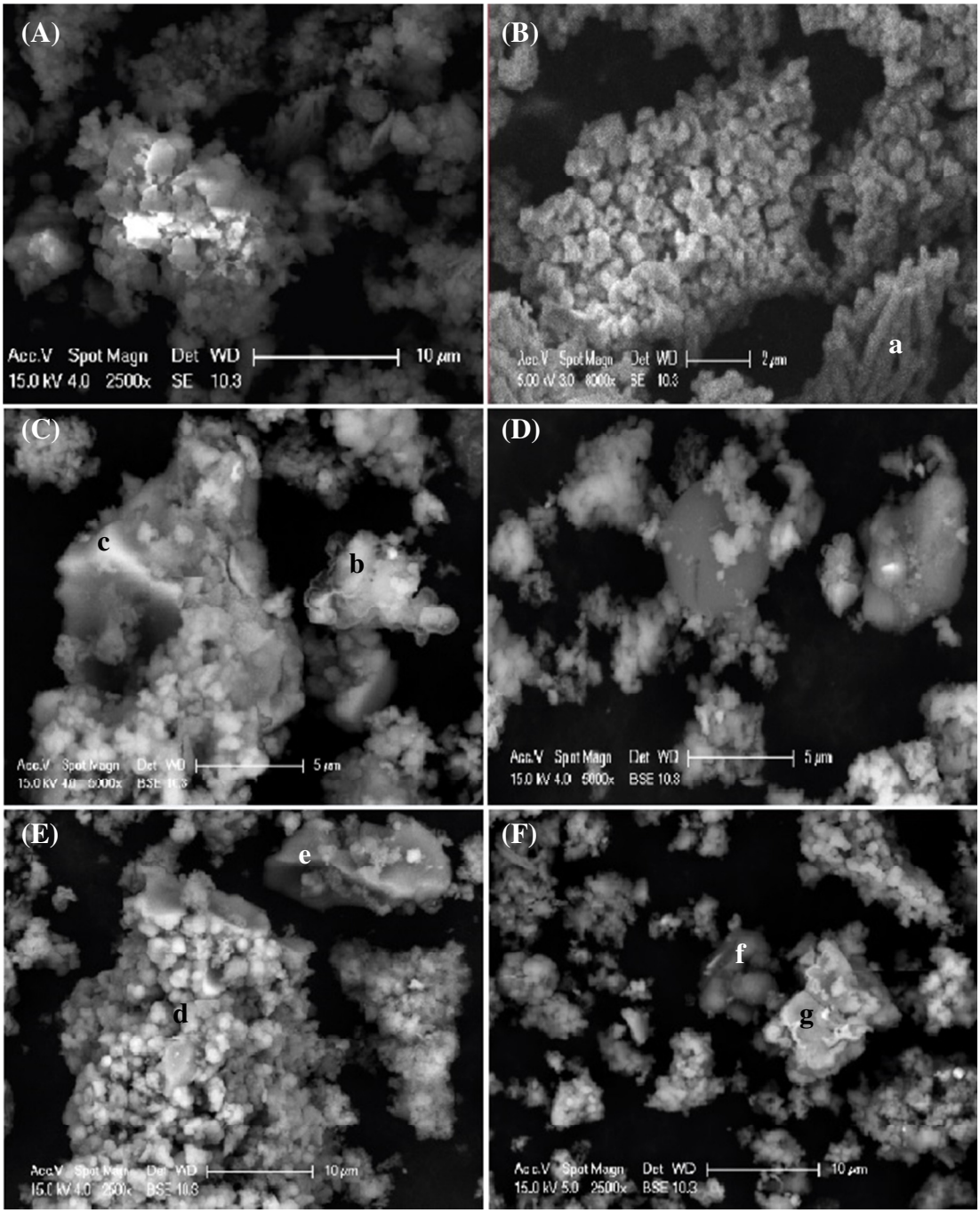


Figure 4.23 : SEM images of the Ochre1 sample: (A) Different morphologies of secondary ochre precipitates in AMD environment. (B) A closer look to Figure 4.24A (by 5 fold): Jarosite (at left-center) and tubular akageneite-like mineral (at bottom-right). (C) Spherical or globular secondary precipitation (possibly gibbsite) around a mineral grain (possibly pyrite). (D) Gibbsite, some metal (Cu, Fe and Zn) sulfides or hydroxides/hydroxysulfates and an unidentified spherical (spore-like) morphology. (E) Al, Cu and Zn bearing secondary Fe hydroxide/hydroxysulfate precipitates (due to combined EDS results; see Table 4.9). (F) Fe and Al hydroxides/hydroxysulfates (jarosite, goethite, gibbsite, etc.) precipitates (Table 4.9).

EDS measurements coupled with SEM imaging (Table 4.9) pointed generally to chlorite group clay minerals, which can be detected by high Si content with Fe, Mg and Al that are mainly corresponding to clinochlore or chamosite's chemical formula (also supported by XRD); whereas high Fe with O and S content may point to secondary iron precipitates. Enrichment of S, Zn and Cu can be locally detected. Moreover, some minerals are rarely enriched in Sr.

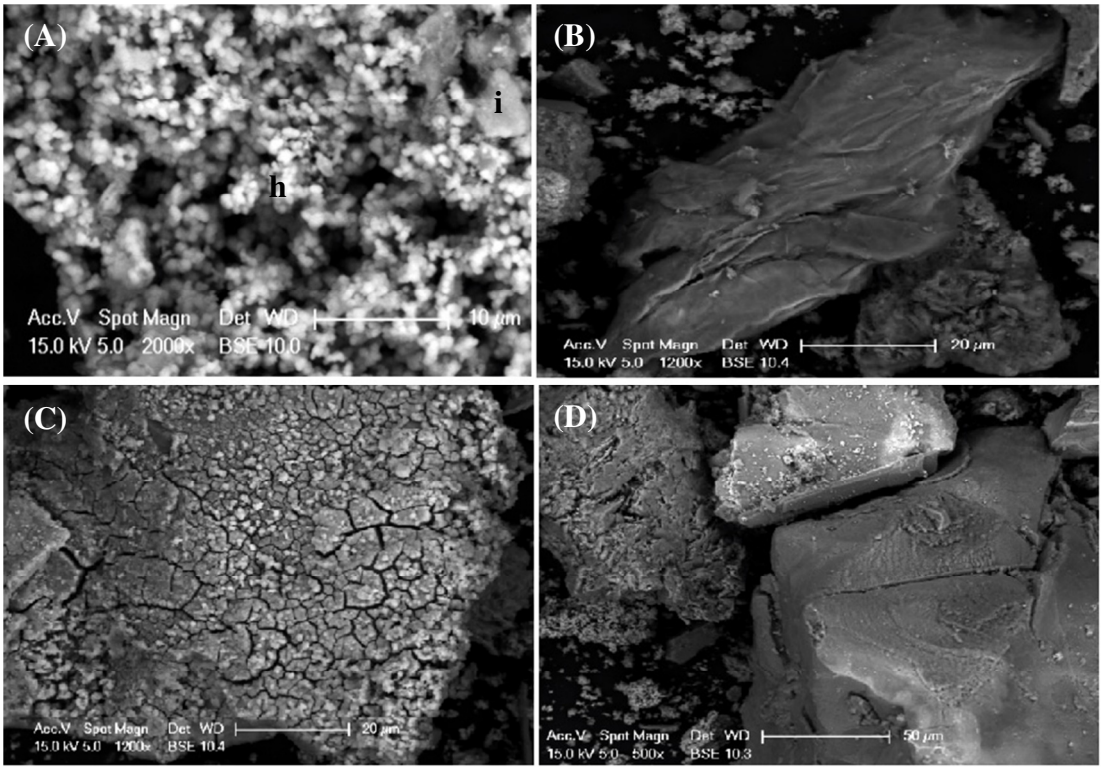


Figure 4.24 : SEM images of the GFe sample: (A) Spherical Fe hydroxide/hydroxysulfate precipitates. (B) Chlorite (probably clinochlore due to EDS results) with secondary precipitates. (C) Fe, Al-silicate (clay) mineral with tension cracks and secondary precipitation on its surface. (D) Deformed Fe, Al-silicate (clay) minerals and surrounding secondary precipitates.

4.4.3 Simulated Geochemical Shifts in Mixing Zones

To evaluate the changes in chemistry in mixing zones of acidic streams and liquid municipal wastes; acidic and neutral streams or neutralization of acidic streams, titration experiments were conducted on AMD-1 and AMD-7 using MWW and USW or 0,1M NaOH as titrants, respectively. Considering original samples were filtered while sampling, experiments were assumed to be representing only chemical mechanisms operating in mixing zones and maximum level of metal precipitation.

Table 4.9 : EDS results (% mass concentration) of selected sections of SEM images. Lower case letters represent analyzed surfaces displayed in Figure 4.24 and Figure 4.25.

SEM image	Section	C	N	O	Na	Mg	Al	Si	P	S	K	Ca	Fe	Cu	Zn
Figure 4.24A	Overall	22,1	2,0	31,7	0,1	0,4	12,0	2,4	0,3	4,4	0,3	ND	21,8	1,7	0,8
Figure 4.24B	a	27,9	1,6	19,0	0,0	0,3	4,2	1,4	0,2	2,0	0,2	0,2	40,2	2,3	0,7
Figure 4.24C	b	12,1	2,8	26,4	0,8	0,9	7,7	3,8	0,4	3,4	0,1	0,3	38,5	1,7	1,1
Figure 4.24C	c	10,0	1,7	22,0	0,1	0,4	6,6	1,7	0,2	4,1	0,1	0,3	49,9	1,9	1,0
Figure 4.24D	Overall	14,3	2,7	35,4	0,2	0,6	28,8	2,8	0,4	8,0	0,3	0,4	3,2	1,9	1,1
Figure 4.24E	d	7,1	3,8	38,2	0,8	1,0	9,2	1,8	0,6	5,7	0,3	0,6	28,5	1,6	1,0
Figure 4.24E	e	11,5	1,7	17,7	0,2	0,3	11,2	1,3	0,4	6,9	0,4	0,5	44,1	2,5	1,5
Figure 4.24F	f	7,9	2,5	36,2	0,2	0,9	23,1	11,0	0,2	4,3	0,3	0,5	11,1	1,4	0,4
Figure 4.24F	g	3,9	1,8	23,0	0,2	0,4	2,9	1,0	0,3	3,0	0,23	0,3	58,9	2,6	1,4
Figure 4.25A	h	3,1	2,4	23,7	0,2	0,5	1,9	1,0	0,6	7,9	0,3	ND	54,9	1,4	1,4
Figure 4.25A	i	18,9	1,7	18,5	0,2	0,3	1,0	0,8	0,3	5,2	0,3	0,5	50,0	1,3	1,1
Figure 4.25B	Overall	2,7	3,2	36,3	0,9	16,2	5,9	23,7	0,5	0,6	0,3	0,6	7,4	0,8	1,0
Figure 4.25C	Overall	4,0	3,0	30,3	1,2	0,8	6,7	9,0	0,5	5,2	0,2	0,9	35,7	1,1	1,5
Figure 4.25D	Overall	5,3	2,9	32,2	0,8	4,3	11,6	19,8	0,5	0,7	0,2	0,2	20,7	0,7	0,3

Adequate amounts of solid precipitates were not obtained for geochemical and mineralogical analysis. Therefore, chemical shifts in solutions were used as a proxy to predict the amount of metal scavenging by precipitation relative to initial concentrations. NaOH titration was used like a control experiment as it would represent the possible maximum precipitation at similar laboratory simulated conditions. Results revealed that MWW mixing to AMD-7 and USW mixing to AMD-1 causes serious proportions of Fe (93% and 90,7%), Cr (90,3% and 80,4%), Al (73,5% and 42,2%) and As (73,8% and 67,4%) precipitation on the streambed sediments, as well as considerable proportions of Co (22,7% and 33,2%), Mn (13,3% and 32,7%), Zn (34,3% and 28,1%), Ni (16,7% and 37,8%) and Cd (16,6% and 25,6%). Those results are below the values obtained from NaOH titration, indicating relative accuracy of the method. Only unexpected result is the increase in Sr concentrations by 11,1% in AMD-7 via MWW titration, whereas titrating AMD-1 using USW as a titrant caused 23,8 precipitation. Initial and final metal concantrations before and after titration experiments are comparatively displayed in Figure 4.25.

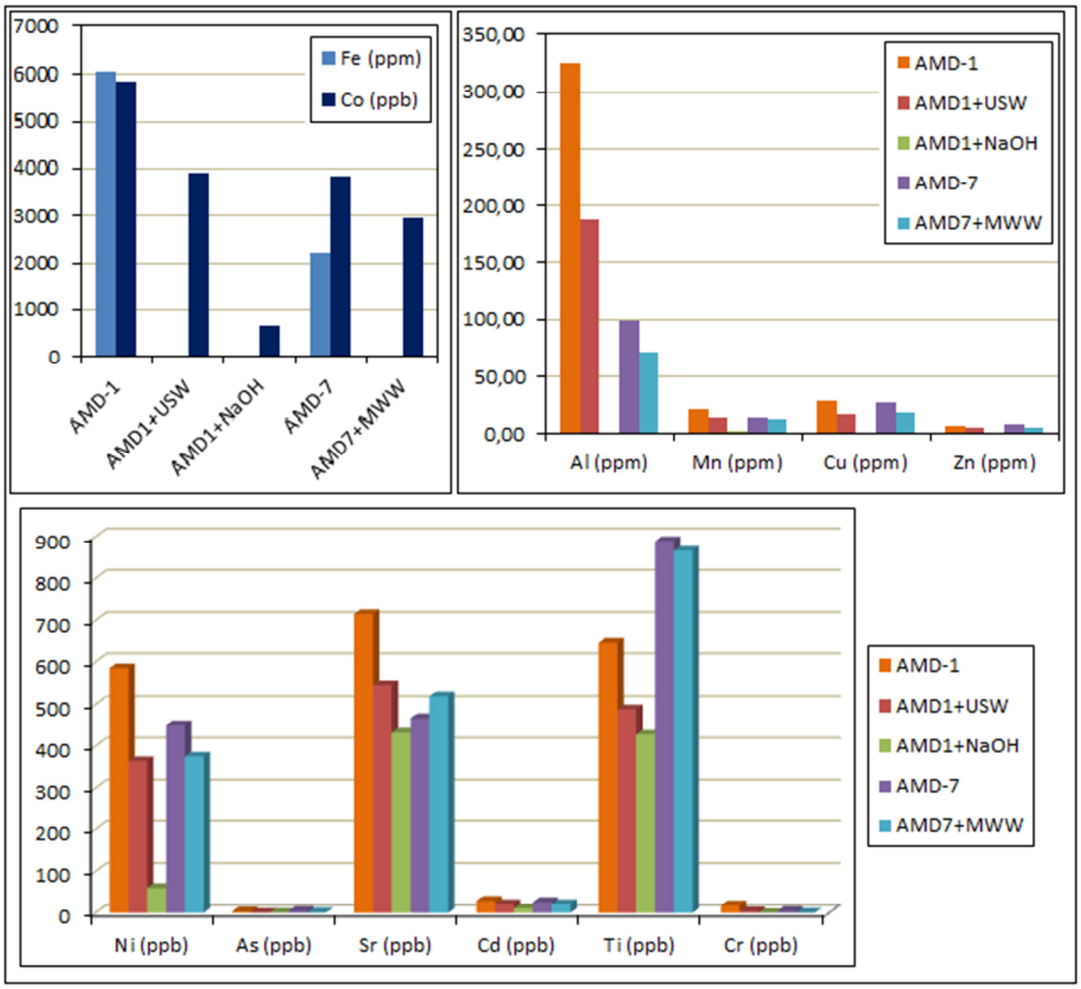


Figure 4.25 : Graphs illustrating the metal concentration before and after titrations.

4.5 Mechanisms Operating on Küre AMD System

This chapter will discuss all results on AMD generation together.

4.5.1 Possible contamination pathways derived from bioleaching experiments

Chemical composition of the supernatants after the massive ore residue collection was determined via ICP-MS analysis are presented in Table 4.10; which represent the shifts in chemistry in the solution after 6 months for B1 experiments and 2 months for B2 experiments. Regardless the limitations of the methodology (pulp density, bacterial cells/ml medium, etc.), results revealed that simulated AMD generated by biological oxidation of the massive sulfide ore caused sulfate rich acidic waters with a great deal of Fe, Cu, Zn, Co and Al contamination in the aquatic system. Lowest pH values were obtained in the presence of mixed acidophiles (pH 0,95), whereas *Acidithiobacillus ferrooxidans* and chemical oxidation caused pH

values of 2 and 2,9, respectively. It should be noted that some amount of Zn, Pb, and As could be carried with the enrichment isolate considering AMD environment of Balya (Balıkesir/Turkey) is highly contaminated with those metals (Çelik-Balcı et al., 2014) and results could more diluted in natural systems. On the other hand, in some extreme cases like Iberian Pyrite Belt AMD discharges, heavy metal and sulfate concentrations exceed a g/L unit in a highly acidic and oxic AMD system (i.e. Sánchez-España et al., 2005). Acceptable metal concentrations for human health, determined for drinking and tap water by WHO (2008), EPA (2012) and TS (TS 266, 2005) standards (Table 4.11) can be used as tools for determining the level of contamination.

Table 4.10 : Chemical composition (%) of the supernatants after residue collection after 6 months for B1 experiments and 2 months for B2 experiments.

Experiment	Fe	Cu	Zn	Co	S	Al	Pb	Ti	As	Mn	Ni	Mo	Cd	Sb
B1-Af	628,5	543	223,9	10,1	10,8	3,8	0,03	0,4	0,7	0,8	0,2	0,05	0,3	0,04
B1-E	1040	171,3	123,3	4,6	11,2	7,7	2,1	0,7	2,4	0,7	0,1	0,1	0,2	0,3
B1-C	161,5	985	462,1	10,8	10,8	2,4	0,04	0,4	0,03	0,3	0,1	0,05	0,6	0,3
B2/26-Af	141,1	1176	392,1	10,8	11,2	4,6	0,02	0,4	0,02	0,4	0,1	0,05	0,5	0,03
B2/26-E	1738	385	246,6	11,8	10,1	33,9	1,3	0,6	6,3	0,4	0,1	0,2	0,3	0,6
B2/40-Af	860	1236	482,8	16,2	11,4	8,2	0,03	0,5	0,7	0,4	0,2	0,05	0,6	0,05
B2/40-E	578,5	1166	412,2	11,7	9,2	12,3	0,04	0,4	0,2	0,5	0,1	0,05	0,5	0,05

Simulated AMD contamination for Küre mining site could have occurred via several pathways consisting of dissolution and oxidation of metals sulfides. Initially, when chalcopyrite encountered aqueous media in the absence of bacteria (groundwater, surface water or rain water in our case), ferrous iron oxidation took place very slowly (Stott et al., 2003) and copper started to dissolve chemically, causing a slight pH increase in the system (Xia et al., 2012). However, this caused acidic rock drainage production in the end (Eq. **(4.1)**) (Kimball et al., 2010). Pyrite was not easily oxidized in the absence of bacteria, owing to its valance bands (Borg and Dienes, 1992) that make it resistant to proton attacks, unless the strong oxidizing agent Fe(III) was present in the aquatic system (Sand et al., 2001; Schippers, 2004) and initiated chemical oxidation. Acid production due to pyrite dissolution in the presence of molecular oxygen is represented in Eq. **(4.2)** (Leahy and Schwarz, 2009).

$$CuFeS_{2(s)} + 16Fe^{3+}_{(aq)} + 8H_2O \rightarrow Cu^{2+}_{(aq)} + 17Fe^{2+}_{(aq)} + 2SO_4{}^{2-}_{(aq)} + 16H^{+}_{(aq)} \quad \textbf{(4.1)}$$

$$FeS_2 + 8H_2O + 14Fe^{3+} \rightarrow 15Fe^{2+} + 2SO_4^{2-} + 16H^+ \quad \textbf{(4.2)}$$

In the presence of bacteria as a catalyzer and Fe(III) as oxidizing agent in aqueous environment, first products of pyrite oxidation are hydrated (Luther, 1987) or liberated form of Fe(II) ions and thiosulfate (Reedy et al., 1991; Parker et al., 2003) (Eq. **(4.3)**), according to thiosulfate mechanism of acid insoluble metal disulfides (Schippers, 2004). In the continuous circle of thiosulfate mechanism with polythionate intermediates, sulfate combined with liberated H^+ ions formed sulfuric acid (Eq. **(4.4)**) as an intermediate or end product (Schippers and Sand, 1999). Produced ferrous iron was immediately oxidized to ferric iron, in turn attacked the ore, leading to indirect oxidation (Sand et al., 2001; Rohwerder et al., 2003) and excess values of ferric iron lead to contamination.

$$FeS_2 + 6Fe^{3+} + 3H_2O \rightarrow 7Fe^{2+} + S_2O_3^{2-} + 6H^+ \quad \textbf{(4.3)}$$

$$S_2O_3^{2-} + 6Fe^{3+} + 3H_2O \rightarrow 8Fe^{2+} + 2SO_4^{2-} + 10H^+ \quad \textbf{(4.4)}$$

Meanwhile pyrite oxidation accelerated chalcopyrite leaching (Dutrizac, 1989), bacteria also oxidized the acid-soluble monosulfide chalcopyrite via polysulfide mechanism which overall ended with elemental sulfur or polysulfide (Eq. **(4.5)**) and lead to sulfiric acid formation via bacterial sulfur oxidation (Eq. **(4.6)**) (Schippers and Sand, 1999; Schippers, 2004) and liberated copper ions contaminated the aquatic environment. Bacterial oxidation or dissolution of sphalerite or copper sulfides that may be present in the ore deposits (Çağatay et al., 1980) can be explained by polysulfide mechanism (Schippers, 2004) and data on metal liberation is available elsewhere (i.e. Balcı, 2010; Dutrizac and MacDonald, 1974; Dong et al., 2013a, 2013b).

$$CuFeS_2 + Fe^{3+} \rightarrow 0{,}125S_8 + Fe^{2+} + Cu^{2+} \quad \textbf{(4.5)}$$

$$0{,}125S_8 + 1{,}5O_2 + H_2O \rightarrow 2H^+ + SO_4^{2-} \quad \textbf{(4.6)}$$

In every mechanism, jarosite precipitated under the control of the solution pH and Fe(III) concentrations (Eq. **(4.7)**) (Watling, 2006; Leahy and Schwarz, 2009; Thurston et al., 2010), co-precipitating with some metals like Zn in mixing zones, which is consistent with the SEM-EDS results. Potassium in Eq. **(4.7)** can also be replaced by Na^+ or NH_4^+ ions (Watling, 2006). Schwertmannite also precipitated as a secondary phase; however, only abiotic oxidation provided necessary pH conditions of schwertmannite stability (Bigham et al., 1996).

$$K^+ + 3Fe^{3+} + 2SO_4^{2-} + 6H_2O \rightarrow KFe_3(SO_4)_2(OH)_6 + 6H^+ \quad \textbf{(4.7)}$$

Considering its well-studied capability of releasing various metals, *A. ferrooxidans* is most likely the bacteria having the most important role in providing a heavy metal rich system, relative to other pure cultures of acidophiles in the system (Bevilaqua et al., 2002, 2004). However, synergetic bioleaching by *A. ferrooxidans* with other dominant acidophiles like *A. thiooxidans* is the main source of excessive acidity and contamination (Stott et al., 2003, Akçıl et al., 2007) in our simulated AMD system, as well as it is the most likely case in natural AMD systems (Baker and Banfield, 2003; Schippers, 2004).

Table 4.11 : Drinking and tap water quality standards showing maximum acceptable levels for human health (TS 266, 2005; WHO, 2008; EPA, 2012).

Chemicals	EPA (2012) mg/L	WHO (2008) mg/L	TS 266 (2005) mg/L
Antimony	0.006[b]	0.02[c]	0.005[g]
Arsenic	0.01[b]	0.01[c]	0.01[g]
Cadmium	0.005[b]	0.003[c]	0.005[g]
Chromium	0.1[b]	0.05[c]	0.05[g]
Copper	1.3[b]	2[c]	2[g]
Lead	0.015[b]	0.01[c]	0.01[g]
Manganese	0.05[e]	0.4[c]	0.05[f]
Molybdenum	0.04[a]	0.07[c]	-
Nickel	0.1[a]	0.07[c]	0.02[g]
Strontium	4[a]	-	-
Zinc	5[e]	3-5[d]	-
Iron	0.3[e]	0.3-3[d]	0.2[f]
Sulfate	500[h]	500[d]	250[f]
Aluminum	0.05-0.2[e]	0.2[d]	0.2[f]
Silver	0.1[e]	0.1[d]	-
pH	6.5-8.5[e]	6.5-9.5[d]	6.5-9.5[f]

[a]Life-time exposure (EPA, 2012)

[b]Maximum contamination level (EPA, 2012)

[c]Guideline value (WHO, 2008)

[d]Referred previous guideline value (WHO, 2008)

[e]Secondary quality regulations (EPA, 2012)

[f]Controlled standards on drinking water quality (TS 266, 2005)

[g]Maximum allowed levels for drinking and tap waters (TS 266, 2005)

[h]Health-based value (EPA, 2012)

4.5.2 Effect of lithological features on water acidity

A mining environment with a long exploitation history could lead to extensive oxidation resulting in extreme acidity like the example of Rio Tinto (Spain) having 5000 years of mining history resulted in extremely acidic waters with pH values down to 0,37 (Buckby et al., 2003); unlike Küre district with over a thousand years of mining history but, having moderately acidic mine drainage, which displays a clear example of the effect of surrounding lithology on water chemistry. According to the geological map of the area combined with drainage network (Figure 4.6), Karanlık Stream cuts through basalt (pillow lava), diabase, subgraywacke and blackshale outcrops; while having inputs from tributaries cutting through peridotite (see sampling points AMD-6 and AMD-7 on Figure 3.1) or passing by gossan. XRD data of basalt and ore bearing wall-rock samples commonly revealed peaks of illite, albite, calcite and montmorillonite with the most intense peaks of chlorite, where sediment and ochre mineralogical compositions only displayed albite and illite among those (Figure 4.7). Consistent with our interpretations on our findings, Galan et al. (1999) found that smectite and calcite immeadiately dissolved in AMD waters, increasing the pH value from 2,2 to 2,8 as a result of their experiments on chlorite-bearing slate and smectite-rich clays that they sampled around Rio Tinto AMD waters. Galan et al. (1999) also concluded that illite and kaolinite did not show major changes after AMD water treatment, while chlorite shows little mineralogical changes along with extensive dissolution leading to Fe, Al and Mg solubilization. Moreover, they noted lack of smectite and calcite in sediments and the precipitation of gypsum Al and Fe oxy-hydroxides and secondary silica phases rich in Al and Mg as a result of neutralization processes; which can be used to explain the lack of calcite with montmorillonite (smectite) in our sediment samples with the abundance of gypsum, jarosite, gibbsite and relatively minor schwertmannite. Those results also support the fact that surrounding lithology and their suspended transported particles contribute to the metal input to AMD riverine systems via dissolution or cause metal scavenging via secondary precipitation after dissolution of neutralizing agents.

Our previous studies on groundwater chemistry obtained from Bakibaba mining tunnels (Demirel et al., 2014a, 2014b) showed that mine drainage waters in the vicinity of the massive ore could have lower pH values down to 2,7, unlike the neutral drainage waters that are flowing relatively distant from the ore through ore

bearing wall-rocks and surface AMD waters with moderate acidity. Combined results of static tests and groundwater pH values measured in Bakibaba underground mining tunnels and waste effluent dam show that, final paste pH values mostly coincide with actual pH values of the water samples, except the waste effluent dam samples. At the lowest elevated sampling point in Bakibaba underground tunnels (512 m above sea level), OBR-3 was sampled along with groundwater which represented the farthermost point from mineralization. Actual pH value of the GW-5 corresponds with the final paste pH of OBR- 3 measured as 8,1. At the 630 m elevation level, also ore bearing rock and groundwater samplings were made, revealing an equal actual and paste pH value of 7,9 for GW-4 and OBR-2. OBR-1 and O samples did not have corresponding groundwater samples. Therefore, actual pH values were evaluated in the closest elevation interval, assuming the groundwater followed a single trend in between two sampling points. OBR-1 sample corresponds to 600-650 m interval which displays predicted pH values of groundwater between 6,7 and 8,1, which is compatible with the final paste pH of 7,6. Groundwater in the vicinity of the ore sample was represented in between 650 and 700 m elevations having pH shifting between 4,5 and 7. However, final paste pH of the ore sample was measured as 3,2. This inconsistency could be attributed to the unknown lithology between sampling points, pointing out a relatively higher neutralization potential or the pulp density. Groundwater sampling point with the highest elevation (780 m) had a pH value of 2,9, suggesting being in the close vicinity of the extent of mineralization or sulfur enrichment on the groundwater's path leading to further oxidation and sulfuric acid release and/or bacterially catalyzed increase in oxidation rates. Waste effluent water had a pH value of 7,7 conflicting with the low paste pH of 3,9. This is mostly because the neutralizing agents anthropogenically mixed with water, creating a higher neutralization potential higher than the acid production potential, stoichiometrically. However, paste pH suggests that high solid/liquid ratio (pulp density) may generate considerable amount of acidity. Therefore, waste effluent dam chemistry can be taken as a model of neutralized stream or river chemistry, with or without any anthropogenic effect. Other static test results show expected trends, which an increase in the sulfur content leads to an increase in the acid production and net acid generation potential with a decrease in the neutralization potential and the final paste pH (except than for sample B, explained above).

Combined with the current results, those findings point to the fact that pH shifts of Küre mine drainage system is mainly controlled by the lithology and distance from ore or material with high sulfur content, if we were to exclude the effects of microbiological activity (i.e. bioleaching).

4.5.3 Sources and fate of metals around Küre VMS deposits

Combined results of series of geochemical and mineralogical studies on water, sediment, ochre and any ore containing material showed that sources of metals are mainly massive ore in addition to ore bearing wall rocks. Dissolution of lithological units, mainly containing clay minerals, and gossan outcrops by rain or AMD waters was also found to be contributing to the metal input to riverine systems. Chemical analysis on the AMD waters samples revealed that complex geochemical systems are regulating the metal fluxes between the stream or riverbed sediments and supernatant water bodies.

Unlike expected in ideal natural systems suggesting a pH increase would decrease metal concentrations in water and increase concentrations in sediments towards downstream direction, metal concentrations of Küre AMD stream waters and sediments show fluctuations instead of following a single coherent trend. Only Fe concentrations in Karanlık Stream tends to decrease towards downstream direction (6042 to 2172 ppm) with increasing pH (3,7 to 4,1); until the stream passes by a mining waste dump area and a gossan outcropping (according to geological maps with our exploratory observations in the area) that lead to a sudden increase in aqueous Fe concentrations up to 4300 ppm (AMD-5). An increase was also detected in Ti, Pb and Sr values that were also attributed to input from gossan and waste dissolution or leaching in contact zones with AMD waters. We don't have any geochemical data on gossan outcrops; however, it can be interpreted from geochemical analysis results of Güner (1980) that the limonite, hematite, alterated basalt and quartz containing gossan of Küre VMS deposits have 48,3% Fe, 0,3% Ti, 26 ppm and 13 ppm Pb, which may explain the increase in aqueous metal concentrations. One of the expected situations was the decrease in metal concentrations after mixing with slightly alkaline Küçükali Stream (pH= 8,1) as evidenced in AMD-2 and AMD-3 sampling points. Yet, metal concentrations in sediments did not always display opposite trends with the concentrations in water of

corresponding locations. The other expected phenomenon was the excessive decrease of metal concentrations in river water and increase in sediments of polluted Zemberekler River, only considering the slightly alkaline pH value of 7,9. Nevertheless, Zemberekler River should have had acidic pH values, considering it is the continuation of Karanlık Stream after passing through underground mining construction site. This implies intervention by the current mining operation in terms of anthropogenically adding neutralizing agents that could suddenly increase the pH from 4,2 to about 8 and result in the precipitation of heavy metals, which can be supported by field observations of carbonate-like material visible near the slopes above the greenish colored Zemberekler River; our XRD results on the samples revealing the presence of Mg-bearing calcium carbonate (calcite) and XRF result revealing abruptly high amounts of Ca (12,5%) with Mg (6,6%). Moreover, filtered river water samples (PRW) taken back to the laboratory had a pH value of 4,4; which should have been the actual pH value of the river, due to previous sampling points and also proved the anthropogenic input.

XRD measurements combined with SEM-EDS analysis of ochre samples displayed main secondary Fe and Al phases as jarosite, schwertmannite, goethite and gibbsite, which are generally known as metal scavengers in AMD systems. Average chemical compositions of the samples showed high concentrations of Fe (23,6%), Cu (0,37%), Zn (0,02%), Co (0,02%) and As (0,008%), which are relatively higher than the average sediment compositions. Sulfur is also more concentrated in ochre than corresponding sediment samples, as expected from their ore mineral and secondary iron hydroxysulfate content. Rest of the elemental composition is either same with or lower than the sediment bulk composition. XRF analyses on ochre samples are in good agreement with the results of mineralogical investigations and proving major proportion of metals are precipitated and transported with secondary iron hydroxide, iron hydroxysulfate and aluminum hydroxide minerals.

5. CONCLUSIONS

A series of field and laboratory studies were carried out to predict AMD generation potential of Küre VSM deposits for the first time. During this research, the massive ore, ore bearing wall rocks, wall rocks and wastes were geochemically and mineralogically characterized and subjected to AMD static tests to predict their acid generation or neutralization potentials. Furthermore, oxidation mechanisms of the massive ore were investigated via the leaching experiments to elucidate acid generation and metal release mechanisms during AMD formation around Küre VSM deposits. ABA test results showed that the ore, ore bearing wall rocks rich in disseminated pyrite and waste effluent precipitate are potentially acid generating with net neutralization potentials (NNP) of -38.4 to -1617.8, and NPR_{SABA} ranging from 0.05 to -0.16. The highest AP (1400.3 ppt) and MPA (1370.9 ppt) values of the ore sample with the lowest NNP (-1617.8 ppt) exhibited threshold values for the mining area. The ore bearing wall rocks (OBR-2, OBR-3) with insignificant sulfur content (0.45% and 0.03%, respectively) showed relatively high NNP values of 261 and 286.4, respectively, indicating non acid producing potentials. Relatively high NP values of some of ore bearing wall rocks (up to 287.5 kg $CaCO_3$/t) compared to the ore itself indicate that AMD may be locally generated. Pyrite and sulfur rich ore bearing wall rocks (i.e. OBR-1; 2.4% S) may locally contribute to AMD generation and heavy metal release in the region. Consistent with this determination, elevated concentrations of Mn, Fe, Co, Cu, Cr, Zn were only determined in the groundwater collected from the underground ore zones in addition to surface water from the stream in the vicinity of the VSM deposits (Table 4.7). The high AP (75.9 ppt) and NAG (100 kg H_2SO_4/t) values of the ore and some of ore bearing wall rocks (OBR-1) indicate that upon exposure to oxidizing conditions they will produce significant amount of acidity causing leach of metals into the environment. Consistent with this, the NAGpH value of the massive ore (pH 2.39) indicate that massive chalcopyrite ore of Küre copper deposits may generate acidic waters with pH values lower than 3.

Furthermore, waste effluent precipitates have the potential to generate acidity and a great deal of heavy metal contamination in case of leakage or dam failure.

XRD and SEM-EDS analysis of ochre samples collected from the AMD impacted surface water showed jarosite, schwertmannite, goethite and gibbsite as main secondary Fe and Al phases. Average chemical compositions of the ochre samples showed high concentrations of Fe (23,6%), Cu (0,37%), Zn (0,02%), Co (0,02%) and As (0,008%). These results suggest that release and precipitation of metals can be controlled by Fe-oxyhydroxides in the filed. Moreover, combined XRD and SEM-EDS measurements also reveal the abundance of clay minerals (mainly clinochlore and illite) and metal-bearing (Zn and Sr) silicate phases, which points out the importance of the stability of clay minerals in the transport, release or stability of metal (mainly Fe, Al, Zn and Sr).

The results from the leaching of the massive ore revealed that biological oxidation of the massive sulfide ore caused sulfate rich acidic waters with a great deal of Fe, Cu, Zn, Co and Al contamination in the aquatic system. Lowest pH values were obtained in the presence of mixed acidophiles (pH 1.26), whereas *Acidithiobacillus ferrooxidans* and chemical oxidation caused pH values of 2.3 and 3.29, respectively. Overall, biological oxidation mechanism and leaching time are proposed to be crucial for environmental implications around mining operations. Therefore, this study may contribute to rehabilitation models as an initial basis.

This study also revealed that short-term leaching studies are useful in successful and quick metal recovery from low grade copper ores for industrial applications. Nevertheless, environmental assessments require a longer period of leaching, considering neglected and important shifts in natural systems.

The field and laboratory investigations revealed generation of AMD in Küre with pH values between 2.9-4.5 and high concentration of Cu, Fe, Zn, Co, Mn and $SO4^{2-}$. Combined results of series of geochemical and mineralogical studies on water, sediment, ochre and ore containing material showed that sources of metals are mainly massive ore in addition to ore bearing wall rocks. The sources of Sr-bearing mineral phaeses and Sr concentrations in riverbed sediments weren't determimed in this study and suggested to be investigated in further environmental studies. Dissolution of lithological units, mainly containing clay minerals, and gossan

outcrops by rain or AMD waters was also found to be contributing to the metal input to riverine systems. Chemical analysis on the AMD waters samples revealed that complex geochemical systems are regulating the metal fluxes between the stream or riverbed sediments and supernatant water bodies.

The static test results compatible with the field data indicated applicability of those methods to this particular field. Consistency in results from both ABA and NAG tests justify that static tests can be used as tools for preliminary evaluation of AMD possibilities and its impact on surface and groundwater quality in VMS mining environment. Therefore, the test results obtained from the current study can hold important implications for depositional conditions of the mining wastes to prevent further AMD generation around the Kure VSM deposits environment.

Mining wastes of the current mining operation running Kure VMS deposits is stored in a flotation tailings dam (waste effluent dam), which is acting as a settlement pond, and afforestation was carried out in the close vicinity. Those are widely accepted methods in mine waste handling. However, because of the long mining history of Kure copper deposits, age of the surface and groundwater contamination is unknown and natural acid rock drainage could also have occurred. Therefore, this study can be considered as a database of a long-term AMD-contaminated environment, which can be used as input data for future rehabilitation models for acid mine drainage streams of Kure area. Exact locations of AMD groundwater discharges on the surface, that could be generating AMD surface waters, are suggested to be detected before building rehabilitation plants or any attempts on surface water quality enhancement.

REFERENCES

Ahmadi, A., Schaffie, M., Manafi, Z., Rrnjbar, M. (2010). Electrochemical bioleaching of high grade chalcopyrite flotation concentrates in a stirred bioreactor. *Hydrometallurgy, 104*, 99-105.

Ahmadi, A., Schaffie, E.M., Petersen, J., Schippers, A., Ranjbar, M. (2011). Conventional and electrochemical bioleaching of chalcopyrite concentrates by moderately thermophilic bacteria at high pulp density. *Hydrometallurgy, 106*, 84–92.

Akçay, M., and Moon, C.J. (2004). The environmental impact of mining in the Pontides, Turkey: reconnaissance sampling and GIS-based analysis. *Geochemistry: Exploration, Environment, Analysis, 4*, 317-328.

Akçıl, A. (2002). A preliminary research on acid pressure leaching of pyritic copper ore in Küre copper mine, Turkey. *Minerals Engineering, 15*(12), 1193–1197.

Akçıl, A., and Çiftçi, H. (2003). Bacterial leaching of Küre copper ore. *Journal of the Chamber of Mining Engineers of Turkey, 42*, 15–26.

Akçıl, A., Çiftçi, H., Deveci, H. (2007). Role and contribution of pure and mixed cultures of mesophiles in bioleaching of a pyritic chalcopyrite concentrate. *Minerals Engineering, 20*, 310–318.

Altun, I., Şengün, M., et al. (1990). *Kastamonu 1/100 000 ölçekli jeoloji haritası*. MTA, Ankara.

Arslan, F., Acarkan, N., Perek, T., Önal, G. (1995). Recovery of precious metals from sulfidic flotation concentrates. In B. Krstev and B. Golomeov (Ed.), *Proceedings of the 6th Balkan Conference on Mineral Processing,* pp. 134–140. Ohrid, Macedonia, September 18–21.

Arslan, F., Bulut, G., Kangal, O., Perek, K. T., Gül, A., Gürmen, S. (2003). Studies on leaching of massive rich copper ore in acidic ferric sulfate solution. *Scandinavian Journal of Metallurgy, 33*, 6–14.

Arslan, F., Kangal, O., Bulut, G. Gül, A. (2004). Leaching of massive rich copper ore with acidified ferric chloride. *Mineral Processing and Extractive Metallurgy Review: An International Journal, 25*(2), 143-158.

Asloğlu, K. (1919). Küre yatakları rapor özeti hakkında: Küre Bakırlı Pirit İşletmesi Müessesesi. Report, (unpublished).

Atabey, E. (2010). Türkiye'de İnsan Kaynaklı (Antropojenik) Unsurlar ve Çevresel Etkileri, *MTA Yerbilimleri ve Kültür Serisi – 7* , pp. 1-136, Ankara. ISBN: 978-605-4075-77-5.

Aykol, A., Budakoğlu, M., Kumral, M., Gültekin, A.H., Turhan, M., Esenli, V., Yavuz, F., Örgün, Y. (2003). Heavy metal pollution and acid

drainage from the abandoned Balya Pb-Zn sulfide Mine, NW Anatolia, Turkey. *Environmental Geology, 45*, 198-208.

Bailey, E.H., Barnes, J.W., Kupfer, D.H. (1966). Geology and Ore Deposit of Küre District, Kastamonu Province, Turkey. In *CENTO Summer Training Program in Geological Mapping Techniques*, pp. 17-73.

Baker, B.J., and Banfield, J.F. (2003). Microbial communities in acid mine drainage. *FEMS Microbiology Ecology, 44*, 139–152.

Baker, R.A. and Wilshire, A.G. (1970). Microbiological factor in acid mine drainage formation: a pilot plant study. *Environmental Science & Technology, 4*(5), 401-407.

Balcı, N. (2010). Effect of bacterial activity on trace metals release from oxidation of sphalerite at low pH (<3) and implications for AMD environment. *Environmental Earth Sciences, 60*, 485–493.

Balcı, N., Bullen, T.D., Witte-Lien, K., Shanks III, W.C., Motelika, M., Mandernack, K.W. (2006). Iron isotope fractionation during microbially stimulated Fe(II) oxidation and Fe(III) precipitation. *Geochimica et Cosmochimica Acta, 70*, 622–639.

Balcı, N., Mandernack, K.W., Shanks III, W.C., Mayer, B., Gemery-Hill, P. (2007). Oxygen and sulfur isotope systematics of sulfate produced by bacterial and abiotic oxidation of pyrite. *Geochimica et Cosmochimica Acta, 71*, 3796–3811.

Balcı, N., Mayer, B., Shanks III, W.C., Mandernack, K.W. (2012). Oxygen and sulfur isotope systematics of sulfate produced during abiotic and bacterial oxidation of sphalerite and elemental sulfur. *Geochimica et Cosmochimica Acta, 77*, 335–351.

Becker, U., Rosso, K.M., Hochella, M.F., Jr. (2001). The proximity effect on semiconducting mineral surfaces: A new aspect of mineral surface reactivity and surface complexation theory?. *Geochimica et Cosmochimica Acta, 65*, 2641-2649. doi: 10.1016/S0016-7037(01)00624-X.

Bethke, C.M. (2008). *Geochemical and Biogeochemical Reaction Modeling (2nd ed.).* Cambridge University Press. ISBN: 978-0-521-87554-7.

Bevilaqa, D., Leite, A.L.L.C., Garcia Jr, O., Tuovinen, O.H. (2002). Oxidation of chalcopyrite by *Acidithiobacillus ferrooxidans* and *Acidithiobacillus thiooxidans* in shake flasks. *Process Biochemistry, 38*, 587–592.

Bevilaqua, D., Diez-Perez, I., Fugivara, C.S., Sanz, F., Benedetti, A.V., Garcia, O. (2004). Oxidative dissolution of chalcopyrite by *Acidithiobacillus ferrooxidans* analyzed by electrochemical impedance spectroscopy and atomic force microscopy. *Bioelectrochemistry, 64*, 79–84.

Bevilaqua, D., Lahti-Tommila, H., Garcia Jr., O., Puhakka, J.A., Tuovinen, O.H. (2014). Bacterial and chemical leaching of chalcopyrite concentrates as affected by the redox potential and ferric/ferrous iron ratio at 22 °C. *International Journal of Mineral Processing, 132*, 1–7.

Bigham, J.M., Schwertmann, U., Traina, S.J., Winland, R.L., Wolf, M. (1996). Schwertmannite and the chemical modeling of iron in acid sulfate waters. *Geochimica et Cosmochimica Acta, 60*, 2111-2121.

Borg, R.J., and Dienes, G.J. (1992). *The Physical Chemistry of Solids*. Academic Press, Boston, USA.

Bosecker, K. (1997). Bioleaching: metal solubilisation by microorganisms. *FEMS Microbiology Reviews, 20*, 591–604.

Bouzahzah, H., Benzaazoua, M., Bussiere, B., Plante, B. (2014). Prediction of acid mine drainage: importance of mineralogy and test protocols for static and kinetic tests. *Mine Water and the Environment, 33*, 54-65.

Boztuğ, D. (1992). Orta-Batı Pontidlerdeki Küre yöresi (K Kastamonu) magmatiti-metamorfitlerinin petrografisi ve magmatitlerin ana element jeokimyası. In *C. Ü. Müh. Fak. Dergisi, Seri-A, Yerbilimleri, 9*(1), pp. 75-106.

Boztuğ, D., Debon, F., Le Fort, P., Yılmaz, O. (1984). Geochemical characteristics of some plutons from the Kastamonu granitoid belt (northern Anatolia, Turkey). *Schweizerische Mineralogische und Perrographische Mitteilungen, 64*(3), 389-403.

Boztuğ, D., Debon, F., Le Fort, P., Yılmaz, O. (1995). High compositional diversity of the Middle Jurassic Kastamonu Plutonic Belt, northern Anatolia, Turkey. *Turkish Journal of Earth Sciences, 4*, 67–86.

Brierley, J.A., and Brierley, C.L. (2001). Present and future commercial applications of biohydrometallurgy. *Hydrometallurgy, 59*, 233–239.

Brodie, M.J., Broughton, L.M., Robertson, A. (1991). A conceptual rock classification system for waste management and a laboratory method for ARD prediction from rock piles. In MEND Program (Ed.), *Proceedings of Second International Conference on the Abatement of Acidic Drainage*, *3*, pp. 119-135. Montreal, Quebec, Quebec Mining Association, Ottowa, September 16-18.

Bruynesteyn, A., and Hackl, R.P. (1984). Evaluation of acid production potential of mining waste materials. *Minerals and the Environment, 4*(1), 5-8.

Buckby, T., Black, S., Coleman, M.L., Hodson, M.E. (2003). Fe-sulphate-rich evaporative mineral precipitates from the Rio Tinto, southwest Spain. *Mineralogical Magazine, 6*, 263–278.

Bulut, G., Kangal, O., Gül, A., Perek, K. T., Arslan, F. (2001a). Recovery of metallic values from a massive rich copper ore. In *Proceedings of IX Balkan Mineral Processing Congress*, pp. 531–536. Istanbul, Turkey, 11–13 September.

Bulut, G., Kangal, O., Perek, K. T., Yasan, I., Arslan, F. (2001b). A comparative study on ferric chloride and ferric sulphate leaching of sulphidic copper ores from Turkey. In *Proceedings of VI Southern Hemisphere Meeting on Minerals Technology*, pp. 348-552. Rio De Janerio, Brazil, May 27–31.

Çağatay, A., Pehlivanoğlu, H., Altun, Y. (1980). Küre piritli bakır yataklarının kobalt-altın mineralleri ve yatakların bu metaller açısından ekonomik

değeri. In *Mineral Research and Exploration Institute of Turkey (MTA) Bulletin, 93/94*, pp. 110-117.

Çakır, Ü. (1995). Aşıköy-Toykondu (Küre-Kastamonu) massif sülfid yataklarının jeolojik özellikleri. In *Mineral Research and Exploration Institute of Turkey (MTA) Bulletin, 117*, pp. 29-40.

Caruccio, F.T., Geidel, G., and Pelletier, M. (1981). Occurrence and prediction of acid drainages. Journal of the Energy Division. In *Procedings of American Society of Civil Engineers, 107*, pp. 167-178.

Casagrande, D.J., Finkelman, R.B., Caruccio, F.T. (1989). The nonparticipation of organic sulfur in acid mine drainage. *Environmental Geochemistry and Health, 11*, 187-192.

Çelik-Balcı, N., Gül, S., Menekşe-Kılıç, M., Karagüler, N., Sarı, E., Sönmez, M.Ş. (2014). Biogeochemistry of Balıkesir Balya Pb-Zn mine tailings site and its effect on generation of acid mine drainage. *In Geological Bulletin of Turkey, 57*(3), pp. 1-22.

Chen, P., and Shakhnovich, E.I. (2010). Thermal adaptation of viruses and bacteria. *Biophysical Journal, 98*(7), 1109–1118.

Córdoba, E.M., Muñoz, J.A., Blázquez, M.L., González, F., Ballester, A. (2008). Leaching of chalcopyrite with ferric ion. Part III: effect of redox potential on the silver-catalyzed process. *Hydrometallurgy, 93*, 97–105.

Córdoba, E.M., Muñoz, J.A., Blázquez, M.L., González, F., Ballester, A. (2009). Passivation of chalcopyrite during its chemical leaching with ferric ion at 68 °C. *Minerals Engineering, 22*, 229-235.

Das, A., Modak, J.M., Natarajan, K.A. (1998). Surface chemical studies of *Thiobacillus ferrooxidans* with reference to copper tolerance. *Antonie van Leeuwenhoek, 73*, 215–222.

Demirbaş, T.T. and Ağaoğlu, F. (1980). Küre-Aşıköy cevher yataklarının gelişme dönemleri ve bugünkü durumu hakkında rapor. *Etibank Küre Bakirli Pirit işletmesi Müessesesi* Report **31**, (unpublished).

Demirel, **C., Balcı, N., Gül, S., Sönmez, Ş.** (2014a). Environmental geochemistry of Küre (Kastamonu) massive sulfide deposits. In *67th Geological Congress of Turkey*, Ankara, Turkey, 14-18 April 2014.

Demirel, **C., Sönmez, Ş., Balcı, N.** (2014b). Understanding Cu release into environment from Küre massive sulfide ore deposits, Kastamonu, NW Turkey. In EGU General Assembly 2014, *Geophysical Research Abstracts, 16*, Abstract: EGU2014-3890. Vienna, 27 April-2 May 2014.

Deveci, H., Akçıl, A., Alp, I. (2004). Bioleaching of complex zinc sulphides using mesophilic and thermophilic bacteria: comparative importance of pH and iron. *Hydrometallurgy, 73*, 293–303.

Dong, Y., Lin., H., Xu, X., Zhou, S. (2013a). Bioleaching of different copper sulfides by *Acidithiobacillus ferrooxidans* and its adsorption on minerals. *Hydrometallurgy, 140*, 42–47.

Dong, Y., Lin., H., Xu, X., Zhang, Y., Gao, Y., Zhou, S. (2013b). Comparative study on the bioleaching, biosorption and passivation of copper sulfide minerals. *International Biodeterioration & Biodegradation Journal, 84*, 29-34.

Dong, Y., Lin., H., Xu, X., Zhou, S. (2013c). Effects of quartz addition on chalcopyrite bioleaching in shaking flasks. *Minerals Engineering, 46–47*, 177–179.

Dopson, M., Halinen, A.-K., Rahunen, N., Özkaya, B., Şahinkaya, E., Kaksonen, A.H., Lindström, E.B., Puhakka, J.A. (2006). Mineral and iron oxidation at low temperatures by pure and mixe cultures of acidophilic microorganisms. *Biotechnology and Bioengineering, 97*(5), 1205-1215.

Dopson, M., and Lindström, E.B. (2004). Analysis of community composition during moderately thermophilic bioleaching of pyrite, arsenical pyrite and chalcopyrite. **Microbial Ecology, 48**, 19–28.

Dreisinger, D.B., Muñoz, J.A., Cooper, W.C., Young, S.K. (2007). Silver-catalyzed bioleaching of low-grade copper ores. Part I: Shake flasks tests. *Hydrometallurgy, 88*(1–4), 3–18.

Duncan, D.W., and Bruynesteyn, A. (1979). Determination of the acid production potential of waste materials. *Metallurgical Society of AIME Annual Meeting*, Paper A79-29. New Orleans, USA.

Duncan, D., and Walden, C. (1975). Prediction of acid generation potential. *Report to Water Pollution Control Directorate*, Environmental Protection Service, Environment Canada.

Dutrizac, J.E. (1978). The kinetics of dissolution of chalcopyrite in ferric ion media. *Metallurgical Transactions B, 9*, 431–439.

Dutrizac, J.E. (1989). Elemental sulphur formation during the ferric sulphate leaching of chalcopyrite. *Canadian Metallurgical Quarterly, 28*, 337–344.

Dutrizac, J.E., and MacDonald, R.J.C. (1974). Ferric ion as a leaching medium. *Minerals Science and Engineering 6*(2), 59–100.

Edwards, K.J., Bond, P.L., Gihring, T.M., Banfield, J.F. (2000). An archaeal iron-oxidizing extreme acidophile important in acid mine drainage. *Science, 279*, 1796–1799.

Ehrlich, H.L. (1996). *Geomicrobiology* (3rd edn.), Marcel Dekker, New York, USA.

Ehrlich, H.L. (2004). Beginnings of rational bioleaching and highlights in the development of biohydrometallurgy: A brief history. *The European Journal of Mineral Processing and Environmental Protection, 4*, 102-112.

Ehrlich, H.L., and Newman, D.K. (2009). *Geomicrobiology* (5th edn.), CRC Press/Taylor & Francis, Boca Raton, FL.

Environmental Australia (1997). Managing sulphidic mine wastes and acid drainage. In *Best Practice Environmental Management in Mining Booklet Series*.

EPA (1994). U.S. Environmental Protection Agency. Technical Document: Acid Mine Drainage Prediction. Office of Solid Waste Special Branch, U.S. EPA, Washington, USA.

EPA (2012). U.S. Environmental Protection Agency. 2012 Edition of the Drinking Water Standards and Health Advisories. *Report:* **EPA 822-S-12-001**. Office of Water, U.S. EPA, Washington, USA.

Feng, S., Yang, H., Xin, Y., Gao, K., Yang, J., Liu, T., Zhang, L., Wang, W. (2013). A novel and highly efficient system for chalcopyrite bioleaching by mixed strains of *Acidithiobacillus*. *Bioresource Technology, 129*, 456–462.

Förstner, U. (1999). Introduction. In: Azcue, J.M. (Ed.), *Environmental Impacts of Mining Activities – Emphasis on Mitigation and Remedial Measures*, pp. 1-3. Springer, Berlin, Germany.

Galan, E., Carretero, M.I., Fernandez-Caliani, J.C. (1999). Effects of acid mine drainage on clay minerals suspended in the Tinto River (Rio Tinto, Spain). An experimental approach. *Clay Minerals, 34*, 99-108.

Gomez, E., Blazquez, M. L., Ballester, A., Gonzalez, F. (1996). Study by SEM and EDS of chalcopyrite bioleaching using new thermophilic bacteria. *Minerals Engineering, 9*(9), 985–999.

Gomez, E., Ballester, A., Blazquez, M. L., Gonzalez, F. (1999). Silver-catalysed bioleaching of a chalcopyrite concentrate with mixed cultures of moderately thermophilic microorganisms. *Hydrometallurgy, 51*(1), 17–46.

Gray, N.F. (1997). Environmental impact and remediation of acid mine drainage: a management problem. *Environmental Geology, 30*, 62-71.

Gu, G., Hu, K., Zhang, X., Xiong, X., Yang, H. (2013). The stepwise dissolution of chalcopyrite bioleached by *Leptospirillum ferriphilum*. *Electrochimica Acta, 103*, 50–57.

Güner, M. (1980). Küre civarının massif sülfid yatakları ve jeolojisi, Pontidler (Kuzey Türkiye). In *Mineral Research and Exploration Institute of Turkey (MTA) Bulletin, 93/94*, pp. 65-109.

Habashi, F. (1978). *Chalcopyrite. Its chemistry and metallurgy*. McGraw-Hill.

Hackl, R.P., Dreisinger, D.B., Peters, E. (1995). Passivation of chalcopyrite during oxidative leaching in sulfate media. *Hydrometallurgy, 39*, 25-48.

Harneit, K., Göksel, A., Kock, D.H., Gehrke, T., Sand, W. (2006). Adhesion to metal sulfide surfaces by cells of *Acidithiobacillus ferrooxidans*, *Acidithiobacillus thiooxidans* and *Leptospirillum ferrooxidans*. *Hydrometallurgy, 83*, 245–254.

He, H., Xia, J.L., Hong, F.F., Tao, X.X., Leng, Y.W., Zhao, Y.D. (2012). Analysis of sulfur speciation on chalcopyrite surface bioleached with *Acidithiobacillus ferrooxidans*. *Minerals Engineering, 27*(1), 60–64.

İbret, Ü. (2007). *Küre Bakır Diyarının Coğrafyası*. Aktif Yayınevi-Ders Kitapları. ISBN: 9758986439.

Jambor, J.L., Dutrizac, J.E., Raudsepp, M. (2007). Measured and computed neutralization potentials from static tests of diverse rock types. *Environmental Geology, 52*, 1019-1031.

James, L.D. (1966). Demonstration and application of some simple geochemical prospecting techniques in the küre district. In *CENTO Summer Training Program in Geological Mapping Techniques*.

Jiang, L., Zhou, H.Y., Peng, X.D., Ding, Z.H. (2008). Bio-oxidation of galena particles by *Acidithiobacillus ferrooxidans*. *Particuology, 6*, 99–105.

Kangal, O., Bulut, G., Gül, A., Ö zaksoy, G., Arslan, F. (2001). Cupric chloride leaching of sulphidic copper ores. In *Proceedings of VI Southern Hemisphere Meeting on Minerals Technology*, pp. 445–450. Rio De Janerio, Brazil, May 27–31.

Karadeniz, M. (2008). *Sülfürlü Madenlerin Sorunu: Asit Maden Drenajı ve Çözümü.* Chamber of Mining Engineers of Turkey, No. 146.

Karimi, G.R., Rowson, N.A., Hewitt, C.J. (2010). Bioleaching of copper via iron oxidation from chalcopyrite at elevated temperatures. *Food and Bioproducts Processing, 88*, 21–5.

Kelly, J.P. (1988). *Oxidation of Sulfur Compounds- The Nitrogen and Sulphur Cycles*. Society of General Microbiology, Cambridge University, Boston.

Ketin, İ., and Gümüş, Ö. (1962). Sinop-Ayancık arasındaki III. Bölgeye dahil sahaların Jeolojisi hakkında rapor. *TPAO* Report **213**, Ankara.

Ketin, İ., and Gümüş, Ö. (1963). Sinop-Ayancık arasında III. bölgeye dahil sahaların jeolojisi. *TPAO* Report **288**, Ankara.

Kim, J., Koo, S.-Y., Kim, J.-Y., Lee, E.-H., Lee, S.-D., Ko, K.-S, and Cho, K.-S. (2009). Influence of acid mine drainage on microbial communities in stream and groundwater samples at Guryong Mine, South Korea. *Environmental Geology, 58*, 1567-1574.

Kimball, B.E., Rimstidt, J.D., Brantley, S.L. (2010). Chalcopyrite dissolution rate laws. *Applied Geochemistry, 25*(7), 972-983.

Klauber, C., Parker, A., van Bronswijk, W., Watling, H. (2001). Sulphur speciation of leached chalcopyrite surfaces as determined by X-ray photoelectron spectroscopy. *International Journal of Mineral Processing, 62*, 65–94.

Koç, Ş., Ünal, A., Kadıoğlu, Y.K. (1995). Küre (Kastamonu) cevherleşmelerini içeren volkanitlerin jeolojisi, jeokimyasi ve jeotektonik konumu. In *Mineral Research and Exploration Institute of Turkey (MTA) Bulletin, 117*, pp. 41-54.

Kovenko, V. (1944). Küredeki eski bakır yatağı ile yeni keşfedilen Aşıköy yatağının ve Karadeniz orta ve doğu kesimleri sahil bölgesinin metallojenisi. In *Mineral Research and Exploration Institute of Turkey (MTA) Bulletin, 2/32*, pp. 180-212.

Krebs, W., Brombacher, C., Bosshard, P.P., Bachofen, R., Brandl, H. (1997). Microbial recovery of metals from solids. *FEMS Microbiology Reviews, 20*, 605–617.

Kuşçu, İ., and Erler, A. (2002). Pyrite deformation textures in the deposits of Küre mining district (Kastamonu-Turkey). *Turkish Journal of Earth Sciences, 11*, 205-215.

Kwong, Y.T.J. (1993).Mine site acid rock drainage assessment and prevention; a new challenge for a mining geologist. In *Proceedings of the international mining geology conference*, pp. 213-217, Kalgoorlie.

Lapakko, K.A. (1994). Evaluation of neutralization potential determinations for metal mine waste and a proposed alternative. *International Land Reclamation and Mine Drainage Conference and Third International Conference on the Abetment of Acidic Drainage*. Pittsburg, USA.

Lapakko, K.A. (2002). Metal mine rock and waste characterization tools: an overview. *Mining, Minerals and Sustainable Developmehynt*, **No. 67**.

Lawrence, R.W., and Scheske, M. (1997). A method to calculate the neutralization potential of mining wastes. *Environmental Geology, 32*(2), 100-106.

Lawrence, R.W., Poling, G.P., Marchant, P.B. (1989). Investigation of predictive techniques for acid mine drainage. Report on DSS Contract No. 23440-7-9178/01-SQ, *MEND* Report **1.16.1(a)**. Energy Mines and Resources, Canada.

Leahy, M.J., Schwarz, M.P. (2009). Modelling jarosite precipitation in isothermal chalcopyrite bioleaching columns. *Hydrometallurgy, 98*, 181–191.

Lee, J., and Pandey, B.D. (2012). Bio-processing of solid wastes and secondary resources for metal extraction – A review. *Waste Management, XXXII*(1), 3–18.

Li, H.M., Ke, J.J. (2001). Technical note: influence of Cu^{2+} and Mg^{2+} on the growth and activity of Ni^{2+} adapted *Thiobacillus ferrooxidans*. *Minerals Engineering, 14*, 113–116.

Li, Y., Kawashima, N., Chandra, A.P., Gerson, A.R. (2013). A review of the structure, and fundamental mechanisms and kinetics of the leaching of chalcopyrite. *Advances in Colloid and Interface Science, 197–198*, 1–32.

Lottermoser, B.G. (2010). *Mine Wastes: Characterization, Treatment and Environmental Impacts* (3rd ed.). Springer, Berlin, Heidelberg.

Luther, G.W., III. (1987). Pyrite oxidation and reduction: molecular orbital theory considerations. **Geochimica et Cosmochimica Acta, 51**, 3193–3199.

Luther, G.W., III. (1990). The frontier-molecular-orbital theory approach in geochemical processes. In Stumm, W. (Ed.), *Aquatic Chemical Kinetics,* pp. 173-198., John Wiley & Sons, Inc, New York, USA.

Luther, G.W., III, Glazer, B.T., Hohmann, L., Popp, J.I., Taillefert, M., Rozan, T.F., Brendel, P.J., Theberge, S.M., and Nuzzio, D.B. (2001). Sulfur speciation monitored in situ with solid state gold amalgam voltammetric microelectrodes: Polysulfides as a special case in

sediments, microbial mats and hydrothermal vent waters. *Journal of Environmental Monitoring, 3*, 61-66.

McLemore, V.T. (2008). *Basics of Mining Influenced Water*, pp. 31-46. Society for Mining, Metallurgy, and Exploration, Inc. ISBN: 978-0-87335-259-8.

Mehta, K.D., Pandey, B.D. (2013). Bacterial leaching kinetics for copper dissolution from a low-grade Indian chalcopyrite ore. *REM - Revista Escola de Minas, 66*(2), 245-250.

MEND (1991). Acid Rock Drainage Prediction Manual, *Coastech Research, MEND Project* Report **1.16.1b**, Ottawa, Ontario, Canada.

Mielke, R.E., Pace, D.L., Porter, T., Southam, G. (2003). A critical stage in the formation of acid mine drainage: Colonization of pyrite by *Acidithiobacillus ferrooxidans* under pH-neutral conditions. *Geobiology, 1*, 81-90.

Miller, S.D., and Murray, G.S. (1988). Application of Acid Base Analysis to Wastes from Base Metal And Precious Metal Mines. In *Proceedings: Mine Drainage And Surface Mine Reclamation, 1, Mine Water and Mine Waste*, pp. 29-32. Bureau of Mines IC 9183.

Miller, S., and Jeffery, J. (1995). Advances in the Prediction of Acid Generating Mine Waste Materials. In N.J. Grundon and L.C. Bell (Eds.), *Proceedings of the Second Australian Acid Mine Drainage Workshop*, pp. 33-43. Charters Towers, Queensland, Australian Centre for Minesite Rehabilitation Research, Brisbane, 28-31 March 1995.

Miller, S.D., Jeffrey, J.J., Murray, G.S.C. (1990). Identification and management of acid generating mine wastes – procedures and practices in South East Asia and the Pacific regions. In *Proc. Lisboa 90:Acid Mine Water in Pyritic Environments*, pp. 57-70. Lisbon, Portugal, September 16-19.

Miller, S., Robertson, A., Donahue, T. (1997), Advances in Acid Drainage Prediction using the Net Acid Generation (NAG) Test. *In Proc. 4th International Conference on Acid Rock Drainage*, pp. 533-549. Vancouver, BC.

Mo, X.L., Lin, H., Fu, K.B., Xu, C.Y., Wang, H. (2012). Influence factors of pyrite promotion on the bioleaching of chalcopyrite. *Journal of University of Science and Technology Beijing, Mineral, Metallurgy, Material, 34*, 761–768.

Morin, K.A., and Hutt, N.M. (1997). *Environmental geochemisty of minesite drainage*. MDAG Publication, Vancouver.

Moses, C.O., Nordstrom, D.K., Herman, J.S., Mills, A.L. (1987). Aqueous pyrite oxidation by dissolved oxygen and ferric iron. *Geochimica et Cosmochimica Acta, 51*, 1561-1571.

Munk, L.-A., Faure, G., Pride, D.E., Bigham, J.M. (2002). Sorption of trace metals to an aluminum precipitate in a stream receiving acid rock-drainage; Snake River, Summit County, Colorado. *Applied Geochemistry, 17*, 421-430.

Nazari, B., Jorjani, E., Hani, H., Manafi, Z., Riahi, A. (2014). Formation of jarosite and its effect on important ions for *Acidithiobacillus ferrooxidans* bacteria. *Transactions of Nonferrous Metals Society of China, 24*, 1152-1160.

Nikitin, V. (1926). Küre bakır madeni, *MTA* Report, (unpublished).

Nordstrom, D.K., and Alpers, C.N. (1999). Negative pH, efflorescent mineralogy, and consequences for environment restoration at the Iron Mountain Superfund site, California. In *Proceeding of the National Academy of Science*, *U.S.A., 96*, pp. 3455–3462.

Nordstrom, D.K., and Southam, G. (1997). Geomicrobiology of sulfide mineral oxidation. In Banfield, J.F., and Nealson, K.H. (Eds.), *Geomicrobiology: Interactions between microbes and minerals, Reviews in Mineralogy, 35*, pp. 361-390. Washington D.C., Mineralogical Society of America.

Norris, P.R. (1983). Iron and mineral oxidation with Leptospirillum-like bacteria. In Rossi, G., Torma, A.E. (Eds.), *Recent Progress in Biohydrometallurgy*, pp. 83–96. Associazione Mineraria Sarda, Iglesias, Italy.

Norris, P.R., and Barr, D.W. (1988). Bacterial oxidation of pyrite in high temperature reactors. In P.R., Norris and D.P. Kelly (Eds.), *Proceedings of Biohydrometallurgy '87*, *Science and Technology Letters*, pp. 532–536. Surrey, United Kingdom.

Ohmura, N., Kitamura, K., Saiki, H. (1993). Selective adhesion of *Thiobacillus ferrooxidans* to pyrite. *Applied and Environmental Microbiology, 59*, 4044–4050.

Okay, A.I., Tüysüz, O., Satır, M., Özkan-Altıner, M., Altıner, D., Sherlock, S., Eren, R.H. (2006). Cretaceous and Triassic subduction-accretion, HP/LT metamorphism and continental groeth in the Central Pontides, Turkey. *Geological Society of America Bulletin, 118*, 1247-1269.

Okay, A.I., Sunal, G., Tüysüz, O., Sherlock, S., Keskin, M., Kylander-Clark, A.R.C. (2014). Low-pressure-high temperature metamorphism during extension in a Jurassic magmatic arc, Central Pontides, Turkey. *Journal of Metamorphic Geology, 32*, 49-69.

Olson, G.J., Brierley, J.A., Brierley, C.L. (2003). Bioleaching review part B: progress in bioleaching: applications of microbial processes by the minerals industries. *Applied Microbiology and Biotechnology, 63*, 249–57.

Page, A.L., Miller, R.H., Keeney, D.R. (1982). Methods of Soil Analysis Part 2. In *Chemical and Microbiological Properties (2nd ed.), Agronomy No. 9*, ASA Publications, Madison, WI.

Paktunç, A.D. (1998). Characterization of mine wastes for prediction of acid mine drainage. In Azcue J.M. (Ed.), *Environmental impacts of mining activities*, pp. 19-40. Springer, Heidelberg.

Paktunç, A.D. (1999). Mineralogical constraints on the determination of neutralization potential and prediction of acid mine drainage. *Environmental Geology, 39*(2), 103-112.

Pan, H.-D., Yang, H.-Y., Tong, L.-L., Zhong, C.-B., Zhao, Y.-S. (2012). Control method of chalcopyrite passivation in bioleaching. *Transactions of Nonferrous Metals Society of China, 22*, 2255–2260.

Parker, A., Klauber, C., Kougianos, A., Watling, H.R., van Bronswijk, W. (2003). An X-ray photoelectron spectroscopy study of the mechanism of oxidative dissolution of chalcopyrite. *Hydrometallurgy, 71*, 265–276.

Pehlivanoğlu, H. (1985). Kastamonu-Küre piritli bakır yatakları (Bakibaba-Aşıköy) ve çevresinin jeoloji raporu. *MTA* Report **1744**, (unpublished), Ankara, Turkey.

Perek, K.T., and Arslan, F. (2010) Effect of mechanical activation on pressure leaching of Küre massive rich copper ore. *Mineral Processing and Extractive Metallurgy Review: An International Journal, 31*(4), 191-200.

Perry, E. (1998). Interpretation of acid-base accounting, Chapter 11. In *Coal Mine Drainage Prediction and Pollution Prevention in Pennsylvania*. Pennsylvania Department of Environmental Protection, Harrisburg.

Petersen, J., and Dixon, D.G. (2006). Competitive bioleaching of pyrite and chalcopyrite. *Hydrometallurgy, 83*, 40–9.

Price, W.A., and Errington, J.C. (1995). ARD Guidelines for Mine Sites in British Columbia. *British Columbia Ministry of Energy* Report, Mines and Petroleum Resources, Mine Review and Permitting Branch.

Rawlings, D.E. (2002). Heavy metal mining using microbes. *Annual Review of Microbiology, 56*(1), 65–91.

Reedy, B.J., Beattie, J.K., Lowson, R.T. (1991). A vibrational spectroscopic ^{18}O tracer study of pyrite oxidation. *Geochimica et Cosmochimica Acta, 55*, 1609 – 1614.

Richmond, W.W., Cowley, J.M., Parkinson, G.M., Saunders, M. (2006). An electron microscopy study of β-FeOOH (akaganéite) nanorods and nanotubes. *CrystEngComm, 8*, 36–40.

Rohwerder, T., Gehrke, T., Kinzler, K., Sand, W. (2003). Bioleaching review part A: progress in bioleaching: fundamentals and mechanisms of bacterial metal sulfide oxidation. *Applied Microbiology and Biotechnology, 63,* 239–48.

Rojas-Chapana, J.A., Bärtels, C.C., Pohlnmann, L., Tributsch, H. (1997). Co-operative leaching and chemotaxis of *thiobacilli* studied with spherical sulphur/sulphide substrates. *Process Biochemistry, 33*(3), 239-248

Rossi, G. (1990). *Biohydrometallurgy*. McGraw-Hill, New York, USA.

Sahoo, P.K., Tripathy, S., Panigrahi, M.K., Equeenuddin, Sk.Md. (2014). Geochemical characterization of coal and waste rocks from a

coalfield, India. Implication for acid and metal generation. *Journal of Geochemical Exploration, 145*, 135-147.

Sánchez-España, J., López Pamo, E., Santofimia, E., Aduvire, O., Reyes, J., and Barettino, D. (2005). Acid mine drainage in the Iberian Pyrite Belt (Odiel river watershed, Huelva, SW Spain): geochemistry, mineralogy and environmental implications. Applied Geochemistry 20, 1320–1356.

Sand, W., and Gehrke, H. (2006). Extracellular polymeric substances mediate bioleaching/biocorrosion via interfacial processes involving iron(Ⅲ) ions and acidophilic bacteria. *Research in Microbiology, 157*, 49–56.

Sand, W., Gehrke, T., Jozsa, P.-G, Schippers, A. (2001). Biochemistry of bacterial leaching direct vs indirect bioleaching. *Hydrometallurgy, 59*, 159–175.

Sand, W., Rohde, K., Sobotke, B., Zenneck, C. (2002). Evaluation of *Leptospirillum ferrooxidans* for leaching. *Applied and Environmental Microbiology, 58*(1), 85-92.

Sanliyuksel-Yucel, D., and Baba, A. (2013). Geochemical characterization of acid mine lakes in northwestturkey and their effect on the environment. *Archives of Environmental Contamination and Toxicology, 64*, 357-376.

Schippers, A. (1998). Untersuchungen zur Schwefelchemie der biologischen Laugung von Metallsulfiden, PhD Thesis, University of Hamburg, Shaker-Verlag, Aachen, Germany.

Schippers, A. (2004). Biogeochemistry of metal sulfide oxidation in mining environments, sediments and soils. In Amend, J.P., Edwards, K.J., Lyons, T.W. (Eds.), *Sulfur Biogeochemistry — Past and Present: Special Paper, 379*, pp. 49–62. Geological Society of America, Boulder, Colorado, USA.

Schippers, A., and Jørgensen, B.B. (2001). Oxidation of pyrite and iron sulfide by manganese dioxide in marine sediments. *Geochimica et Cosmochimica Acta, 65*, 915-922.

Schippers, A., and Jørgensen, B.B. (2002). Biogeochemistry of pyrite and iron sulfide oxidation in marine sediments. *Geochimica et Cosmochimica Acta, 66*, 85-92.

Schippers, A., Jozsa, P.-G., Sand, W. (1996). Sulfur chemistry in bacterial leaching of pyrite. *Applied and Environmental Microbiology, 62*, 3424-3431.

Schippers, A., Jozsa, P.-G., and Sand, W., Kovacs, Zs.M., Jelea, M. (2000). Microbiological pyrite oxidation in a mine tailings heap and its relevance to the death of vegetation. *Geomicrobiology Journal, 17*, 151-162.

Schippers, A., and Sand, W. (1999). Bacterial leaching of metal sulfides proceeds by two indirect mechanisms via thiosulfate or via polysulfides and sulfur. *Applied and Environmental Microbiology, 65*, 319–321.

Schippers, A., Hedrich, S., Vasters, J., Drobe, M., Sand, W., Willscher, S. (2014). Biomining: Metal recovery from ores with microorganisms. In *Geobiotechnoloy 1 Advances in Biochemical Engineering/Biotechnology, 141*, pp. 1-47, Springer, Berlin, Germany.

Silverman, M.P., and Ehrlich, H.L. (1964). Microbial formation and degradation of minerals. *Advances in Applied Microbiology, 6*, 153–206.

Singer, P.C., and Stumm, W. (1970). Acidic mine drainage: the rate-determining step. *Science, 167*, 1121-1123.

Skousen, J., Simmons, J., McDonald, L.M., Ziemkiewicz, P. (2002). Acid-base accounting to predict post-mining drainage quality on surface mines. *Journal of Environmental Quality, 31*, 2034-2044.

Sobek, A.A., Schuller, W.A., Freeman, J.R., Smith, R.M. (1978). Field and laboratory methods applicable to overburdens and minesoils, *EPA* Report, **600/278-054**.

Steudel, R. (1996). Mechanisms for the formation of elemental sulfur from aqueous sulfide in chemical and microbiological desulfurization processes. *Industrial & Engineering Chemistry Research, 35*, 1417-1423.

Stott, M.B., Watling, H.R., Franzmann, P.D., Sutton, D. (2000). The role of ironhydroxy precipitates in the passivation of chalcopyrite during bioleaching. *Minerals Engineering, 13*(10), 1117–1127.

Stott, M.B., Sutton, D.C., Watling, H.R., Franzman, P.D. (2003). Comparative leaching of chalcopyrite by selected acidophilic bacteria and archaea. *Geomicrobiology Journal, 20*, 215–230.

Stumm, W., and Morgan, J.J. (1996). Aquatic Chemistry. Wiley, New York.

Sverdrup, H.U. (1990). *The kinetics of base cation release due to chemical weathering*. Lund University Press, Lund.

Third, K.A., Cord-Ruwisch, R., Watling, H.R. (2000). The role of iron-oxidizing bacteria in stimulation or inhibition of chalcopyrite bioleaching. Hydrometallurgy 57, 225–233.

Third, K.A., Cord-Ruwisch, R., Watling, H. (2002). Control of the redox potential by oxygen limitation improves bacterial leaching of chalcopyrite. *Biotechnology and Bioengineering, 78*, 433–441.

Thurston, R.S., Mandernack, K.W., Shanks III, W.C. (2010). Laboratory chalcopyrite oxidation by *Acidithiobacillus ferrooxidans*: Oxygen and sulfur isotope fractionation. *Chemical Geology, 259*, 252-261.

Thomas, J.E., Skinner, W.M., Smart, R.St.C. (2003). A comparison of the dissolution behavior of troilite with other Fe(II) sulfides; implications of structure. *Geochimica et Cosmochimica Acta, 67*, 831-843.

Tributsch, H. (2001). Direct versus indirect bioleaching. *Hydrometallurgy, 59*, 177-185.

TS 266 (2005). Sular - İnsanî Tüketim Amaçli Sular (Water intended for human consumption). **ICS 13.060.20**. Türk Standardlari Enstitüsü, Ankara, Turkey.

Tüysüz, O. (1990). Tectonic evolution of a part of the Tethyside orogenic collage: The Kargı Massif, northern Turkey. *Tectonics, 9*, 141-160.

Tüysüz, O. (1999). Geology of the Cretaceous sedimentary basins of the Western Pontides. *Geological Journal, 34*, 75-93.

Ustaömer, T., and Robertson, A.H.F. (1994). Late Paleozoic marginal basin and subduction-accretion: The Paleotethyan Küre Complex, Central Pontides, northern Turkey. *Journal of the Geological Society, London, 151*, 291-305.

Vaughan, D.J., and Craig, J.R. (1978). *Mineral chemistry of metal sulfides*. Cambridge University Press, Cambridge, England.

Wang, Z-h., Xie, X-h., Liu, J-s. (2012). Experimental measurements of short-term adsorption of *Acidithiobacillus ferrooxidans* onto chalcopyrite. *Transactions of Nonferrous Metals Society of China, 22*, 442-446.

Watling, H.R. (2006). The bioleaching of sulphide minerals with emphasis on copper sulphides - a review. *Hydrometallurgy, 84*, 81–108.

Weber, P.A., Stewart, W.A., Skinner, W.M., Weisener, C.G., Thomas, J.E., Smart, R.S.C. (2004). Geochemical effects of oxidation products and framboidal pyrite oxidation in acid mine drainage prediction techniques. *Applied Geochemistry, 19*, 1953-1974.

WHO (2008). Guidelines for Drinking-water Quality, *Volume 1* (3rd ed.). World Health Organization, Geneva.

Wong, J.W.C., Ip, C.M., Wong, M.H. (1998). Acid-forming capacity of lead-zinc mine tailings and its implications for mine rehabilitation. *Environmental Geochemistry and Health, 20*(3), 149-155.

Xia, L-x., Liu, X., Zeng, J., Yin, C., Gao, J., Liu, J., Guanzhou, Q. (2008). Mechanism of enhanced bioleaching efficiency of *Acidithiobacillus ferrooxidans* after adaptation with chalcopyrite. Hydrometallurgy 92, 95–101.

Xia, L-x., Tang, L., Xia, J-l., Yin, C., Cai, L-y., Zhao, X-j., Nie, Z-y., Liu, J-s., Qiu, G-z. (2012). Relationships among bioleaching performance, additional elemental sulfur, microbial population dynamics and its energy metabolism in bioleaching of chalcopyrite. *Transactions of Nonferrous Metals Society of China, 22*, 192-198.

Xu, Y. and Schoonen, M.A.A. (1995). The stability of thiosulfate in the presence of pyrite in low-temperature aqueous solutions. *Geochimica et Cosmochimica Acta, 59*, 4605-4622.

Yılmaz, O, and Boztuğ, D. (1986). Kastamonu granitoid belt of northern Turkey: First are plutonism product related to the subduction of the Paleo-Tethys. *Geology, 14*, 179-183.

Zhang, J.-Z., and Millero, F.J. (1993). The products from the oxidation of H_2S in seawater. *Geochimica et Cosmochimica Acta, 57*, 1705-1718.

Zhao, X., Wang, R., Lu, X., Lu, J., Li, C., Li, J. (2013a). Bioleaching of chalcopyrite by *Acidithiobacillus ferrooxidans. Minerals Engineering. 53*, 184–192.

Zhao, H., Wang, J., Hu, M., Zhang, Y., Qiu, G. (2013b). Synergistic bioleaching of chalcopyrite and bornite in the presence of *Acidithiobacillus ferrooxidans*. *Bioresource Technology, 149*, 71–76.

URL-1 <*http://www.kastamonu.gov.tr/sayfa.asp?id=3*>, date retrieved 05.02.2015.

URL-2 <*http://www.mta.gov.tr*>, date retrieved 17.09.2013.

CURRICULUM VITAE



Name Surname: Cansu Demirel

Place and Date of Birth: İstanbul (Üsküdar) – 03/08/1990

E-Mail: cns_demirel@hotmail.com

EDUCATION:

B.Sc.: Istanbul Technical University, Geological Engineering

PROFESSIONAL EXPERIENCE AND REWARDS:

2014-2015

Project Assistant / TÜBİTAK-İTÜ (113Y464)

2011

Laboratory Intern / ITU Geochemical Research Laboratories

Engineering Geology Intern / Zemin Teknolojileri Merkezi (ZTM)

2010

Engineering Geology Intern / Zemar Zemin Araştırma

2008

Accounting Intern (Volunteer) / SO CHIC (Sezgin Silver)

PUBLICATIONS, PRESENTATIONS AND PATENTS ON THE THESIS:

▪ **Demirel, C.**, Balcı, N., Sönmez, Ş. (2015). Evaluation of feasibility of static tests applied to Küre VMS ore deposits. *Geophysical Research Abstracts, Vol 17*, Abstract: EGU2015-2833 EGU General Assembly, Vienna, Austria, 12 – 17 April.

▪ **Demirel, C.**, Kurt, M.A., Balcı, N. (2015) Simulation of acid mine drainage generation around Küre VMS Deposits, Northern Turkey. *Geophysical Research Abstracts, Vol 17*, Abstract: EGU2015-4048. EGU General Assembly, Vienna, Austria, 12 – 17 April 2014.

▪ **Demirel, C.**, Sönmez, Ş., Balcı, N., 2014. Understanding Cu release into environment from Küre massive sulfide ore deposits, Kastamonu, NW Turkey. *Geophysical Research Abstracts, Vol 16,* Abstract: EGU2014-3890. EGU General Assembly 2014, Vienna, 27 April-2 May 2014.

▪ **Demirel,** C., Balcı, N., Gül, S., Sönmez, Ş. (2014) Environmental geochemistry of Küre (Kastamonu) massive sulfide deposits. 67th Geological Congress of Turkey, Ankara, Turkey, 14-18 April 2014.

OTHER PUBLICATIONS, PRESENTATIONS AND PATENTS:

▪ Bulkan, Ö., **Toksoy, B.**, Yalamaz, B., Acığınar, S., Çağatay, N.M., Gürevin, C., Acar, D., Aydın, H., Demirel., C. (2014) Environmental controls on the organic matter enrichment processes in the Lake Bafa sediments (Eastern Mediterranean Region), during the last 150 years. ISEMG, Muğla, Turkey, 13 – 17 October 2014.

▪ Demirel, C., Menekşe, M., Balcı, N., **Sönmez, Ş.** (2014) Bioleaching of metals from printed circuit boards by *Acidithiobacillus thiooxidans*. IMMC 2014, Istanbul, Turkey, 11 – 13 September 2014.

▪ **Balcı, N.**, Gül, S., Demirel, C., Sarı, E., Sönmez, M.Ş. (2014) O and S isotope ratios of sulfate and Implications for AMD generation A case study: Balıkesir-Balya Pb-Zn Mine Waste Site. 67th Geological Congress of Turkey, Ankara, Turkey, 14-18 April 2014.

▪ Mahmutoğlu, Y., **Demirel, C.**, Şahin, M., Güreş, B., Güler, F., Şans, G. (2013) Investigation of the Slope Stability of Gürpinar Region, Istanbul in Engineering Geological Approach. 66th Geological Congress of Turkey, Ankara, Turkey, 1-5 April 2013.

COURSES & CERTIFICATES

2014

ECORD Summer School on "Subseafloor Biosphere: Current Advances and Future Challenges", MARUM, University of Bremen, Germany, 22 September - 2 October 2014 / Workshop and certificate of attendance.

2013

Awareness of disasters course for individuals and families – Official instructor certificate / AFAD

First Aid – Education and certificate (Ministry of Health) / Hayat Yıldızı Education Center.

Light and Heavy Search and Rescue Operations – Education and certificate / AKA Search and Rescue

Community awareness of disasters – Education and certificate / AKA Search and Rescue

2011

Certificate of completion for A 1.2 (A1 - beginner) level, certificate of attendance to A 2.1 level.

LANGUAGES

English (Advanced)

German (Basic)

COMPUTER SKILLS

Microsoft Office (Good)

ArcGIS (Good)

AutoCAD (Good)

Surfer (Basic)

RockWorcks (Basic)

Photoshop (Basic)